Diffusion mechanism of aromatic hydrocarbons within zeolites in liquid phase and sub- and super-critical fluids

液相・亜臨界・超臨界流体中のゼオライトの芳香族炭化水素の拡散機構

2022 年

北海道大学大学院　総合化学院

総合化学専攻　化学システム工学研究室

SU XINLUONA

Table of Contents

Chapter 1
Introduction

The need for sustainable production of everyday materials in addition to market volatility of petroleum-based feedstocks has motivated research into the production of renewable aromatic chemicals from biomass. Porous materials such as zeolites with their unique property, which are widely used in chemical industry and petrochemical industry such as selective catalysis and adsorption separation. Through the adsorption and diffusion properties of diffusion substance within zeolites were studies. Further understanding of diffusion mechanism within zeolites could offer some new information, which is of guiding significance for studying the intrinsic reaction kinetics of catalytic reaction, designing zeolite catalyst and reactor in the reaction engineering. In this study, we focused on the diffusion within zeolites in the liquid phase and sub- and super-critical fluids, which can clarify the diffusion mechanism within the pore of zeolites.

1.1. Zeolites

Zeolites are usually defined as a crystalline aluminosilicate with a three-dimensional framework structure that forms regularly sized pores in each dimension. They consist of connection of SiO_4 and AlO_4 tetrahedrons through oxygen bridges (Fig.1.1) [1]. Among them, Si (Al) tetrahedrons is the most primary building units of zeolites framework. At some places in the framework Al ions have charge of plus three and the framework carries a negative charge. In order to balance the valence state, coordination cations such as H^+ exist (Fig.1.2) within the cavities preserve the electroneutrality of the zeolite. This cation within the cavities has solid acid, which can become an active site for reversibly adsorb polar molecules. The active site contains various alkali metals, alkaline earth metals and transition metal species. According to the regulations of the International Union of Pure and Applied Chemistry (IUPAC) and the size of pore channels, porous materials can be divided into three categories: macroporous materials with a diameter greater than 50 nm, microporous materials with a diameter of 2 nm, and mesoporous materials with a range of 2-50 nm [2]. The pore size is one of the most important characteristics in the structure of zeolite molecular. In addition, the diameter of some lighter hydrocarbons approaches the pore diameter of the

zeolites. The molecule which is smaller than the pore size of the zeolite can enter the pores, and the molecule which is larger than the pore size of zeolite cannot enter the pores.

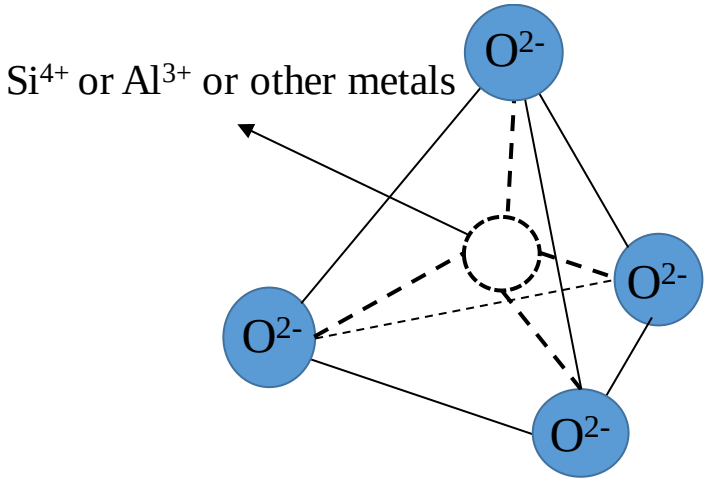

Fig.1.1 Unit in the zeolites structure.

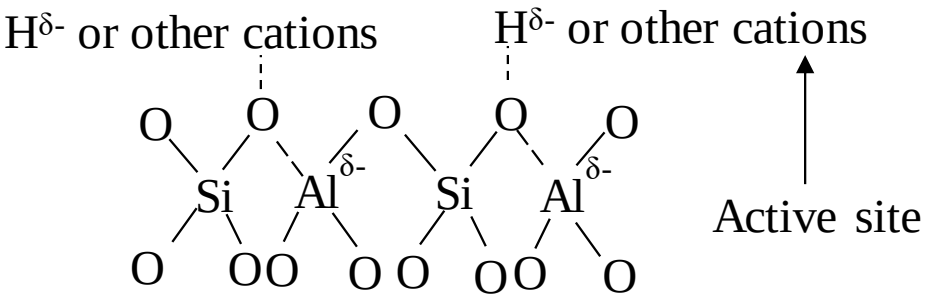

Fig.1.2 acid site of zeolite

In 1756, the Swedish mineralogist Cronstedt discovered the first natural aluminosilicate and it was named zeolite by Cronstedt [3]. In the 1960s, the artificial synthesis of zeolite made this kind of porous materials begin to play its application value [4]. In 2006, there were approximately 170 molecular sieve structures were

registered [5]. According to the different framework structure of zeolites, zeolites can be divided into different types, such as MFI type, BEA type, USY type, MOR type, MWW type zeolite, etc [6-8].

In general, the internal structure of molecular sieves is mainly composed of channels and cages. In this paper, the structure of MFI type zeolites, BEA type zeolites, Y type zeolites were investigated.

1.1.1. Structure and application of MFI type zeolites, BEA type zeolites, Y type zeolites

The unique crystal structure of zeolite determines its unique properties: possessed tunable solid acidity, flexible frameworks, ion exchange and high adsorption capacity [9], which is widely used in various fields including petrochemistry and fine chemicals as catalysts, adsorbents, and separators by utilizing these characteristics [10-14].

In the framework of MFI type zeolite (ZSM-5 zeolite and high-silica silicalite-1 zeolite), the tetrahedron composed of silicon oxygen or aluminum oxygen atoms forms a five membered ring through a common vertex oxygen bridge, and eight five membered rings are connected with each other to form its basic structural unit (Fig.1.3 a). Each sheet is linked by oxygen bridges to the next to form the 3-dimensional structure. Thus, two kinds of 10-ring cross channels are formed, i.e., the straight-line channel with an aperture of 0.53 x 0.56 nm and a zigzag Z-shaped sinusoidal channel with an aperture of 0.51 x 0.55 nm (Fig.1.3 b) [15-16]. The ZSM-5 has attracted attention as a catalyst with shape selectivity in refinery and petrochemical processes, and it has been put into practical for catalytic decomposition of fluidized bed [17-20].

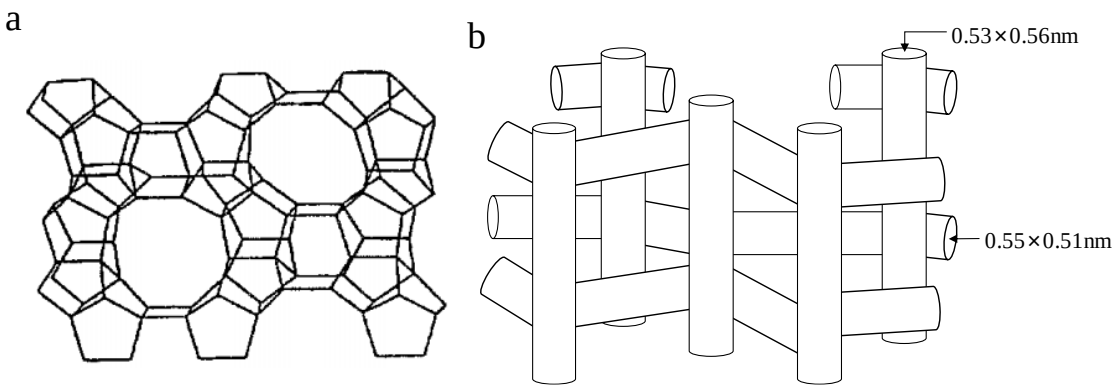

Fig.1.3 a Representative zeolite structures of MFI zeolite [15] and b porous structure of MFI zeolite

Y zeolite is one of the most widely used microporous molecular sieves in industry, which has FAU topology. (Fig.1.4 a). In this case, they are arranged in the same way as the carbon atoms in diamond, which are joined to one another via double 6-rings. This creates the so-called supercage with four, tetrahedrally oriented, 12-ring pore openings, and a 3-dimensional channel system, and pore size of Y zeolite is 0.74 x 0.74 nm. (Fig.1.4 b). Because of its large pore volume and three-dimensional 12 membered ring channel system, octahedral zeolite has a large pore volume, Y zeolite has become the main active component of Fluidized Catalytic Cracking (FCC) and hydrocracking catalysts [21-25].

BEA zeolite is tetragonal with high density of crystal defects, which have a high silica zeolite with three-dimensional twelve membered ring channel structured (0.76 x 0.64 nm). The units are joined to one another via 4-rings to form layers with saddle-shaped 12-rings (Fig.1.5). BEA zeolite has good adsorption performance, which is widely used in the removal of thiophene sulfide from FCC gasoline. The results show that the microporous mesoporous structure of BEA zeolite can remove organic sulfur compounds with different molecular sizes, which can be applied to the desulfurization of oil products with multi-component organic sulfur components [26]. In addition, BEA zeolites are also widely used in vehicle emission control, industrial waste gas purification, and emission reduction of volatile organic compounds (VOC), NOx and N_2O [27-30].

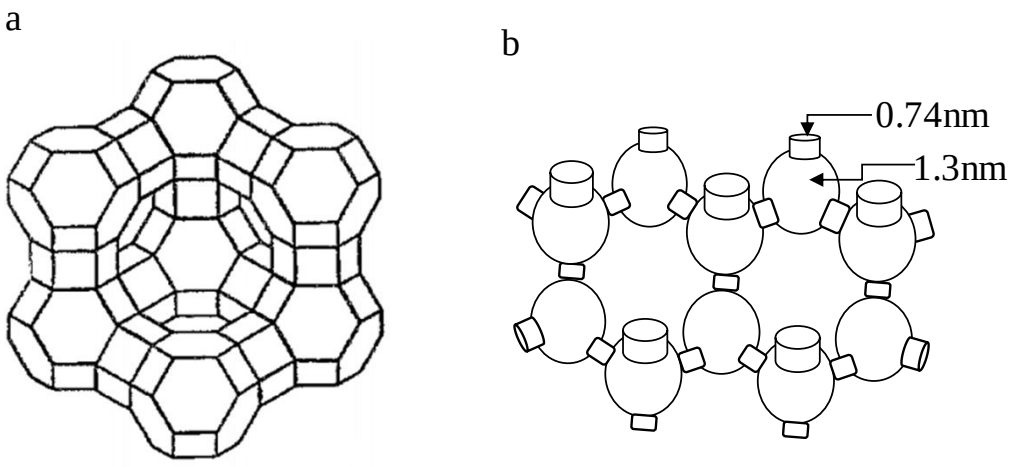

Fig.1.4. a. Representative zeolite structures of Y zeolite [15] and b. porous structure of Y zeolite generally by viscous flow.

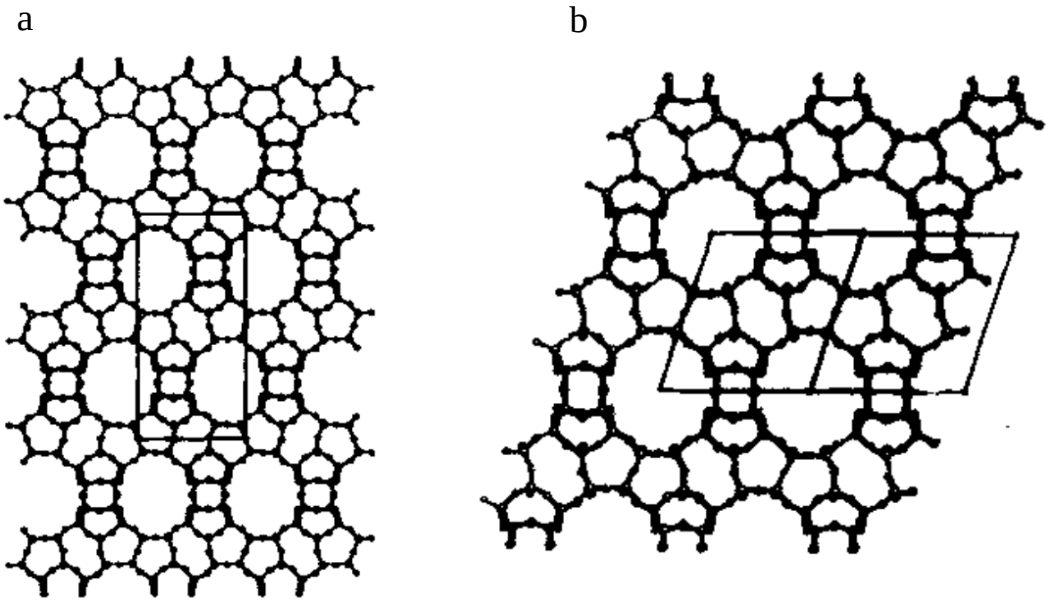

Fig.1.5 a. Framework structure viewed of BEA zeolite approximately along [010]
b. Framework structure viewed of BEA zeolite approximately along [110][26]

1.2. Adsorption of Zeolite

1.2.1. Adsorption

Adsorption occurs due to the interaction between the adsorbate molecules and the adsorbent surface, such as catalysis, dissolution, etc. The solid that can be adsorbed is called adsorbent, and the substance adsorbed is called adsorbate. The adsorption rate of fluid molecules on zeolite is relatively fast, and the adsorption process is mainly controlled by intragranular diffusion. The pore size of the zeolite determines the size of the molecules that can enter the crystal cavity. The adsorption of adsorbate molecules in zeolite channels not only interacts with the pore walls of zeolites, but also between adsorbate molecules and molecules.

The Si/Al ratio of zeolites also affects the properties of zeolites. For example, the surface of zeolites with high Si/Al ratio is nonpolar, and the effect of nonpolar surface on adsorption is not obvious. The aluminum content in zeolite also has an effect on the adsorption performance of zeolite. For Al rich zeolites, the electrostatic effect plays a dominant role in the adsorption process due to the strong electrostatic field in the pore

channel.

1.2.2. Type of adsorption isotherms

In the IUPAC recommendations there are six physical adsorption isotherm types were shown in Fig1.6. Type I: adsorption on microporous adsorbents. TypeII: adsorption on nonporous or macroporous adsorbents with strong adsorbate-adsorbent interactions. TypeIII: adsorption on non-porous or macroporous adsorbents with weak adsorbate-adsorbent interactions. Type IV: mesoporous adsorbents with capillary condensation is accompanied by hysteresis. TypeV: it is related to the Type III isotherm and the adsorbent-adsorbate interaction is weak. TypeVI: stepwise layer-by-layer adsorption on a highly uniform nonporous surface [31].

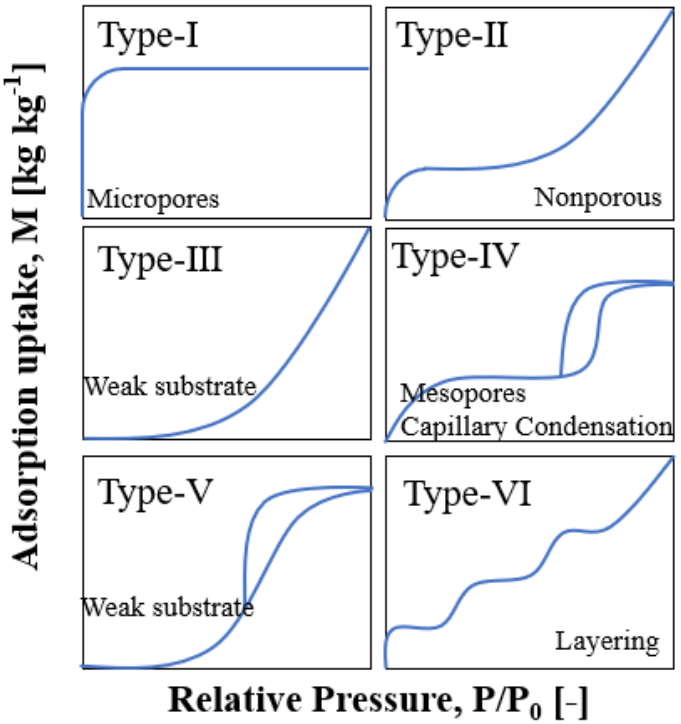

Fig.1.6 Classification of adsorption isotherms according to IUPAC [32]

1.2.3. Equation of adsorption isotherms

The mathematical formula to express the isothermal adsorption curve is called isothermal adsorption formula. The following formulas are commonly used:

(1) The Henry isotherm

At a certain temperature, the solubility of gas in liquid is directly proportional to its partial pressure, which is Henry's law. In the process of adsorption, the adsorption amount is directly proportional to the pressure (or concentration). This is the same as the solubility of gas in dissolution, so it is called Henry adsorption.

$$Q=KC \tag{1-1}$$

Here, Q is amount of adsorbed, K is equilibrium constant which is estimated from the slope of isotherms, and C is concentration or pressure in adsorbed phase at equilibrium condition.

(2) The Langmuir isotherm

The Langmuir isotherm theory assumes monolayer coverage of adsorbate over a homogenous adsorbent surface [33]. Therefore, a saturation point is reached where no further adsorption can occur at equilibrium. A basic assumption is that sorption takes place at specific homogeneous sites within the adsorbent. Once a dye molecule occupies a site, no further adsorption can take place at that site. The Langmuir equation is expressed as:

$$q=\frac{aq_sP}{1+aP} \tag{1-2}$$

Here, q is amount of adsorbed, a is sorption equilibrium constant, q_s is amount of saturated sorption and P is pressure at equilibrium condition.

The Langmuir equation is used in homogeneous sorption, where the sorption of each molecule has equal sorption activation energy. The equation is thermodynamically consistent and follows Henry's Law at low concentrations.

(3) The Freundlich isotherm

The Freundlich expression is an exponential equation and therefore assumes that as the adsorbate concentration increased with increasing the concentration of adsorbate on the adsorbent surface. The Freundlich equation is expressed as:

$$q = aP^{1/n} \quad (1\text{-}3)$$

In this equation, q is amount of adsorbed, a is sorption equilibrium constant, P is pressure at equilibrium condition, and n is constant. This expression is characterized by the heterogeneity factor, n, and so the Freundlich isotherm may be used to describe heterogeneous systems [34–36].

(4) The Tempkin isotherm

Tempkin and Pyzhev [37] considered the effects of some indirect adsorbate/adsorbate interactions on adsorption isotherms and suggested that because of these interactions the heat of adsorption of all the molecules in the layer would decrease linearly with coverage. The Tempkin isotherm has been used in the following form:

$$q = \frac{RT}{b} \ln AC \quad (1\text{-}4)$$

Here, R is the universal gas constant (8.314 J/mol K), T is the absolute temperature in Kelvin, and b is the Tempkin constant related to heat of sorption (J/mg). The Tempkin constants A and b are calculated from the slope and C is concentration.

1.3. Intracrystalline diffusion phenomenon within zeolite

1.3.1. Diffusion

Due to the widely application of porous materials in petrochemical industry, the diffusion behavior of molecules in adsorbents is very crucial because the diffusion performance of reactants/products in catalyst channels is closely related to the efficiency of the catalytic process. Porous materials are used as catalysts in catalytic reactions. When the molecular size of reactants/products are close to the pore size of porous materials, there are interactions between the reactant/product molecules and the pore channels, the diffusion of the reactants/products within the pores of the porous materials is limited. Therefore, the diffusion of reactants/products is strongly affected by the pore size and configuration of porous materials, and not only by temperature and adsorbent concentration. In this way, it can greatly reduce the mass transfer rate (i.e. diffusion limitation), and seriously affects the activity and selectivity of the porous materials catalysts.

In these diffusion processes, the effective diffusion coefficient is very significant for studying the intrinsic reaction kinetics of catalytic reaction, designing reactor and predicting the ideal concentration distribution of active components on the catalyst. Therefore, it is very essential to measure the diffusion performance of the probe molecules in the catalyst by various experimental instruments and methods, and to carry out theoretical research on diffusion related to the catalyst development and industrial application technology [38].

Heterogeneous catalytic reaction of porous materials plays an important role in petrochemical and fine chemical production Use. In the process of heterogeneous catalytic reaction, the catalytic reaction performance of the catalyst is closely related to the diffusion performance of porous materials. The catalytic reaction process of porous materials includes (Fig.1.7): a. the reactant first diffuses from reaction fluids to the outer surface of zeolite (external diffusion). b. the reactant diffuses from the surface of the zeolite to the inside of the channel (internal diffusion). c. catalytic reaction on the inner surface of the inner channel of zeolites (chemical reaction). d. the product diffuses from the inner channel to the outer surface of the zeolites (internal diffusion). e. the product diffuses from the outer surface of the zeolite (external diffusion).

From the above process, whether a catalytic reaction can take place or not, how efficient the catalytic reaction is, the diffusion of reactants plays an important role within zeolite. For the reaction that can be carried out in thermodynamics, if the reactant molecules are limited in the diffusion process, the efficiency of the whole catalytic reaction will be reduced; similarly, if the product molecules generated cannot leave the active site and reach the gas phase, liquid phase or other phases in time that we often called product poisoning. Therefore, the study of the diffusion properties of porous materials is very important for understanding the catalytic process.

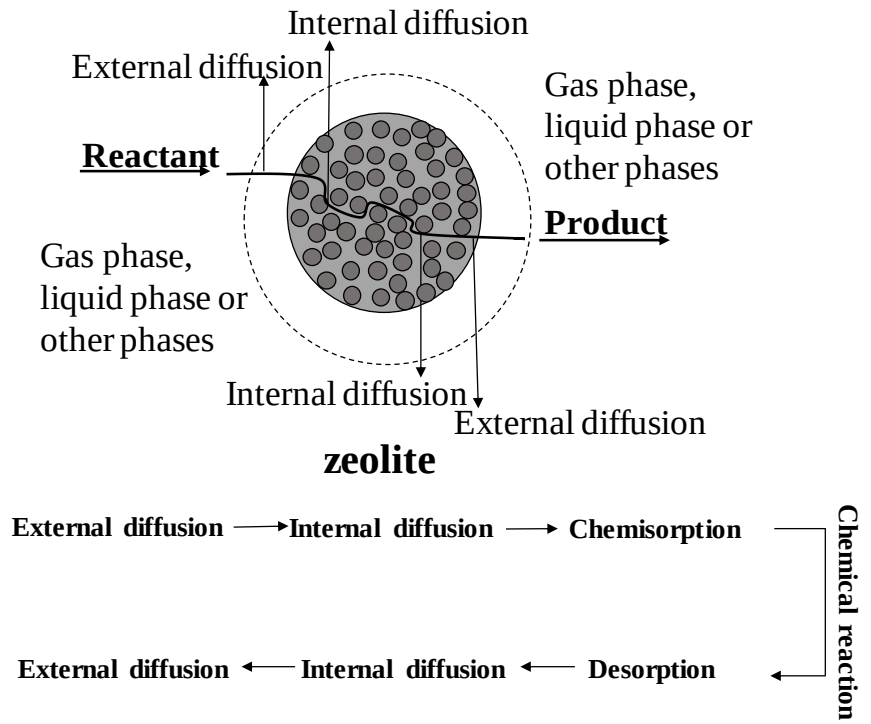

Fig.1.7 Heterogeneous catalytic reaction on zeolite catalyst particles

1.3.2. Affect factor of diffusion

Generally, the pore size of zeolite is less than 1.3nm, which belongs to microporous material, and the molecular kinetics diameter of most of hydrocarbon is about 1nm. Therefore, the diffusion of hydrocarbon within zeolite is affected by the size and configuration of adsorbent and adsorbate structure. Zeolite is composed of crystals with uniform pore size. The adsorption molecules will produce steric hindrance with adsorbent molecules in the diffusion process. In this case, only small or appropriate shape hydrocarbon molecules can diffuse into the zeolite, while other hydrocarbon molecules are excluded, which reflects the shape selective property of zeolite.

The porosity of zeolites gives rise to their unique shape selectivity characteristic, as certain reactions are facilitated while others are suppressed due to the high or low accessibility of reactants to reaction sites, and slow transport of products out of these sites.According to the average free path length of diffusion molecules (λ) and the pore size of porous solid particles (d_p), diffusion in porous materials can be divided into the following three regions: 1. Molecular diffusion; 2. Knudsen diffusion; 3. Configurational diffusion(Fig.1.8 a) [39-42].

1) Molecular diffusion(d_p>>λ): also known as host diffusion or bulk diffusion. When the pore diameter is much larger than the average free path of molecules, there is no effect of pore wall effect, and guest molecules can easily pass through the pore. When the pore diameter is large or the system pressure is high, molecular diffusion plays a major role.

2) Knudsen diffusion(d_p≅λ): the pore diameter of the medium is smaller than the average free path of the guest molecule, and there is a strong interaction between the guest molecule and the pore wall, and the pore wall will have a significant impact on the adsorption and diffusion of molecules in the medium.

3) configurational diffusion: also known as “Intracrystalline diffusion,” [43], For molecules with strong adsorption capacity on the pore surface, or the size of the guest molecule is very close to the pore size of zeolite, such diffusion occurs. The diffusion is not only related to the temperature of the system and the concentration of guest molecules, but also affected by the shape and size of the channels of zeolite. In the configuration region, the diffusion resistance is greatly increased due to the influence of the force field gradient and the diffusion potential of molecules through the pore channel.

From the relationship between the pore size and the three kinds of diffusion, which can be seen that the diffusion coefficient decreases with the decrease of the pore diameter. The most obvious diffusion type affected by pore size is intracrystalline diffusion. The small change of pore size can lead to the change of diffusion coefficient by multiple or even several orders of magnitude. Intracrystalline diffusion is an activated process, the energy of activation arising largely from steric hindrance. The diffusional activation energy and therefore the diffusivity, for a given sorbate, are therefore directly related to the pore size, as shown schematically in Fig.1. 8b.

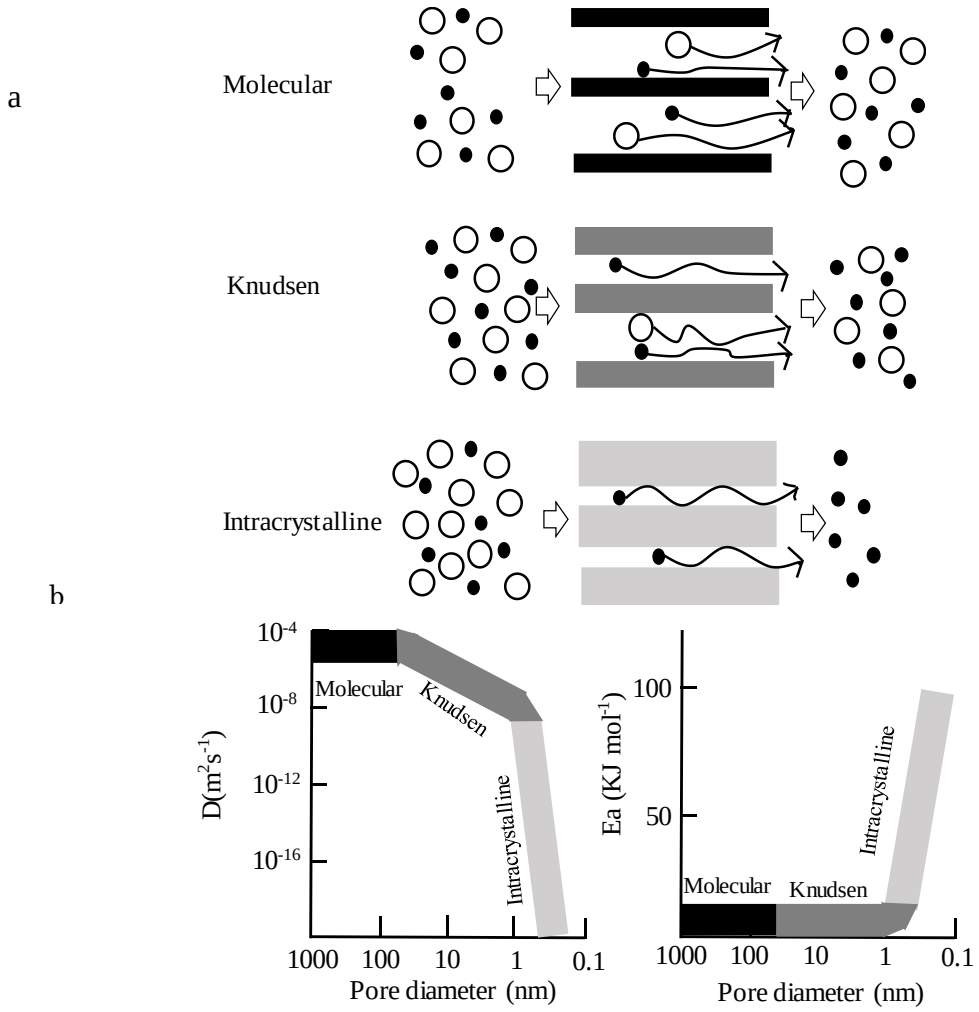

Fig.1.8 Diffusion of guest molecule in zeolites a) Schematic representation of the effect of pore size on the diffusion of large and small molecules; b) Effect of pore diameter on molecular diffusivity (D) and energy of diffusional activation (Ea) with the different regimes.

The main expressions of molecular diffusion in particle channels are shown in the Table 1.1. Ruthven et al. reported that the adsorption of gas on porous materials mainly occurred in the intracrystalline of the porous material, which considered that the adsorption contribution of the macroporous connector and the outer surface of the crystal could be ignored. Because the diffusion rate of adsorbate molecules in the porous material crystal was very slow, and the diffusion time constant D/R^2 is usually lower than $10^{-3}s^{-1}$, so the diffusion of adsorbate molecules in porous materials plays an

important or even decisive role in the process of adsorption and desorption. The diffusion coefficient of adsorbate molecules in porous materials is about 10^{-9}-$10^{-20}$$m^2$/s.

Table 1.1 Main expressions of molecular diffusion in particle channels

Molecular diffusion type	Diffusion coefficient formula	Diffusion coefficient order of magnitude
Intracrystalline diffusion	$D= D_0\exp(-\frac{E}{RT})$	$D<10^{-9}m^2/s$
Knudsen diffusion	$D = \frac{2r}{3}\sqrt{\frac{8RT}{\pi M}}$	$D\approx10^{-6}m^2/s$
Molecular diffusion	$D = \frac{T^{1.5\ -\ 2}}{P}$	$D\approx10^{-5}$-$10^{-4}m^2/s$

where D_0, E, R, r, T, M and P are correction diffusion coefficient, activation energy, universal gas constant, pore radius, absolute temperature, mass of gas molecule and equilibrium pressure, respectively.

The diffusion of hydrocarbons within zeolite belongs to intracrystalline diffusion, and its diffusion value depends on the geometric characteristics, connectivity, size and lattice defects of zeolite channels. Diffusion coefficient is the most basic transfer parameter to describe the characteristics of diffusion process. The definition and expression of diffusion coefficient are different, which can be divided into three categories: (1) the corrected diffusion coefficient(D) defined in Maxwell-Stefan diffusion theory, also known as Ms diffusion coefficient, which is applied to the diffusion of multicomponent in porous materials[44], zeolite membranes are used to separate Alkane Isomers and experimental techniques are used to study the diffusion of probe molecules in porous materials [45-47].(2) Diffusion coefficient through a tracer molecular marker, self-diffusion coefficient (D_{self}) [48-49]; (3) effective diffusion coefficient given according to Fick's law (D_{eff}) [50-52]. In this paper, we choose Fick diffusion coefficient.

When the diffusion of molecules in zeolite is controlled by intracrystalline

diffusion, the diffusion coefficient obtained by adsorption kinetics mainly depends on the following factors:

(1) The shape, size, polarity and deformability of the adsorbate molecules.

(2) The results show that the size of zeolite crystal particles, the shape and size of channels in the crystal, the connection mode, the distribution and charge number of cations in the crystal lattice, the surface properties of zeolite and lattice defects.

(3) The concentration of adsorbate molecules in adsorbent crystal.

(4) System temperature, humidity. Temperature is very sensitive to the effect of diffusion. The degree of influence on the reaction should be measured under the reaction temperature. The diffusion coefficient measured at different temperatures is different. The activation energy of the sample can be calculated by *Arrhenius* formula and the diffusion coefficient measured at reaction temperature. etc.

1.3.3. Measurement method of diffusion coefficient within porous crystals

The measurement of diffusion coefficient is a very challenging work [53-54]. So far, many experimental methods have been developed to measure the diffusion coefficient of probe molecules on zeolite. The most basic principle is to change the pressure or composition of the surrounding environment of the adsorbent system, and then record the time response of the system. By analyzing the response curve, the diffusion coefficient can be obtained [55].

At present, there are many methods to measure diffusion. According to their characteristics, these methods are mainly divided into three categories: macroscopic method, microscopic method and molecular simulation technology.

The macroscopic method usually measures the change of adsorbate concentration, and the analysis of the response curve is often based on Fick diffusion law. The diffusion coefficient measured by this method is usually mass transfer diffusion coefficient, and self-diffusion coefficient can also be measured by using marker molecules. Compared with the macroscopic method, the microscopic method measures the movement of molecules in the pore channel in a very short time and a very small space. According to the measurement principle, this method can measure the mass transfer rate of molecules in a single zeolite crystalline grain, which can directly explain the microscopic diffusion mechanism of molecules.

Measurement method for diffusivity in macroscopic method and microscopic

method were shown in Table1.2, respectively. Macroscopic method includes transient method and steady state method. The transient method can be divided into the following five categories. The characteristic of volumetric method and gravimetric method is that the operation is carried out under isothermal condition, the experiment directly observe and the data processing is relatively simple, but it is greatly affected by the external heat and mass transfer restrictions, so it is not suitable for the rapid adsorption process. Zero-length column technique (ZLC) method is simple equipment, convenient operation and small amount of sample consumption, which can effectively eliminate the external mass transfer restriction and the influence of thermal effect. Frequency response (FR) method is influence of external heat and mass transfer restrictions, so it is seldom used. Its advantage is that almost free from the rate limit of diffusion system. Chromatographic method is applied in the rapid diffusion system, which has the advantages of not being disturbed by external diffusion and thermal effect [68]. However, there are some problems, such as the broadening of chromatographic response peak and the agglomeration of zeolite grains, resulting in the deviation of axial diffusion behavior. The steady state method can be divided into the following two categories. Wiche-Kallenbach method has no effect of external heat transfer and mass transfer limitation. However, large single crystal or membrane with uniform thickness and high density is required. The experimental process of effectiveness factor method is very complicated, which is affected by external heat and mass transfer limitations [56-64].

Microscopic method can be divided into the following three categories. The advantage of pulsed field gradient NMR (PFG NMR) method is that it does not destroy the sample, the particle size of the sample to be measured is small, and the diffusion behavior of multiple components in the same system can be studied by studying the different chemical shifts, which can directly distinguish the intragranular diffusion and the extragranular diffusion. Quasi elastic neutron scattering (QENS) method can be used to measure the self-diffusion coefficient and average free path of molecules. And neutron itself is not charged, which can measure data that cannot be measured by other methods. However, this technology is not suitable for rapid diffusion system [69], and its application has certain limitations [65-67].

Table 1.2 Measurement Method for Diffusivity

Technique	viewpoint	Ref.
Gravimetric method	macroscopic(transient)	56
Volumetric method	macroscopic(transient)	57
Chromatography method	macroscopic(transient)	58-59
Frequency response method (FR)	macroscopic(transient)	60
Zero length column method (ZLC)	macroscopic(transient)	61
Cone element oscillating microbalance (TEOM)	macroscopic(transient)	62
Wiche-Kallenbach	macroscopic (steady state)	63
Effectiveness factor	macroscopic (steady state)	64
Pulsed field gradient NMR (PFG NMR)	microscopic	65
Quasi elastic neutron scattering (QENS)	microscopic	66
Interference microscopy technique	microscopic	67

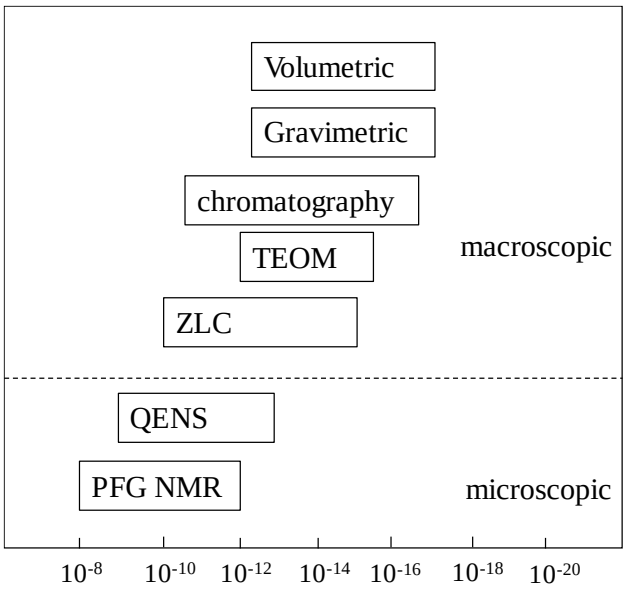

Fig.1.9 The range of diffusivities measures by different methods

Figure 1.9 showed that the approximate range of diffusion coefficient values measured by different measurement methods. It can be seen that difference of diffusion coefficient obtained by different measurement methods may be very large for the same system, due to the different principles, assumptions, measurement time and displacement range of different measurement methods. Therefore, we can't directly compare the diffusion coefficient measured by different methods. We should choose the most appropriate measurement method according to different systems and the specific purpose of the research. Microscopic method and molecular simulation technology are used to study the diffusion of guest molecules in porous materials at the molecular level. The measurement is not affected by the heat transfer in the diffusion process, so it is suitable for theoretical research. However, the test conditions are strictly and the experimental cost is pricey. The measured diffusion data only represent the nature of local diffusion. In contrast, the measurement conditions of macroscopic method are closer to the industrial practice, so most of the macroscopic methods are widely used in diffusion research.

There is a big difference between the diffusion constants obtained by macroscopic method and microscopic method. Because the diffusion of adsorbate molecules on zeolites belongs to the molecular level that is very necessary for theoretical research. However, from the perspective of application, the experimental conditions of microscopic method are very strict, and the macroscopic method is closer to industrial application. Therefore, gravimetric method, constant volume method, frequency response (FR) method and zero-length column technique (ZLC) method are often used for measuring the diffusivity of hydrocarbon within porous materials.
Among these measurement methods, Takao Masuda et al. reported that measurement of diffusivity of hydrocarbons within zeolite in the gas phase and liquid phase by using the constant volume method. [70-74] In this paper, the constant volume method is used to measurement of diffusion coefficient of hydrocarbons within porous materials.

1.4. Supercritical fluid

1.4.1. Definition

The supercritical fluid is defined as the temperature and pressure of a substance are above the critical temperature (T_C) and the critical pressure (P_C), the material is in supercritical state. The critical point in the Figure1.9 refers to the point

where the vapor-liquid interface just disappears when the vapor-liquid equilibrium line extends to high temperature. The corresponding temperature and pressure here are critical temperature (T_C) and critical pressure (P_C). Moreover, the fluid is in supercritical state when the temperature and pressure of fluid exceed the critical temperature and pressure at the same time. It is possible to continuously change the density from the dilute state near the ideal gas to the dense state close to the liquid. This means that the solvent can be controlled as a function of the density, and it is possible to control the solvent specially represented by the transport property such as the diffusion coefficient. When it is applied to the reaction, separation, and material production [75-76], it is possible to obtain the different effect in the conventional liquid solvent from the characteristic of the liquid equivalent solubility and the expected diffusion property. (Fig.1.10)

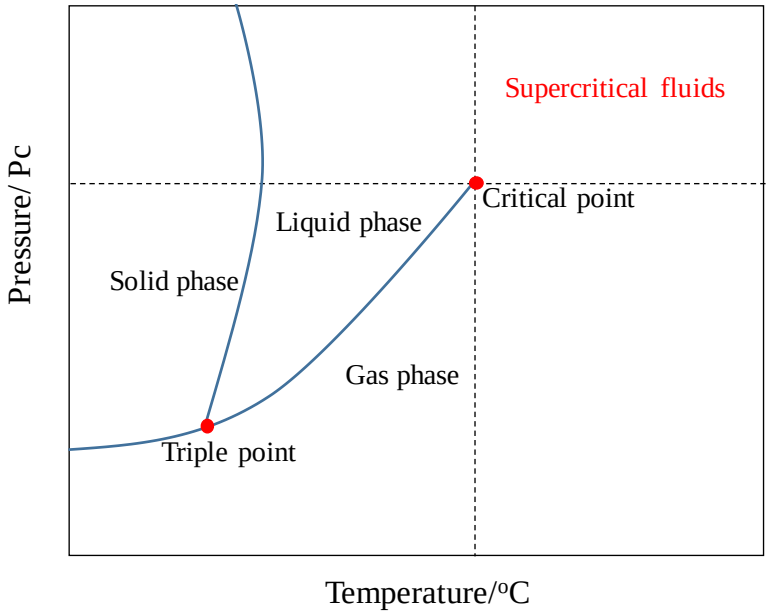

Fig.1.10 Typical phase diagram demonstrating where the supercritical fluid region is located.

1.4.2. Property of supercritical fluid

Supercritical fluid has some characteristics of gas and liquid, and many properties are between the properties of gas and liquid [77]. Supercritical fluid densities are comparable to those of liquids, whereas the diffusivities and viscosities are comparable to those of gases. The density is sufficient to afford substantial dissolution power, the high diffusivities and low viscosities enhance mass transfer rates of reactants to the active sites on catalyst dispersed in supercritical fluids (catalyst are insoluble in all supercritical fluids) [78]. Reactions which are limited by the rates of diffusion, rather than intrinsic kinetics, will proceed faster in supercritical fluids than in liquids.

It has been found that supercritical fluid has many advantages, whether as extractant or reaction medium [79-80]:

(1) It can eliminate the mass transfer resistance between the gas-liquid interface and the liquid-liquid interface by controlling its phase behavior.

(2) The properties depending on the density (solubility, dielectric constant, diffusion coefficient, etc.) change continuously and greatly with the change of temperature and pressure.

(3) In the presence of solute, the solute and solvent combination may cause the solvent to be mixed around the solute molecule to increase the solubility of solute near the critical point, and the transport properties and reaction rate.

(4) It can enhance the external diffusion effect in multiphase reaction, prevent the accumulation of poison on the catalyst surface, and improve the service life of the catalyst.

(5) In the vicinity of the critical point, the thermal conductivity is larger than that of the liquid, and the heat transfer rate is high.

(6) The yield, conversion, chemical selectivity and stereoselectivity of the reaction can be improved.

1.4.3. Phase behavior and solubility

The importance of system phase behavior involving supercritical fluid can be viewed from two aspects. Firstly, the kinetic analysis of reactions in supercritical fluid obviously needs to calculate the number and composition of equilibrium phase. Secondly, the industrial scale reactions will involve whatever number and compositions of equilibrium phases the overall process economics dictate. Design, scale-up, and

production, therefore, require thermodynamic as well as kinetic analysis.

1.4.4. Molecular aggregation in supercritical solutions

The phase equilibrium behavior of solutions containing supercritical fluids is very complex due to the great differences in molecular size, structure, interaction strength and critical properties between solutes and solvents. Especially in the near critical region, compared with a liquid medium, the supercritical fluid is much more compressible and has a larger free volume so that the attractive forces can move molecules into energetically favorable locations. A consequence of these features is the formation of a nonuniform spatial distribution of solvent molecules about a solute molecule. Therefore, under the effect of intermolecular attraction, molecules in supercritical fluid will gather around solute molecules. This phenomenon, which has been termed as local density enhancement [81], clustering [82], or molecular charisma [83] gives rise to interesting solvation effects not ordinarily found in liquid mixtures. Solvent molecules agglomerate or condense around solute molecules mainly because of the high polarizability of solute molecules and the attraction between solute and solvent molecules is much greater than that of solvent-solvent molecules. For example, the partial molar volume of naphthalene in supercritical fluid carbon dioxide at infinite dilution is -7800 cm^3/mol at 308.5 K and 79.8 bar, which corresponds to the condensation of about 80 solvent molecules around a solute molecule [84-85].

1.4.5. Reactions in supercritical fluids

As an economic and feasible alternative to organic solvents, supercritical fluid is becoming more and more important in chemical synthesis. There are some unique characteristics associated with supercritical fluids which make them suitable for different industrial applications [86-87]. More recently, supercritical fluids have been used as benign solvents (includes Carbon dioxide and water are the fluids used most frequently in reactions at supercritical conditions) in various production stages in the biomedical, pharmaceutical and biofuel industries [88-92]. Supercritical fluids reaction provides a unique process opportunity, which can not only replace the traditional hazardous organic solvents, but also optimize and control the reaction environment by controlling fluid density, pressure and temperature, so as to control the reaction rate,

eliminate the transport limit of reaction rate, and separation of reactants and products. The diffusion coefficient of supercritical fluid is between that of gas and liquid, which lead to possible to increase the reaction rate that are diffusion limited in the liquid phase [93]. It was reported that the reaction rate was significantly affected by the pressure change and increased near the critical point. Under this condition, the local density and composition of the solution changed significantly, and sometimes the formation of solvent clusters controlled the reactivity and selectivity [94-95].

The disadvantages of supercritical fluid were that solubility of high or polar molecular weight substrates and reagents in the reaction was limited, and then some side reaction was occurred in supercritical fluids. In addition, it may have low solubility of ligands and/or transition metal complexes in catalytic applications. In this way, several researchers developed many methods to increase the solubility of catalytic species in supercritical fluid CO_2, for example, addition highly CO_2-philic parts on the ligands [96-97].

Furthermore, supercritical fluid is the effective way to suppresses the formation of coke during reaction. In our laboratory research work, T. Yoshikawa et al. reported that transalkylation of p-propylphenol over zeolites in supercritical benzene solvent that it was considered to be effective for suppressing coke formation [98]. G. Watanabe et al. also explored that 2-methylnaphthalene methylation over the MTW-type zeolites, which the amount of coke loaded could be decreased under high-pressure conditions [99-100]. In addition, the co-solvent effect is sometimes observed in supercritical fluid systems, which can change the reaction environment by chemical methods. In this environment, a specific interaction with a product can be used to change the product distribution or modify the transition state [101].

1.5. Research objective

Porous materials such as zeolites are used in various fields including petrochemical industry as catalysts, adsorbents, and separation membranes, because they have properties such as high surface area, molecular sieve ability and ion exchange ability. On the other hand, since most of the reaction active sites of zeolite are located on the inner surface of the pores, the reaction product diffuses from the bulk fluid into the pores of zeolite and adsorbs to the active sites before the reaction proceeds. Therefore, the apparent reaction rate is observed in the zeolite crystal, because the pore

size of zeolite is close to the molecular size of hydrocarbons, the diffusion rate in the zeolite catalyst has a large effect on the apparent reaction rate. Therefore, information on the intracrystalline diffusivity of diffusion molecules within zeolite is indispensable for the reaction engineering analysis and the catalyst design using the zeolite catalyst. Therefore, in this study, we measured the liquid-phase diffusion coefficients of these molecules in MFI-type zeolite and Y-type zeolite crystals for cyclic hydrocarbons containing heteroatoms in the molecular structure of the liquid-phase system.

Viewed against the consumption of fossil fuels, biomass is considered an environmentally friendly and renewable fuel source. Phenolic compounds are one of the valuable intermediate products that can be obtained from biomass, which further obtained a range of extraordinary chemicals. Moreover, solvents are also needed for most chemical reactions. Most researcher select hydrocarbon as the solvents due to it can avoid heat evaporation. In addition, it is very difficult to measurement of diffusion of phenolic compounds within zeolites in the gas phase because some phenolic compounds are solid at room temperature.

As mentioned above, the study of diffusion of hydrocarbon within zeolites has been reported mainly in the vapor phase. However, there are few reports of the diffusion coefficient of hydrocarbons within zeolites in the liquid phase and no report in the sub-and super-critical fluids. Especially, the reactions of aromatic hydrocarbons (phenolic compounds) containing heteroatoms in the molecular structure are reported in various reactions using zeolite catalysts, but there are few reports of diffusion mechanism for these aromatic hydrocarbons. The purpose of this study is to clarify the intracrystalline diffusion mechanism of aromatic hydrocarbons within zeolites to contribute to catalyst and catalytic reactor design in biomass refinery and desulfurization processes. Therefore, in this study, we measured the diffusivity of these aromatic hydrocarbons within beta-type, MFI-type and Y-type zeolites in liquid phase and sub-and super-critical fluids.

This dissertation consists of five chapter with a conclusion.

Chapter 1 Describes research background including the general characteristics of zeolites, intralystalline diffusion phenomenon within zeolite and the general characteristics of supercritical fluids, and finally introduces the purpose of this study and the structure of this paper.

Chapter 2 Measurement of the adsorption and intracrystalline diffusivities of phenolic compounds within MFI-type zeolites in the liquid phase using a constant volumetric method. Specifically, the effects of the substituent groups of the benzene ring in silicalite-1 and the Brønsted acid sites in H-MFI on the adsorption and diffusion

of phenolic compounds has been investigated.

Chapter 3 The direct and continuous measurement of the intracrystalline diffusivity of phenol and toluene within H-Y in mesitylene, cyclohexane and 2-propanol solutions and the effects of the solvents on the adsorption and diffusion mechanism of phenol and toluene within H-Y has been investigated.

Chapter 4 Developing a method for the direct and continuous measurement of intracrystalline diffusivity of 1-methylnaphathlene and toluene within Si-beta, silicalite-1 and K-ZSM-5 using a Raman spectrometer in the sub- and super-critical fluids and formation of clusters between diffusion substance and solvent molecules near the critical point of solvent at pore mouth of zeolites has been investigated. Moreover, the intracrystalline diffusivity of toluene within Silicalite-1 in the sub- and super-critical fluids was compared with that in the gas phase.

Chapter 5 Measurement of intracrystalline diffusivity of hydrocarbon within porous materials in sub- and super-critical fluids by a constant volumetric method using Raman spectroscopy. This study aimed to measuring the intracrystalline diffusivities of aromatic hydrocarbons within silicalite-1, K-ZSM-5 and K-Y in the in sub- and super-critical fluids. Moreover, the mechanism of aromatic hydrocarbons diffusion within silicalite-1, K-ZSM-5 and K-Y in super-critical fluids has been investigated.

Reference

[1] M. E. Davis. Nature 417 (2002) 813-821.
[2] H. van Bekkum, E. M. Flanigen, P. A. Jacobs, J. C. Jansen, Introduction to Zeolite Science and Practice, Elsevier, (2001).
[3] B. Bogdanov, D. Georgev, K. Angelva, K. Yaneva, Math. Nat. Sci, 4 (2009) 6-11.
[4] R. L. Wadlinger, G. T. Kerr, E. J. Rosinski, U.S. Patent 3 (1967) 69.
[5] E. B. G. Johnson, S. E. Arshad, Appl. Clay Sci., 97(2014) 215-221.
[6] S. Al-Khattaf, S. A. Ali, A. M. Aitai, N. Zikova, D. Kubicka, J. Cejka, Catal. Rev., 56 (2014) 333-402.
[7] J. D. Sherman, Proc. Nat. Acad. Sci. USA 96 (1999) 3471
[8] J. A. Rabo and M. W. Schoonover, Appl. Catal. A, 222 (2001) 261
[9] Y. Li, G. Zhu, Y. Wang, Y. Chai, C. Liu, Micropor. Mesopor. Mater. 312 (2021) 110790.
[10] M. E. Davis, Nature 417 (2002)813-821.
[11] M. O. Daramola, E. F. Aransiola, and T. V. Ojumu, Materials, 5 (2012) 2101-2136.

[12] C. S. Cundy, and P. A. Cox. Chem. Rev., 103 (2003) 663-702.
[13] S. Mitchell, A. B. Pinar and J. Kenvin, P. Crivelli, J. Karger and J. Perez-Ramirez, Nat. Commun., 6 (2015)1-14.
[14] T. Ennaert, J. V. Aelst, J. Dijkmans, R. D. Clercq, W. Schutyser, M. Dusselier, D. Verboekend and B. F. Sel, Chem. Soc. Rev., 45(2016)584-611.
[15] L. Chen, Y. Deng, W. Han, C. Wang, D. Han, C. Feng, Fuel, 310 (2022)122427.
[16] G. J. deA. A. Soler-Illia, C. Sanchez, B. Lebeau and J. Patarin, Chem. Rev., 102(2002)4093-4138.
[17] X. Wu and R.G. Anthony, J. Catal., 184 (1999) 294
[18] M. Berggrund, M. Skoglundh, A.E.C. Palmqvist, Top. Catal., 42-43 (2007) 153
[19] G. Centi, P. Generali, L. Dall'Olio, S. Perathoner, Z. Rak, Ind. Eng. Chem. Res., 39 (2000) 131
[20] T. Nobukawa, K. Sugawara, K. Okumura, K. Tomishige, K. Kunimori, App. Catal. B., 70 (2007) 342.
[21] S. Mi, T. Wei, J. Sun, P. Liu, X. Li, Q. Zheng, K. Gong, X. Liu, X. Gao, B. Wang, H. Zhao, H. Liu and B. Shen, J. Catal., 347 (2017) 116-126.
[22] J. García-Martínez, M. Johnson, J. Valla, K. Li and J. Y. Ying, Catal. Sci. Technol., 2 (2012) 987-994.
[23] J. M. Arandes, J. Erena, J. Bilbao, D. Lopez-Valerio and G. D. L. Puente, Arandes, José M., Ind. Eng. Chem. Res., 42 (2003) 3952-3961.
[24] D. Karami and N. Mahinpey. Chem. Eng. Commun., 203 (2016) 251-257.
[25] E. A. ghaei, R. Karimzadeh, H. R. Godini, A. Gurlo and O. Gorkr, Microporous and Mesoporous Mater., 294 (2020) 109854.
[26] J. M. Newsam, M. M. J. Treacy, W. T. Koetsier and C. B. D. Gruyter, Proceedings of the royal society of London. A. Math. Phys. Sci., 420 (1988) 375-405.
[27] N. Kumar, F. Klingstedt, L. E. Lindfors, Stud. Surf. Sci. Catal., 130(2000) 2981-2986.
[28] R. López-Fonseca, J. I. Gutierrez-Ortiz, M. A. Gutierrez-Ortiz, J. R. Gonzalez-Velasco, Catal. Today, 107 (2005) 200-207.
[29] J. Jiang, H. Pan, G. Sun, Q. Ye, Z. Shao and Y. Shi, Energy & Fuels 25 (2011) 4377-4383.
[30] Y. Shi, X. Wang, Y. Xia, C. Sun, C. Zhao, S. Liand, W. Li, Mol. Catal., 433 (2017) 265-273.
[31] K. S. W. Sing, D. H. Everett, R. A. W. Haul, L. Moscou, R. A. Pierotti, J. Rouquerol, T. Siemieniewska, Pure Appl. Chem., 57 (1985) 603-619.
[32] M. Sultan, T. Miyazaki, and S. Koyama. Renew. Energ., 121 (2018) 441-450.

[33] I. Langmuir, J. Am. Chem. Soc., 40 (1918) 1361.
[34] H. Moon, W.K. Lee, J. Colloid Interface Sci., 96 (1983) 162–170.
[35] B. Al-Duri, G. McKay, Chem. Eng. J., 38 (1988) 23.
[36] G. McKay, J. Soc. Dyers Color., 96 (1980) 576.
[37] M. J. Tempkin, V. Pyzhev, Acta. Physiochim. URSS 12 (1940) 217.
[38] T. Dogu, Industrial &Engineering chemistry research, 6 (1998) 2158-2171.
[39] D. M. Ruthven, M. F. M Post, Stud. Surf. Sci. Catal., 137 (2001) 525-577.
[40] L. Forni, Catal. Today, 52 (1999)147-152.
[41] A. Corma, Chem. Rev. 95 (1995) 559-614.
[42] K. Li, J. Valla, and J. Garcia-Martinez. ChemCatChem, 6 (2014) 46-66.
[43] P.B. Weisz, Chemtech, 3 (1973) 498–505.
[44] R. Krishna, Chem. Eng. Sci., 45 (1990) 1779-1791.
[45] F. Courivaud, E. W. Hansen, A. Karlsson, S. Kolboe and M. Stocker, Micropor. Mesopor. Mater., 35 (2000) 327-339.
[46] M. Bienfait, B. Asmussen, M. Johnson, P. Zeppenfeld, Surf. Sci., 460 (2000) 243-248.
[47] R. C. Runnebaum and E. J. Maginn. J. Phys. Chem. B., 101 (1997) 6394-6408.
[48] N. Noguchi, and T. Okuchi. Icarus, 335 (2020) 113401.
[49] A. G. Guy, Mater. Sci. Eng., 66 (1984)107-114.
[50] A. Liu, P. Liu, and S. Liu. Int. J. Heat Mass Transf., 162 (2020) 120336.
[51] M. Izadmehr, M. Abbasi, M. Mansouri, A. Kazemi, A. Nakhaee and A. Daryaafar, Fuel, 199 (2017) 551-561.
[52] Z. Rong, A. P. Terzyk, P. A. Gauden and P. Vadgama, J. Colloid Interface Sci., 313 (2007) 449-453.
[53] D. M. Ruthven and S. Brandani. J. Membr. Sci., 6(2001)87-212.
[54] M. Khalifi, N. Sabet, M. Zirrahi, H. Hassanzadeh, J. Abedi, AIChE Journal 66 (2020): e16966.
[55] D. M. Ruthven, Principles of adsorption and adsorption processes, John Wiley & Sons, 1984.
[56] D. B. Shah, C. J. Guo, D. T. Hayhurst, J. Chem. Soc., Faraday Trans., 91 (1995) 1143.
[57] L. J. Song, L. V. C. Rees, Micropor. Mesopor. Mater., 6 (1996) 363
[58] B. G. Anderson, F. J. M. M. de Gauw, N. J. Noordhoek, L. J. V. IJzendoorn, R. A. V. Santen and M. J. A. de Voigt, Ind. Eng. Chem. Res., 37 (1998) 815-824.
[59] K. Chihara, T. Terakado, T. Ninomiya, H. Mizuochi, Stud. Surf. Sci. Catal., 154(2004)1991-1998.

[60] L. Song, Z. Sun, L. Duan, J. Gui and G. S. McDougall, Micropor. Mesopor. Mater. 104 (2007) 115-128.
[61] M. A. Jama, M. P. F. Delmas, D. M. Ruthven, Zeolite, 18 (1997) 200.
[62] W. Zhu, J. M. V. de Graaf, L. J. P. V. de Broeke, F. Kapteijn and J. A. Moilijn, Ind. Eng. Chem. Res., 37(1998) 1934-1942.
[63] S.F. Garcia, P.B. Weisz, J. Catal., 142 (1993) 691.
[64] W. Ostwald, Z. Phys. Chem., 15 (1894) 705.
[65] P. Kortunov, S. Vasenkov, J. Kärger, R. Valiullin, P. Gottschalk, M. Fé Elía, M. Perez, M. Stöcker, B. Drescher, G. McElhiney, C. Berger, R. Gläser, and J. Weitkamp, J. Am. Chem. Soc., 127 (2005) 13055-13059.
[66] H. Jobic, and D. N. Theodorou, Micropor. mesopor. mater., 102(2007) 21-50.
[67] U. Schemmert, J. Kärger, and J. Weitkamp, Micropor. Mesopor. Mater., 32 (1999)101-110.
[68] D. Caputo, M. Eić, and C. Colella. Stud. Surf. Sci. Catal., 142(2002)1611-1618.
[69] H. Jobic, A. Methivier, G. Ehlers, B. Farago and W. Haeussler, Angew. Chem. Int. Ed., 43(2004) 364-366.
[70] T. Masuda, K. Fukada, Y. Fujikata, H. Ikeda and K. Hashimoto, Chem. Eng. Sci., 51(1996) 1879.
[71] T. Masuda, Catal. Surv. from Asia, 7(2003)133.
[72] T. Masuda, Y. Fujikata, H. Ikeda, K. Hashimoto, Micropor. Mesopor. Mater., 38 (2000) 323.
[73] T. Masuda, Y. Fujikata, T. Nishida, K. Hashimoto, Micropor. Mesopor. Mater., 23(1998) 157.
[74] T. Masuda, Y. Okubo, S.R. Mukai, M. Kawase, K. Hashimoto, A. Shichi, A. Satsuma, T. Hattori, Y. Kiyozumi, Chem. Eng. Sci., 56 (2001) 889.
[75] J. F. Brennecke, Chem. Ind., 21(1996) 831-4.
[76] C. A. Eckert, B. L. Knutson and P. G. Debenedetti, Nature, 383 (1996) 313-318.
[77] L. T. Taylor, Supercritical fluid extraction, Wiley-Interscience, 4(1996).
[78] A. K. Chaudhary, S. V. Kamat, E. J. Beckman, D. Nurok, R. M. Kleyle, P. Hajdu and A. J. Russell, J. Am. Chem. Soc., 118 (1996) 12891-12901.
[79] B. Subramaniam, and M. A. McHugh. Ind. Eng. Chem. Process. Des. Dev., 25 (1986) 1-12.
[80] G. N. Sapkale, S. M. Patil, U. S. Surwase and P. K. Bhatbhage, Int. J. Chem. Sci, 8(2010) 729-743.
[81] M. P. Ekart, K. L. Bennett, S. M. Ekart, G. S. Gurdial, C. L. Liotta and C. A. Eckert, AIChE J. 39(1993) 235-248.

[82] J. F. Brennecke, P. G. Debenedetti, C. A. Eckert and K. P. Johnston, AIChE J., 36 (1990) 1927-1928.
[83] C. A. Eckert and B. L. Knutson, Fluid Phase Equilib., 83(1993) 93-100.
[84] C. A. Eckert, D. H. Ziger, K. P. Johnston and S. Kim, J. Phys. Chem. 90(1986) 2738–2746
[85] G. Pablo and Debenedetti, Chem. Eng. Sci., 42(1987)2203-2212.
[86] R. Edward, Q. Sun, Z. Zhang, C. Zhang, W. Gou, J Environ Sci, 21(2009)720-726.
[87] J. M. Bernal, P. Lozano, E. Garcia-Verdugo, M. I. Burguete, G. SanchezGomez, G. Lopez, M. Pucheault, M. Vaultier and S. V. Luis, Molecules, 17(2012) 8696–8719.
[88] W. C. Tsai and Y. Wang, Prog. Polym. Sci., 98(2019) 101161.
[89] K. Byrappa, S. Ohara, and T. Adschiri. Adv. Drug Deliv. Rev., 60(2008) 299-327.
[90] L. Baldino, M. Scognamiglio, and E. Reverchon. J. Supercrit. Fluids, 165(2020)104960.
[91] W. Sakdasri, S. Ngamprasertsith, S. Daengsanun and R. Sawangkeaw, Energy Convers. Manag., 182 (2019) 215-223.
[92] D. Wen, H. Jiang and K. Zhang. Prog. Nat. Sci., 19 (2009) 273-284.
[93] P. E. Savage, S. Gopalan, T. I. Mizan, C. J. Martino, E. E. Brock, AIChE J., 41 (1995) 1723–1778.
[94] A. Baiker, Supercritical fluids in heterogeneous catalysis, Chem. Rev. 99(1999) 453–473.
[95] Y. Ikushima, Adv. Colloid Interface Sci., 71(1997) 259–280
[96] J. M. DeSimone and W. Tumas, Green chemistry using liquid and supercritical carbon dioxide, Oxford University Press, 2003.
[97] E. L. VGoetheer, A. W. Verkerk, L. J. P. V. D. Brokrk, E. de Wolf, B-J Deelman, G. V. Kten and J. T. F. Keurentjes, J. Catal., 219 (2003) 126-133.
[98] T. Yoshikawa, T. Umezawa, Y. Nakasaka and T. Masuda, Catal. Today, 347 (2020) 110-114.
[99] G. Watanabe, Y. Nakasaka, T. Taniguchi, T. Yoshikawa, T. Tago and T. Masuda, Chem. Eng. J., 312 (2017) 288-295.
[100] G. Watanabe, Y. Nakasaka and T. Masuda, J. Japan Pet. Inst., 60 (2017)146-153.
[101] J. M. Dobbs, J. M. Wong, R. J. Lahiere and K. P. Johnston, Ind. Eng. Chem. Res.,26 (1987) 56-65.

Chapter 2
Diffusion of phenolic compounds within high-silica MFI-type zeolite in the mesitylene solution

2.1. Introduction

The MFI-type zeolites have attracted considerable attention in many industrially important processes because of their tunable solid acidity, flexible frameworks, high specific surface area, and high adsorption capacity that arise from their typically crystalline aluminosilicate with a three-dimensional structure that forms regularly sized pores in the zeolite framework [1]. Therefore, MFI-type zeolites are widely used as catalysts in the field of petroleum refining, biomass conversion, environmental catalysis, and fine chemical production [2-7]. In an industrial reaction, the diameter of some lighter hydrocarbons approached the pore diameter of the MFI-type zeolites; the diffusion process of the lighter hydrocarbon molecules was strongly controlled by the pore size and the active sites of the zeolites. Moreover, understanding the diffusion of hydrocarbons in MFI-type zeolites is critical because sometimes their apparent reaction rates are limited by the diffusion rates of the reactant and product inside the zeolite [8-13]. Hence, the diffusion coefficient inside the pores and the diffusion mechanism within zeolites, which strongly influence the activity and selectivity of the reaction, can offer some new and useful information for the design of zeolite catalysts in reaction engineering [14]. The literature includes numerous studies related to the intracrystalline diffusivities of hydrocarbons within MFI-type zeolites in the gas phase [15-19]. We have also investigated the intracrystalline diffusivity of paraffins, olefins, and aromatics within zeolites in the gas phase [12,20-24].

In recent years, biomass, which contains abundant carbon renewable feedstocks, has been considered a promising renewable energy resource for conversion into various fuels and chemicals [25]. Phenol, as the most representative phenolic compound, is an important chemical intermediate obtained from biomass and is used in the manufacture of various chemical products, including pharmaceuticals, petrochemicals, paints and dyes [26-28]. Recently, researchers have investigated the effect of porous materials on the hydrogenation [29], oxidation [30], alkylation [31], and carboxylation [32] of phenol for conversion into useful products. In addition, the valorization of raw and fossilized lignocelluloses that contain aromatic structures for

phenolic compounds over zeolite catalysts has been an important industrial and scientific endeavor for several decades. Sels et al. [33] reported the first detailed thermodynamics and kinetics studies of the vapor-phase conversion of ethylphenol over aluminosilicate catalysts in the absence of hydrogen and noble metals, as a method to produce phenol, they found that H-MFI showed strong benefits for achieving the quantitative formation of phenol. Shantz et al. [34] investigated a benzene conversion of 25.5% with a phenol selectivity of 90% on iron-containing hierarchical MFI materials. Wang et al. [35] has been reported that V-containing beta zeolite for the low-temperature liquid-phase methylation of phenol with methanol and found that the V-containing beta provided a high yield, and exhibited good reusability and preferential chemoselectivity toward the C-alkylation products (o- and p-cresols). We have also reported the conversion of alkyl phenols into phenols within MFI-type zeolites under high temperature and high pressure in the liquid phase [36]. Moreover, many researchers have also shown that adsorption properties of zeolites for organic compounds removal, especially for phenolic compounds [37-40]. Therefore, understanding the diffusion mechanism of phenolic compounds within MFI-type zeolites in the liquid phase is important in the design of zeolites for a chemical reaction engineering approach. However, the direct and continuous measurement of intracrystalline diffusivity of phenolic compounds within zeolites in the liquid phase has rarely been investigated.

The current work focuses on measuring the adsorption and intracrystalline diffusivities of phenolic compounds within MFI-type zeolites in the liquid phase using a constant volumetric method [41-42]. Specifically, the effects of the substituent groups of the benzene ring in silicalite-1 and the Brønsted acid sites in H-MFI on the adsorption and diffusion of phenolic compounds are investigated.

2.2. Experimental

2.2.1. Preparation of Silicalite-1 and H-MFI

Conventional silicalite-1 and H-MFI zeolites with an Si/Al ratio of 303 were prepared via a hydrothermal method. Solutions of tetraethyl orthosilicate (TEOS), $Al(OCH(CH_3)_2)_3$, and tetrapropylammonium hydroxide (TPAOH) were used as a Si source, Al source, and an organic structure directing agent (OSDA), respectively, for preparation of silicalite-1 and H-MFI. An aqueous solution containing the Si source, Al source (for H-MFI), and OSDA were prepared and mixed for 24h. A Teflon-lined

stainless-steel hydrothermal synthesis autoclave reactor with the synthesis gel of silicalite-1 or H-MFI zeolite was placed in an oven and heated at 448 or 423 K for 48 or 72 h, respectively. After hydrothermal synthesis, the autoclave was quenched in ice water. The obtained zeolites suspensions were washed with deionized water by centrifugation and then dried in air. The obtained zeolites were calcined in a muffle furnace at 823 K for 24 h to remove the templates completely.

Silicalite-1 and H-MFI were ion-exchanged with NH_4NO_3 aqueous solution at 348 K for 3 h, resulting in NH_4-H-MFI. The H-type samples were subsequently washed with deionized water by centrifugation and calcined at 823 K for 24 h.

2.2.2. Characterization of MFI-type zeolites

The powder X-ray diffraction (XRD) patterns of the zeolites were performed using Cu Kα X-rays; samples were scanned in the 2θ range from 5° to 50° on an Ultima IV, Rigaku Co. Ltd., The scanning electron microscope (SEM) images were obtained with a JSM-6500F, a JEOL. N_2 adsorption-desorption experiments were conducted to determine the Brunauer-Emmett-Teller (BET) surface area and pore volume of the zeolites; the adsorption-desorption experiments were carried out at 77 K, using Microtrac BEL Corp., Belsorp-mini. All of the samples were degassed under vacuum at 673 K for 24 h before being analyzed. NH_3-temperature programmed desorption (NH_3-TPD) was carried out on a BEL CAT with a mass spectrometer. The Si/Al ratios were determined by dissolving the samples in potassium hydroxide and analyzing the resultant solutions by inductively coupled plasma atomic emission spectroscopy (ICP-AES) using an ICPE-9000 (Shimadzu). Thermogravimetric Analysis (TGA) of high-silica MFI zeolites was performed on a DTG-60A, Shimadzu, in the temperature range 293–1073 K with a heating rate of 10 K/min under a N_2 gas atmosphere.

2.2.3. Measurement of intracrystalline diffusivity in the liquid phase

The intracrystalline diffusivity of phenolic compounds within MFI-type zeolites in the liquid phase was investigated using a constant volumetric method. Mesitylene was used as a solvent because mesitylene molecules cannot enter the pores of MFI-type zeolites. The intracrystalline diffusivity in the liquid phase was calculated using the experimental apparatus in Fig.2.1, which is the same apparatus described in our previous work. First, the zeolite sample was placed in a Pt basket that was

subsequently positioned in the middle of the top of the stainless-steel autoclave with mesitylene solution. The autoclave was heated to the experimental temperature (313-353 K), and the solution was magnetically stirred. After the solution reached the desired temperature, 1 mL of phenolic compound (or toluene for comparison) was injected by syringe into the autoclave. Finally, in situ measurement of the change in phenol concentration in the mesitylene solution with time was conducted to measure the intracrystalline diffusivity in the liquid phase.

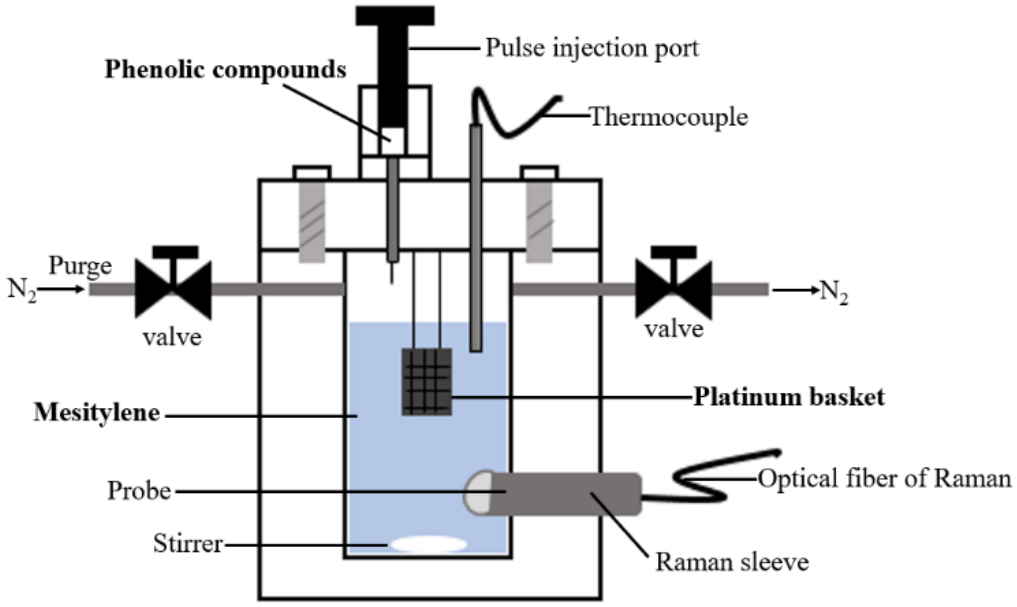

Fig.2.1 Experimental apparatus for measuring the intracrystalline diffusivity in the liquid phase

Raman spectroscopy was conducted [41-42] to measure the concentration change of the phenolic compound as a result of the adsorption of some of the compound onto the zeolite crystals. The obtained intracrystalline diffusivity was correlated using the following theoretical equation for an MFI-type zeolite with a hexagonal slab shape (silicalite-1 and H-MFI)

$$\frac{M_t}{M_e} = \frac{C_0 - C_t}{C_0 - C_e} = 1 - \sum_{n=1}^{\infty} \frac{2\alpha(1+\alpha)}{1+\alpha+\alpha^2 q_n^2} \exp\left(-\frac{D_{ad} q_n^2 t}{L^2}\right) \quad (2\text{-}1)$$

$\alpha = V/(a_m WHL)$ and q_n are the non-zero positive root of $\tan q_n = -\alpha q_n$

where, M_t is the amount of phenolic compound adsorbed at time t; M_e is the M_t value at equilibrium; C_t is the phenolic compound in mesitylene at time t; C_0 and C_e are the initial and equilibrium C_t values, respectively; D_{ad} is the intracrystalline diffusivity of the phenolic compound or toluene; L is the half-thickness of the hexagonal slab-shaped zeolite crystals; a_m is the outer surface area of the zeolite crystals, V is the volume of the liquid phase; W is the weight of the zeolites; and H is the partition factor.

Effective diffusivity is an important parameter for studying kinetic analysis of the actual reaction rate using reaction model by using Thiele model; and can be evaluated by the multiplying partition H factor by the intracrystalline diffusivity, where the value of H is calculated from adsorption isotherms, which shown as follows [41].

$$H = q/C \quad (2\text{-}2)$$

$$D_{eff} = D \times H \quad (2\text{-}3)$$

where, q is the amount of adsorbed diffusion substances at equilibrium in mesitylene, and C is the concentration of diffusion substances in mesitylene at equilibrium.

2.3. Results and Discussion

2.3.1 Characterization of the MFI-type zeolites

Fig.2.2 shows XRD patterns of the prepared silicalite-1 and H-MFI powders. All of the diffraction peaks in the patterns of silicalite-1 and H-MFI correspond to typical characteristic diffraction peaks of MFI-type zeolites. Fig.2.3 shows SEM images of the synthetic silicalite-1 and H-MFI powders. The silicalite-1 and H-MFI zeolites exhibited plate-type structures with a thickness of 0.54 and 0.59 μm, respectively.

Fig.2.4 shows TGA profile of H-MFI and silicalite-1 was measured and confirmed that weigh loss was not observed above 500 degree C indicating these zeolites are stable.

Fig.2.5 shows the NH_3-TPD profiles of H-MFI zeolites. In the profile of H-MFI, two NH_3 desorption peaks are observed at approximately 483 K and 663 K, which correspond to the desorption of physically adsorbed NH_3 and the desorption of NH_3 from strong acid sites, respectively. These results indicate that the H-MFI zeolite exhibited strong acidity, with NH_3 both physically adsorbed and adsorbed onto strong acid sites. A total acid site amount of 0.073 mmol/g (Table 1) and an Si/Al ratio of 291 was calculated on the basis of the amount of NH_3 desorbed from the strong acid sites. N_2 adsorption isotherms of silicalite-1 and H-MFI were recorded at 77K, and the BET specific surface area (S_{BET}), external surface area (S_{EXT}), and the micropore volume (V_m) of the silicalite-1 and H-MFI were estimated (Table 1). The Si/Al ratio of 303 obtained by ICP-AES analyse is also shown in Table2.1; this value is similar to the Si/Al ratio measured by NH_3-TPD (Si/Al=291).

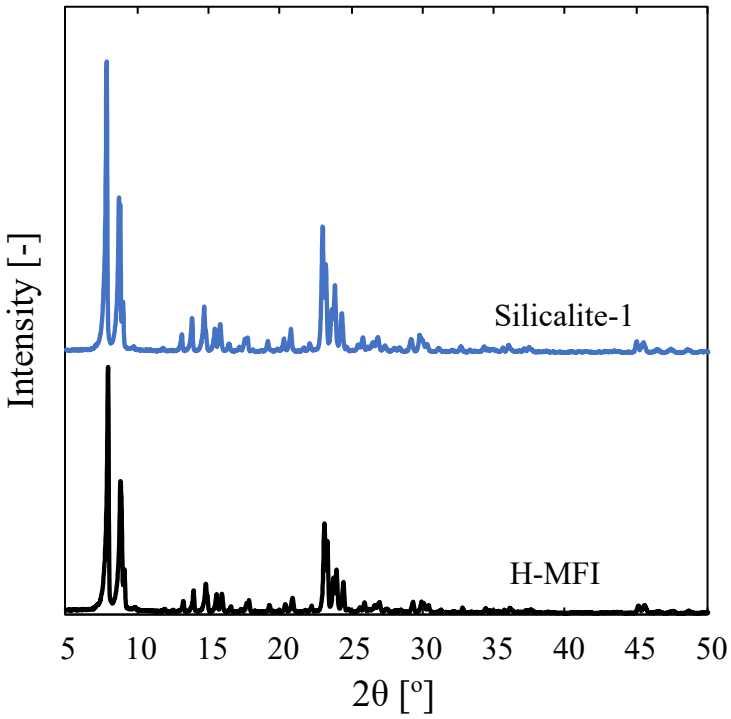

Fig.2.2 XRD patterns of silicalite-1 and H-MFI

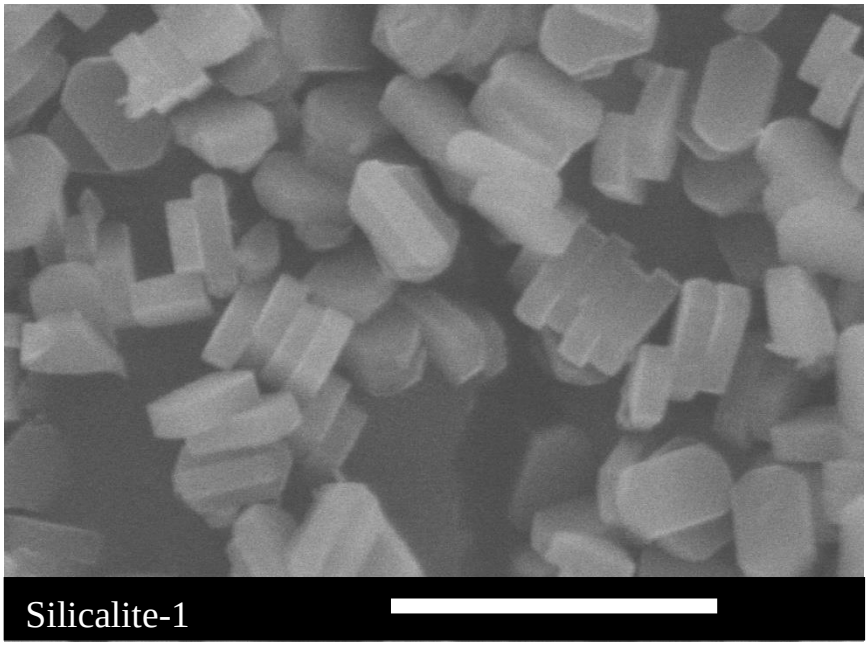

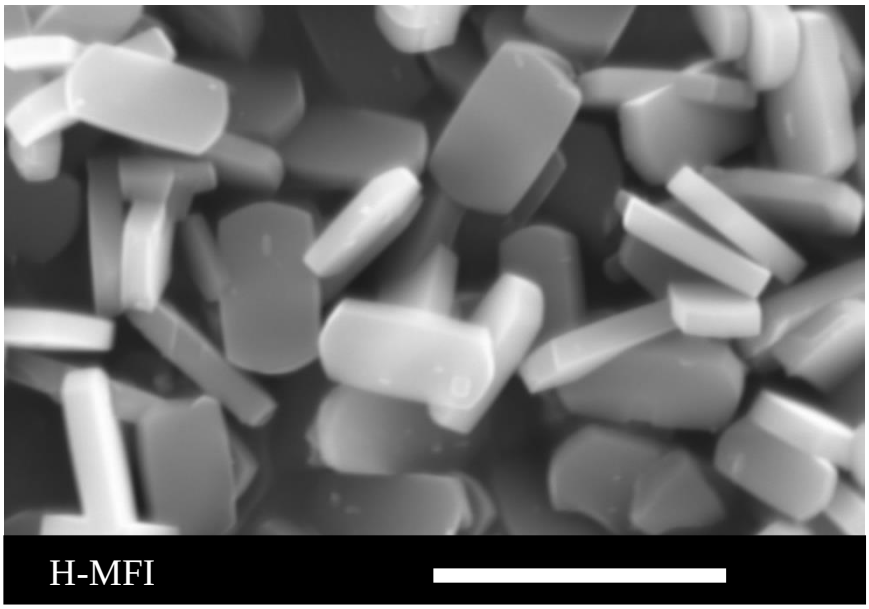

Fig.2.3 SEM images of silicalite-1 and H-MFI

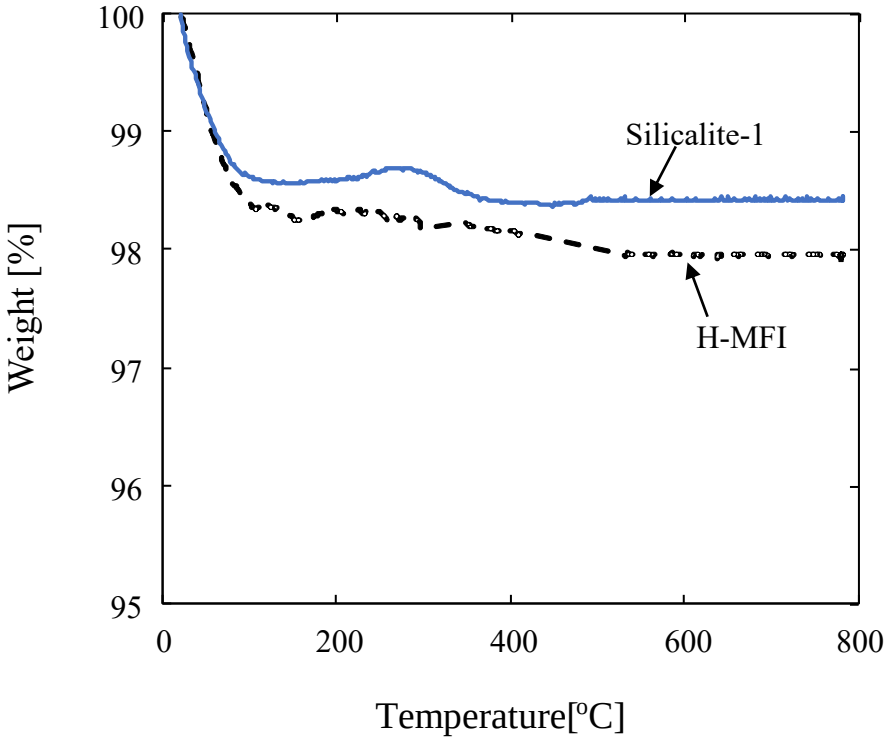

Fig. 2.4 TGA of silicalite-1 and H-MFI

Table 2.1 Properties of MFI-type zeolites

Zeolites	S_{BET} [$m^2\ g^{-1}$]	S_{EXT} [$m^2\ g^{-1}$]	V_m [$cm^3\ g^{-1}$]	Number of acid sites [$mol\ kg^{-1}$]	Si/Al ratio [-]
H-MFI	355	7.56	0.17	0.073	303
Silicalite-1	346	9.76	0.17	—	—

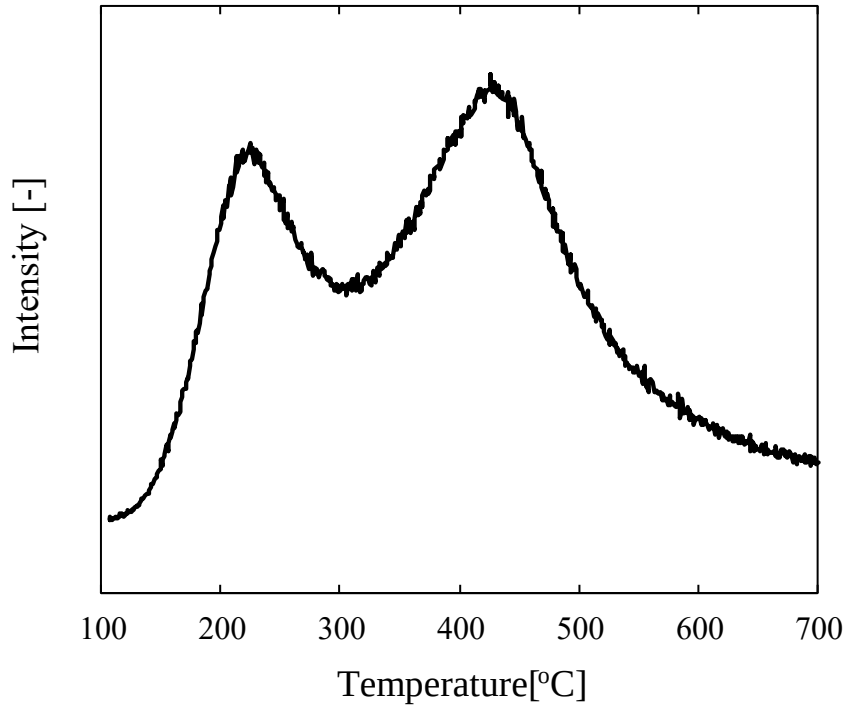

Fig.2.5 NH_3-TPD profile of H-MFI

2.3.2. Adsorption of phenolic compounds within silicalite-1 and H-MFI

2.3.2.1 Adsorption isotherms of phenolic compounds within silicalite-1

Fig.2.6 shows the adsorption isotherms of phenol within silicalite-1 at 313, 323 and 353 K. The adsorption isotherms exhibit a linear correlation, indicating that the adsorption isotherms of phenol within silicalite-1 can be expressed with a Henry-type equation (Eq.(4))

$$q=KC_e \qquad (2\text{-}4)$$

Where q is amount of adsorbed diffusion substance, K is the equilibrium constant, and Ce is the equilibrium concentration of the diffusion substance in the liquid phase.

Adsorption isotherms of phenol within H-MFI can be expressed with a Freundlich-type equation (Eq.(2-5)) in the investigated concentration range.

$$q=K_F C_e^{1/n} \quad (2\text{-}5)$$

where K_F is Freundlich equilibrium constant and the value n was determined to be 1.5.

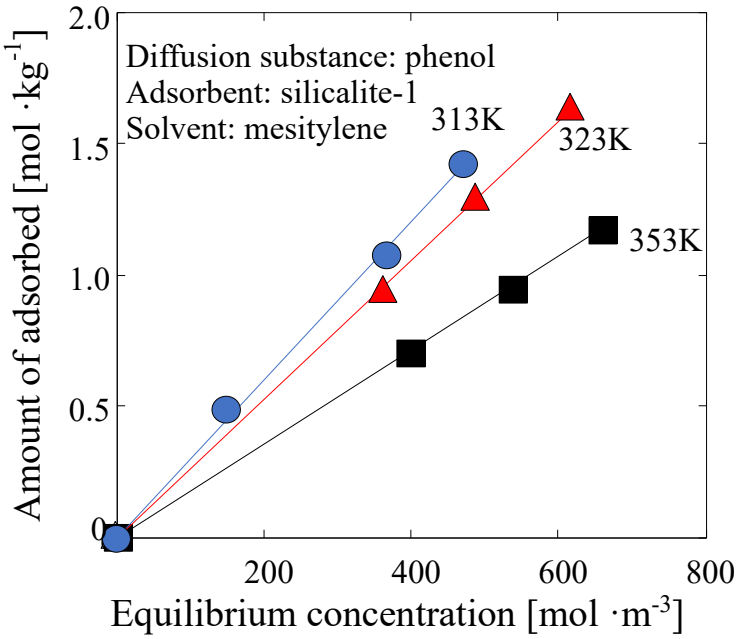

Fig.2.6 Adsorption isotherms of phenol on silicalite-1

In addition, adsorption isotherms of toluene, *p*-propylphenol and *m*-cresol within silicalite-1 at each temperature were confirmed to be expressed by Eq (2-4). The equilibrium constants corresponding to these experimental results are summarized in Table 2.2. Although the equilibrium constants for phenol and *p*-propylphenol are approximately the same as that for toluene, the equilibrium constant for *m*-cresol is smaller than that for toluene. The adsorption enthalpies (ΔH) of these diffusion substances were calculated from the equilibrium constants; the results are shown in Fig. 2.7. The adsorption enthalpies of phenol, *p*-propylphenol and toluene were approximately the same (−11.7 kJ/mol). By contrast, the adsorption enthalpy of *m*-cresol was −8.7 kJ/mol. These negative ΔH values indicate that the adsorption is an exothermic process, which limits the mobility of the adsorbed phenol compared with that of the bulk phase [43]. In particular, the absolute value of the adsorption enthalpy of phenol is slightly greater than that of *m*-cresol, indicating that phenol within silicalite-1 exhibits high stability. These results are attributed to *m*-cresol exhibiting a larger kinetic diameter compared with other diffusion substances.

Table 2.2 Adsorption equilibrium constant of phenol, *p*-propylphenol, *m*-cresol and toluene on silicalite-1

Adsorption equilibrium constant	Temperature [K]		
[m^3kg^{-1}]	313	343	353
phenol	3.0×10^{-3}	2.6×10^{-3}	1.8×10^{-3}
p-propylphenol	3.0×10^{-3}	2.5×10^{-3}	1.8×10^{-3}
toluene	2.8×10^{-3}	2.5×10^{-3}	1.7×10^{-3}
m-cresol	2.1×10^{-3}	1.7×10^{-3}	1.4×10^{-3}

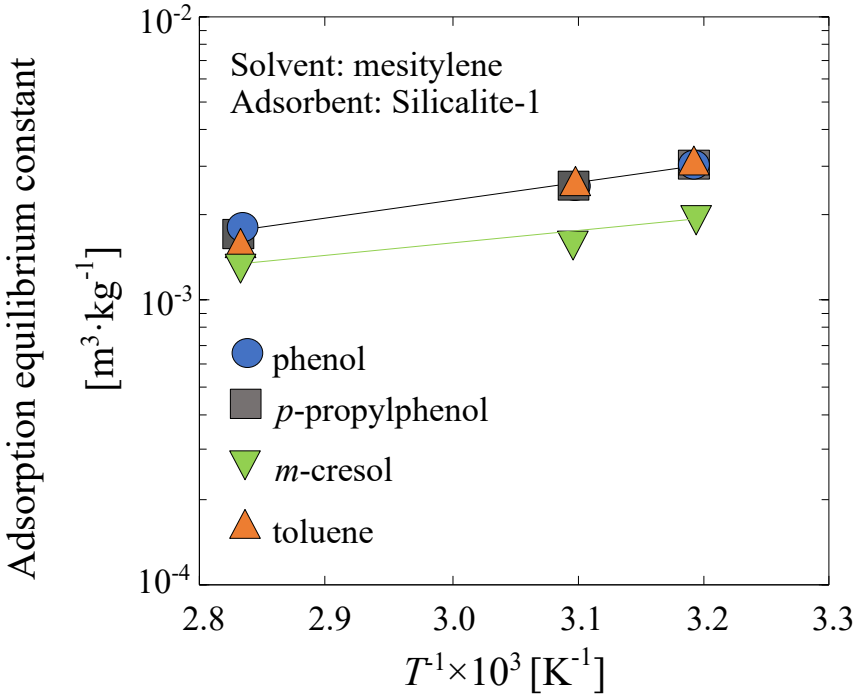

Fig.2.7 Adsorption equilibrium constant of phenol, *p*-propylphenol, *m*-cresol and toluene within silicalite-1in mesitylene solution

2.3.2.2 Adsorption isotherms of phenolic compounds within H-MFI

Because most zeolites have acidic sites on their surface, we investigated the adsorption of phenol within H-MFI in mesitylene solution. Fig.2.8 shows the adsorption isotherms of toluene and phenol within H-MFI at 313 and 353 K. The H-MFI exhibits strongly acidic sites with greater phenol adsorption ability compared with silicalite-1. In addition, the amount of phenol adsorbed onto H-MFI was much greater that of toluene at each temperature. Hydrogen bonding between the OH group in phenol and the Brønsted acid sites within H-MFI is considered to enhance the adsorption of phenol. Javadian and Ektefa [44] calculated the benzene and phenol adsorption conditions in H-MFI using density function theory (DFT) and reported that the interaction between phenol and zeolite is stronger than that between benzene and zeolite. Our experimental results are consistent with their calculation analysis.

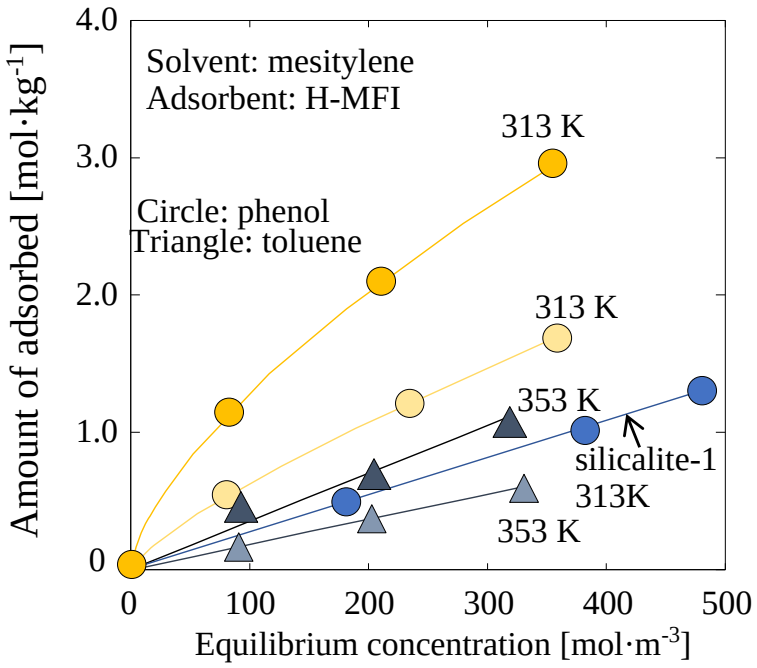

Fig.2.8 Adsorption isotherms of phenol and toluene on H-MFI

2.3.3 Intracrystalline diffusivities of phenolic compounds within silicalite-1 and H-MFI

The typical temperature dependency of intracrystalline diffusivity in silicalite-1 obtained for phenol, *p*-propyphenol, *m*-cresol, and toluene in the liquid phase is shown in Fig.2.9. Under the investigated experimental conditions, the intracrystalline diffusivities of phenol and *p*-propylphenol in silicalite-1 are approximately the same as that of toluene, irrespective of the functional group. By contrast, *m*-cresol exhibits lower intracrystalline diffusivity than toluene. The activation energies of these intracrystalline diffusivities were calculated using the Arrhenius equation. The activation energies calculated from the intracrystalline diffusivity of phenol, *p*-propylphenol and toluene in silicalite-1 were 17 kJ/mol, and this value is smaller than that of m-cresol (23 kJ/mol). Fujikata et al have reported that intracrystalline diffusivities of toluene within silicalite-1 at temperatures ranging from 423 to 723 K in the gas phase are similar to that of *p*-xylene and 10−25 times greater than that of *m*-xylene. In addition, the activation energies for intracrystalline diffusivity of toluene and *m*-xylene within silicalite-1 are 17 kJ/mol and 23 kJ/mol, respectively [23]. Because the pore size of MFI-type zeolite is similar to the molecular diameter of benzene rings, aromatic molecule diffuses widening the MFI-type zeolite pore. Thus, a geometrical limitation determined by the relationship between the pore size and the diameter of diffusion molecules affect the intracrystalline diffusivity. For silicalite-1, although aromatics with different functional groups (phenol, *p*-propylphenol, *m*-cresol, and toluene) were used as diffusion molecules, only the geometrical limitation determined the intracrystalline diffusivity.

Fig.2.10 shows a typical Arrhenius plot for the intracrystalline diffusivities of phenol and toluene within H-MFI in the liquid phase. Two types of mass transfer resistance of diffusion molecules occur inside MFI-type zeolites. One is the geometrical limitation (as previously mentioned), the other is related to the interaction between the diffusion molecule and an acid site. The diffusion molecule adsorbs onto the remains on the acid site. The adsorbed molecule inhibits the diffusion of other molecules because the molecular diameter of hydrocarbons is similar to the pore size of MFI-type zeolites. As shown in Fig.2.10, the intracrystalline diffusivity of phenol and toluene within H-MFI are lower than that within silicalite-1. The presence of acid sites slowed the diffusion of phenol and toluene in the H-MFI pores.

Although phenol exhibited almost the same intracrystalline diffusivity as toluene within silicalite-1, the intracrystalline diffusivity of phenol within H-MFI was

lower than that of toluene. In addition, the calculated activation energy for phenol diffusivity within H-MFI is 31.4 kJ/mol and this value is greater than that of toluene (24.4 kJ/mol). These results indicate that the mass transfer resistance of phenol within H-MFI is high compared with that of toluene. Because the hydrogen bonding interaction between phenol and H-MFI differ from that between toluene and H-MFI, we speculated that the residence time of phenol on acid sites became longer than that of toluene, which led to the observed difference in intracrystalline diffusivity within H-MFI.

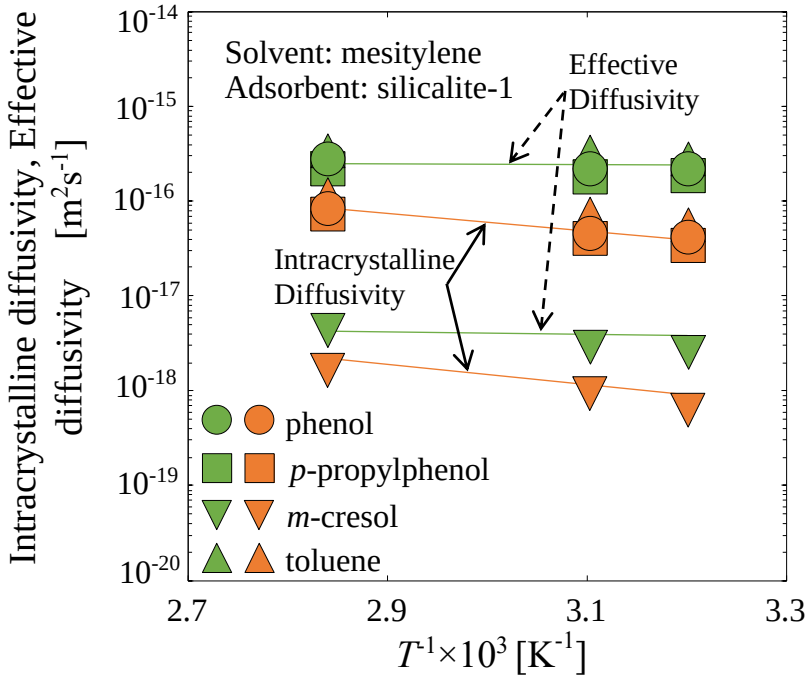

Fig.2.9 Arrhenius plots of the intracrystalline diffusivity and effective diffusivity of phenol, *p*-propylphenol, *m*-cresol, and toluene within silicalite-1

As previously mentioned, effective diffusivities of molecules are useful in catalyst design in a reaction engineering approach, such as the relation between the Thiele modulus and the effectiveness factor. Although effective diffusivities do not have any physical meaning, the values obtained for phenolic compounds in present study are shown in Fig.2.9 and Fig.2.11. In silicalite-1, phenol, *p*-propylphenol and toluene exhibit approximately the same effective diffusivity, whereas *m*-cresol exhibits a lower effective diffusivity than toluene. The effective diffusivity of phenol and toluene within H-MFI are much lower than within siliclite-1.

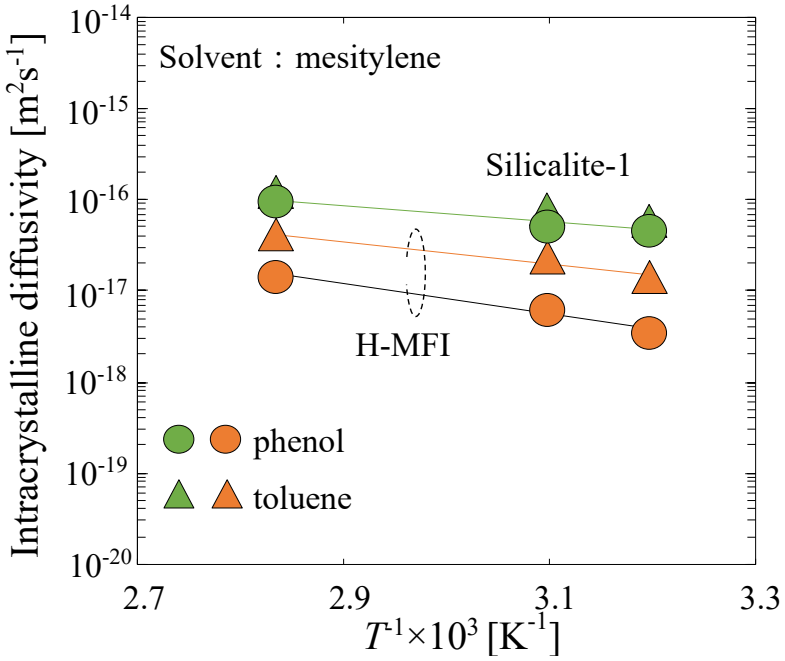

Fig.2.10 Arrhenius plots of the intracrystalline diffusivity of phenol and toluene within silicalite-1 and H-MFI

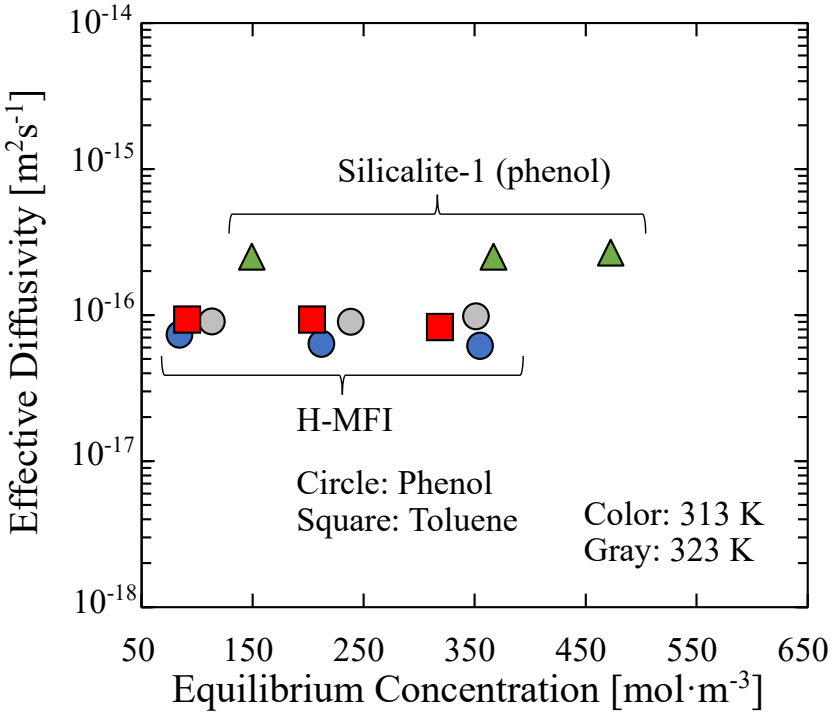

Fig.2.11 Effective diffusivities of phenol and toluene within silicalite-1 and H-MFI

2.4. Conclusions

This study investigated the intracrystalline diffusivity of phenol, p-propylphenol, m-cresol, and toluene within silicalite-1 and H-MFI in the liquid phase. The results are summarized as follows.

(1) The amounts of phenol, p-propylphenol and toluene adsorbed within silicalite-1 are approximately the same, whereas the amounts of adsorbed m-cresol is small, which is attributed to the larger kinetic diameter of m-cresol. In addition, compared with toluene, phenol exhibits a greater adsorption amount in H-MFI, because of strong interaction between hydrogen bonds in phenol molecules and Brønsted acid sites within H-MFI.

(2) The investigation of the intracrystalline diffusivity of phenol, p-propylphenol, and toluene within silicalite-1 indicates that they exhibit approximately the same diffusivity, which is ascribed to geometrical limitations alone determining the intracrystalline diffusivity. However, the m-cresol exhibited a lower intracrystalline diffusivity and effective diffusivity, and a higher activation energy (21.8 kJ/mol) than the other phenolic compounds (~17 kJ/mol). This result is attributed to the larger molecular size of m-cresol strongly limiting its diffusion inside the micropores of silicalite-1. In H-MFI zeolite, the acid sites affect phenol diffusion, leading to a low intracrystalline diffusivity and a high activation energy compared with silicalite-1, indicating a difference in the hydrogen bonding interaction between phenol and H-MFI than between toluene and H-MFI, it is considered that the residence time of phenol on the acid sites was longer than that of toluene, which led to the difference in intracrystalline diffusivity within H-MFI.

References

[1] Y. Li, G. Zhu, Y. Wang, Y. Chai, C. Liu, Microporous Mesoporous Mater. (2020).
[2] C. Martínez, A. Corma, Coord. Chem. Reviews. 255 (2011) 1558-1580.
[3] P.Peng, D. Stosic, X.M. Liu, Z.F. Yan, S. Mintova, Chem. Eng. J. 385 (2020) 123800.
[4] N.K. Razdan, A. Kumar, B.L. Foley, A. Bhan, J. Catal. 381 (2020) 261-270.
[5] A. Saraeian, M.W. Nolte, B.H. Shanks, Renew. Sust. Energ. Rev. 104 (2019) 262-280.
[6] M.W. Schreiber, R. Bermejo-Deval, J.A. Lercher, J. Am. Chem. Soc. 140 (2018) 4849-4859.

[7] D.W. Gardner, J. Huo, T.C. Hoff, J-P. Tessonnier, ACS Catal. 5 (2015) 4418-4422.
[8] Y. Nakasaka, T. Kanda, K.I. Shimizu, K. Kon, G. Shibata, T. Masuda, Catal. Today. 332 (2019) 64-68.
[9] H. Konno, T. Okamura, T. Kawahara, Y. Nakasaka, T. Tago, T. Masuda, Chem. Eng. J. 207 (2012) 490-496.
[10] G.D. Cremer, Catal. Today. 157 (2010) 236-242.
[11] T. Masuda, J. Japan Pet. Inst. 46 (2003) 281-294.
[12] T. Masuda, Chem. Eng. sci. 56 (2001) 889-896.
[13] A.M. Ávila, C.M. Bidabehere, U. Sedran, Chem. Eng. J. 132 (2007) 67-75.
[14] P. Losch, A.B. Pinar, M.G. Willinger, K. Soukup, S. Chavan, B. Vincent, B. Louis, J. Catal. 345 (2017) 11-23.
[15] S.S. Arzumanov, D.I. Kolokolov, A.G. Stepanov, J. Phys. Chem. C. 119 (2015) 18481-18486.
[16] A. Poursaeidesfahani, M.F. deLange, T.J.H. Vlugt, F. Khodadadian, J. Catal. 353 (2017) 54-62.
[17] W.L. Duncan, K.P. Möller, Ind. Eng. Chem. Res. 39 (2000) 2105-2113.
[18] O.P. Keipert, M. Baerns, Chem. Eng. sci. 53 (1998) 3623-3634.
[19] X. Yue, X. Yang, Langmuir. 22 (2006) 3138-3147.
[20] T. Masuda, Catal. Surv. from Asia. 7 (2003) 133-144.
[21] T. Masuda, Y. Fujikata, H. Ikeda, K. Hashimoto, Microporous Mesoporous Mater. 38 (2000) 323-332.
[22] T. Masuda, Y. Fujikata, T. Nishida, K. Hashimoto, Microporous Mesoporous Mater. 23 (1998) 157-167.
[23] Y. Fujikata, T. Masuda, H. Ikeda, K. Hashimoto, Microporous Mesoporous Mater. 21 (1998) 679-686.
[24] T. Masuda, K. Fukada, Y. Fujikata, H. Ikeda, K. Hashimoto, Chem. Eng. sci. 51 (1996) 1879-1888.
[25] R.C. Brown, Thermochemical Processing of Biomass: Conversion into Fuels, Chemicals and Power (2011) 1-12.
[26] N. Deng, M. Li, L. Zhao, C. Lu, S.L. de Rooy, I.M. Warner, J. hazard. mater. 192 (2011) 1350-1357.
[27] Z. Li, M. Wu, Z. Jiao, B. Bao, S. Lu, J. hazard. mater. 114 (2004)111-114.
[28] V.K. Gupta, A. Nayak, S. Agarwal, I. Tyagi, J. colloid interface sci. 417 (2014) 420-430.
[29] N.C. Nelson, J.S. Manzano, A.D. Sadow, S.H. Overbury, I.I. Slowing, ACS Catal. 5 (2015) 2051-2061.

[30] A. Santos, P. Yustos, T. Cordero, S. Gomis, S. Rodriguez, F. Garcia-Ochoa, Catal. Today. 102 (2005) 213-218.
[31] S. Eckstein, P.H. Hintermeier, M.V. Olarte, Y. Liu, E. Baráth, J.A. Lercher, J. Catal. 352 (2017) 329-336.
[32] J. Luo, S. Preciado, P. Xie, I. Larrosa, Chem. Europ. J. 22 (2016) 6798-6802.
[33] Y. Liao, D. Verboekend, B.F. Sels, Appl. Catal. B. 234 (2018) 117-129.
[34] M. Shahami, K.M. Dooley, D.F. Shantz, J. Catal. 368 (2018) 354-364.
[35] J. Xie, W. Chuang, N. Yan, Y. Du, S. Xi, W. Zhang, J. Tang, Y. Zhou, J. Wang, Chem. Eng. J. 328 (2017) 1031-1042.
[36] T. Yoshikawa, T. Umezawa, Y. Nakasaka, T. Masuda, Catal. Today. 347 (2020) 110-114.
[37] R. I. Yousef, B. El-Eswed, A. H. Al-Muhtaseb, Chem. Eng. J. 171 (2011) 1143-1149,
[38] B. Koubaissy, J. Toufaily, M. El-Murr, T. J. Daou, H. Hafez, G. Joly, P. Magnoux, T. Hamieh, Cent. Eur. J. Eng. 2 (2012) 435-444.
[39] M. Ahmaruzzaman, Adv. Colloid Interface Sci.143 (2008) 48-67.
[40] W. P. Cheng, W. Gao, X. Cui, J. H. Ma, R. F. Li. J. Taiwan Inst. Chem. Eng. 62 (2016): 192-198. 62 (20168) 192-198.
[41] Y. Nakasaka, T. Tago, K. Odate, T. Masuda, Microporous Mesoporous Mater. 112 (2008) 162-169.
[42] Y. Nakasaka, T. Tago, K. Yano, T. Masuda, Chem. Eng. sci. 65 (2010) 226-231.
[43] F.Q. Liu, M.F. Xia, S.L. Yao, A.M. Li, H.S. Wu, J.L. Chen, J. hazard. mater. 152 (2008) 715-720.
[44] S. Javadian and F. Ektefa, RSC adv. 122 (2015)100799-100808.

Chapter 3
Effect of solvents coexistence on the intracrystalline diffusivity of toluene and phenol within Y-type zeolite in the liquid phase

3.1. Introduction

Zeolites, especially Y-type zeolites, are attractive catalytic materials because of their important properties of high surface area, large pore structure, strong Brønsted acidity and high thermal stability; structurally, they consist of three-dimensional channels of 12-membered rings with an average pore size of 0.74 nm [1-2]. The superior performance afforded by Y-type zeolites have been exploited extensively in the fluid catalytic cracking of heavy aromatics and in hydrocracking reactions, as well as applications in the petroleum refining industry [3]. Adsorption and diffusion of lighter hydrocarbon molecules within zeolites are strongly dependent on the pore structure and surface acidity of the zeolites, especially with regard to the molecular size of hydrocarbons, which is comparable to the micropore size in the zeolites [4-5]. The utilization of active sites in zeolites may often be hindered by the limited intracrystalline diffusion in their micropores. Enhancing the diffusion rates of the reactants and products within zeolites is critical because the utilization of active sites in zeolites is often hindered by limited intracrystalline diffusion in the micropores [6-9]. Therefore, obtaining new insights regarding the catalytic reaction engineering performance of zeolite catalysts can provide a theoretical basis for designing highly effective zeolite catalysts, which are essential for gaining a thorough understanding of the diffusion mechanism within the zeolite pores and the controlling factors that strongly affect the catalytic activity, selectivity, and lifetime [5, 10-11]. In recent years, experimental studies on the intracrystalline diffusivities of hydrocarbons within MFI-type zeolites in the gas and liquid phase have revealed new information [12–20]. However, in the case of the intracrystalline diffusivities of hydrocarbons within Y-type zeolites in the liquid phase, only a few studies have been reported in the literature.

The selection of solvents and their optimization are also important parts of the design process for new chemical products. Wanmolee et al. studied the depolymerization of organosolv lignin to phenolic monomers with H-USY (Si/Al = 5) in various organic solvents—ethyl acetate, methyl isobutyl ketone (MIBK), methanol, and acetone. Among the solvents, supercritical MIBK was the most efficient with

respect to the conversion process and phenolic monomers were obtained at 350ºC with addition of 2 MPa H_2 [21]. Liu et al. noted that the choice of solvent and alkylation significantly changed the reaction pathway of zeolite catalyzed phenol alkylation in the liquid phase. More carbenium ions are produced by either alcohols or olefins on non-hydrated zeolite Brønsted acid sites (BAS) than hydronium ions on BAS in pores filled with water, resulting in a higher alkylation rate in polar solvents (cyclohexanol and cyclohexene) than in water [22]. Therefore, understanding the effect of solvents on the diffusion of intermediate products such as phenol within zeolites can provide valuable predictor information for chemical reactions in industry.

Viewed against the consumption of fossil fuels, biomass is considered an environmentally friendly and renewable fuel source and contains a range of extraordinary chemicals [23-27]. Phenol is one of the valuable intermediate products that can be obtained from biomass and its chemical reactions have gained traction in recent decades [28-29]. In particular, phenol plays a crucial role in the industrial production of petrochemicals, synthetic resins, and agrochemicals [30-32]. Moreover, zeolites are among the most effective catalysts for adsorption and conversion of phenolic compounds. Khalil et al. reported the satisfactory performance of HY zeolite in removing phenol from a synthetic biofuel by gas phase DFT and DFPT calculations, FT-IR adsorption, and liquid phase adsorption [33]. Verboekend et al. investigated the synergistic effect of unmodified metal-free ZSM-5 zeolite catalysts and showed that water exhibited an extraordinary dealkylation performance for selective conversion of alkylphenols to phenol and olefins [34].

Based on the above, it is therefore of great interest and timely to study in detail the effects of solvents on the diffusion behavior of phenolic molecules on the surface of zeolite catalysts. In this study, the direct and continuous measurement of the intracrystalline diffusivity of phenol and toluene within Y-type zeolite in mesitylene, cyclohexane and 2-propanol solutions and the effects of the solvents on the adsorption and diffusion of phenol and toluene within the zeolites has been investigated.

3.2. Experimental

3.2.1. Preparation of H-Y zeolite and dealuminated H-Y

Y-type zeolite (Na-Y) was purchased from Wako Chemical Ltd., Miyazaki, Japan. The zeolite was subsequently converted to H-type zeolite by centrifugation and

calcination of NH_4^+-type zeolites at 823 K for 24h to remove NH_3. The product was labeled H-Y. The dealuminated-Y was prepared by using H-Y in a tubular quartz reactor within an electric furnace and in a flow of N_2. The steam flow replaced the N2 before continuing to heat to the final reaction temperature at 973 K. After 1 h at the reaction temperature the reactor, the N_2 flow replaced the steam before the reactor was allowed to cool to room temperature. And then the sample was refluxed for 12 h with 150 ml of Ethylenediaminetetraacetic acid (EDTA). The obtained zeolites suspensions were washed with deionized water by centrifugation and then dried in air. The obtained zeolites were calcined in a muffle furnace at 823 K for 12 h [35]. The product was labeled deAl-Y.

3.2.2. Characterization of Y-type zeolite

The micrograph image of H-Y was obtained by scanning electron microscopy (SEM) using a JEOL JSM-6500F system. The pore size distribution in H-Y zeolite were obtained by recording the N_2 adsorption-desorption profiles at 77 K (Belsorp-mini, Microtrac BEL Corp.). The specific surface area and pore volume were calculated by the Brunauer-Emmett-Teller (BET) and t-plot methods, respectively. The H-Y was pretreated by degassing at 673 K for 24 h under vacuum. Amount of acid sites in H-Y and deAl-Y was carried out by NH_3-temperature programmed desorption (NH_3-TPD) on a BEL CAT Ⅱ (MicrotracBEL Corp.) with a Q-mass spectrometer (Bel-mass, MicrotracBEL Corp.). X-ray fluorescence (XRF, JSX-3100R II, JEOL) was employed to characterize the Si/Al molar ratio of H-Y.

3.2.3. Measurement of intracrystalline diffusivity in the liquid phase

The intracrystalline diffusivity of phenol within H-Y or deAl-Y in the liquid phase was investigated using a constant volumetric method. Mesitylene, cyclohexane and 2-propanol served as the solvents. The intracrystalline diffusivity in the liquid phase was calculated using the experimental apparatus shown in Fig.3.1, which is the same as described previously [18]. First, the H-Y or deAl-Y was placed in a Pt basket and immersed in mesitylene, cyclohexane and 2-propanol, and then transferred to a vacuum drier for 3 h. Next, the Pt basket was positioned in the middle of the top of a stainless-steel autoclave with one of the solutions. The autoclave was heated to the experimental temperature (313-353 K), and the solution was magnetically stirred. After the solution reached the experimental temperature, phenol (or toluene for comparison

purposes) was injected by syringe into the autoclave. Finally, *in situ* measurements of the change in phenol concentration with time were undertaken to measure the intracrystalline diffusivity in the respective solvents.

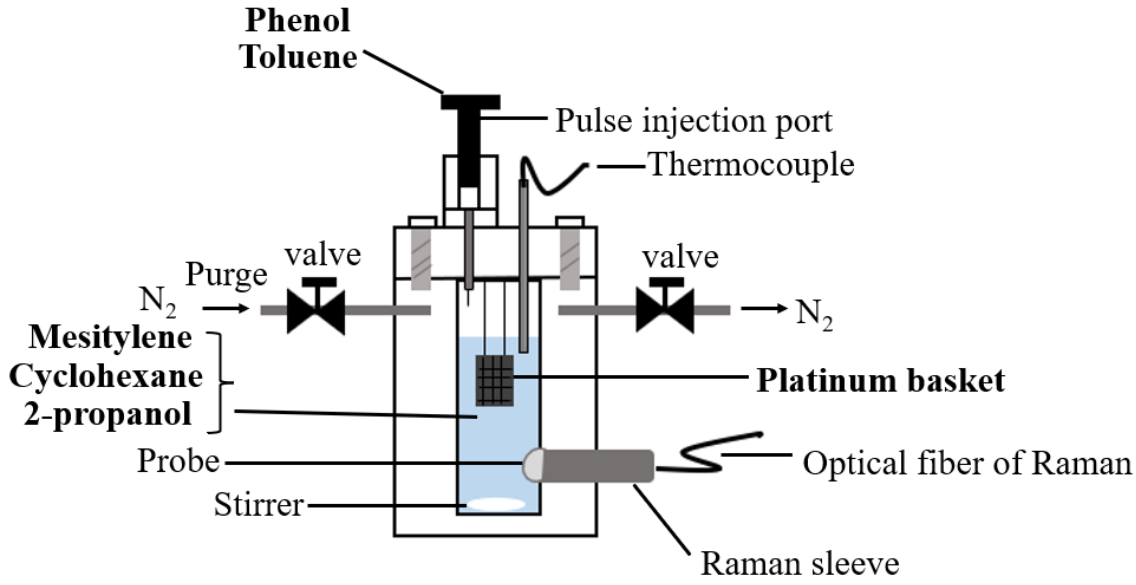

Fig.3.1 Experimental apparatus for measuring the intracrystalline diffusivity of phenol and toluene in mesitylene, cyclohexane and 2-propanol solutions.

Raman spectroscopy was performed [18–19] to measure the change in concentration of phenol as a result of the adsorption of some of the compound onto the zeolite crystals. The intracrystalline diffusivity was estimated using the following equation derived for a spherical shape crystal (Y-type zeolite) [16, 36].

$$\frac{M_t}{M_e} = \frac{C_o - C_t}{C_o - C_e} = 1 - \sum_{n=1}^{\infty} \frac{6\alpha(1+\alpha)}{9 + 9\alpha + \alpha^2 q_n^2} \exp\left(-\frac{D q_n^2 t}{R_0^2}\right) \qquad (3\text{-}1)$$

where $\alpha = V/(a_m WHR)$, and q_n is the non-zero positive root of $\tan q_n = -\alpha(3q_n/3+\alpha q_n^2)$.

M_t is the amount of phenol and toluene adsorbed at time t; M_e is the M_t value at equilibrium, C_t is the phenol and toluene in solvent at time t, C_0 and C_e are the initial and equilibrium C_t values, respectively, D is the intracrystalline diffusivity of the diffusion substance, R_0 is the radius of the spherical-shaped zeolite crystals, a_m is the outer surface area of the zeolite crystals, V is the volume of the liquid phase, W is the weight of the zeolite, and H is the partition factor.

The effective diffusivity is an important parameter for studying the kinetics of the actual reaction rate using a reaction scheme based on the Thiele model, and this can be evaluated by multiplying the partition factor H by the intracrystalline diffusivity, and where the value of H is calculated from the adsorption isotherms, which are as follows [18].

$$H=\rho K \tag{3-2}$$

$$D_{eff}=D\times H \tag{3-3}$$

where K is the equilibrium constant, ρ is the apparent density of the Y-type zeolite crystals.

3.3. Results and Discussion

3.3.1. Characterization of the H-Y zeolite

SEM image of the H-Y zeolite is presented in Fig.3.2. The image reveal that H-Y particles have a spherical shape with a mean crystal size (thickness) of 3.98 μm. The N_2 adsorption-desorption isotherm of H-Y exhibited type I behavior, which is consistent with the presence of micropores. Moreover, deAl-Y exhibited type IV behavior, which is consistent with the presence of micropores and mesopores. (not shown here) The specific surface area (S_{BET}) of 770 and 621 $m^2\ g^{-1}$, the external surface area (S_{EXT}) of 12.54 and 38.6 $m^2\ g^{-1}$ and the pore volume (V_m) of 0.31 and 0.29 $cm^3\ g^{-1}$ for H-Y and deAl-Y are summarized in Table 3.1, respectively. Fig. 3.3 shows the NH_3-TPD profiles of H-Y and deAl-Y zeolite. The peak of H-Y is much higher than that of deAl-Y, which indicated that low Bronsted acid sites in the pore of deAl-Y zeolite. In addition, XRF analysis revealed a Si/Al ratio of 2.8 for H-Y.

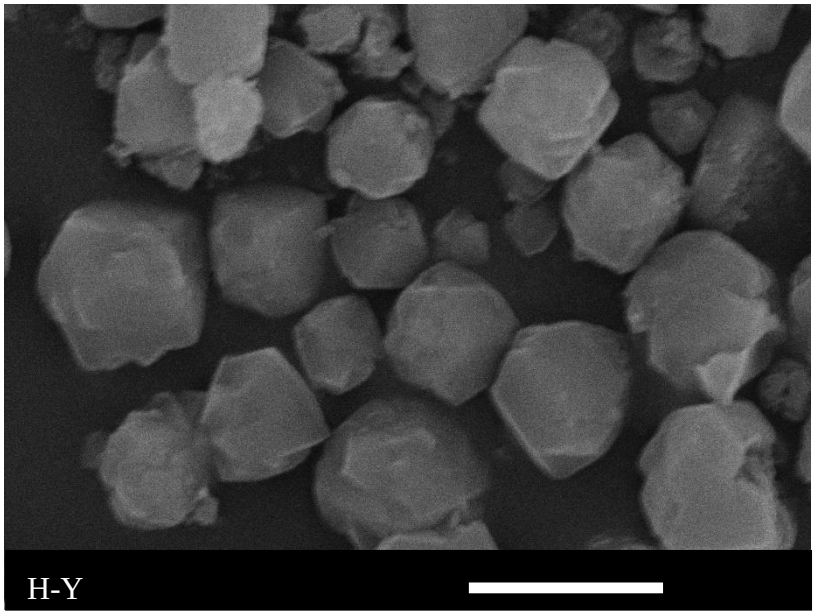

Fig.3.2 SEM image of H-Y.

Table 3.1 Properties of H-Y-type zeolites

Zeolites	S_{BET} [$m^2\ g^{-1}$]	S_{EXT} [$m^2\ g^{-1}$]	V_m* [$cm^3\ g^{-1}$]	Si/Al ratio* [-]
H-Y	770	12.54	0.31	2.8
deAl-Y	621	38.6	0.29	—

* Pore volume (V_m) was calculated by the BJH method, and the Si/Al ratio obtained by XRF analysis.

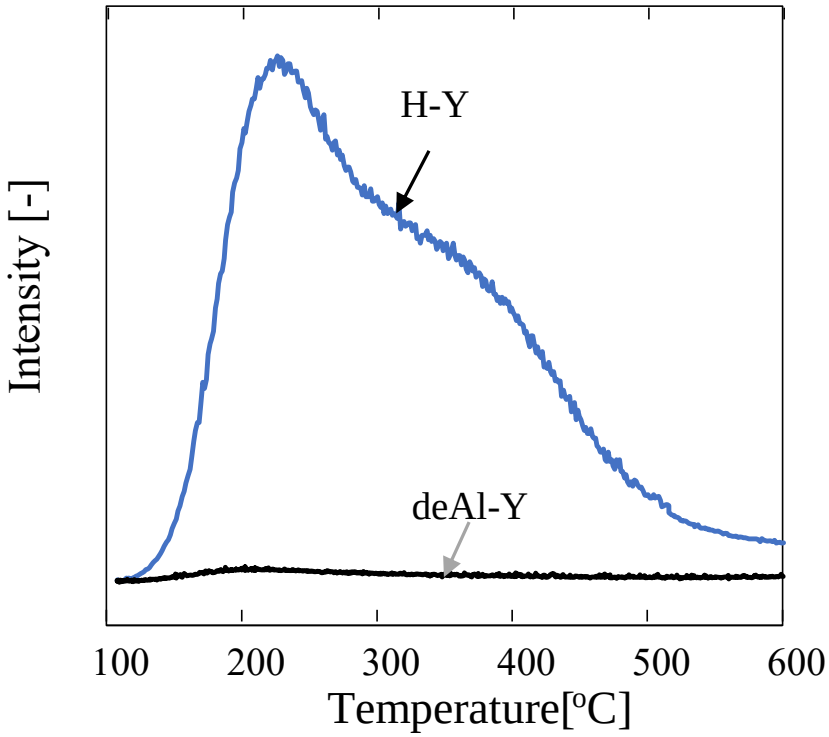

Fig.3.3 NH_3-TPD profile of H-Y and deAl-Y zeolites.

3.3.2. Adsorption of 2-propanol, mesitylene and cyclohexane on H-Y in the vaper phase

Adsorption isotherms for 2-propanol, mesitylene and cyclohexane on H-Y in the vapor phase at 298 K are presented in Fig.3.4. 2-propanol shows a much larger amount of adsorption on H-Y compared with mesitylene and cyclohexane. Moreover, the amount of mesitylene adsorbed is the lowest on H-Y in the low-pressure range. This indicates that the adsorption ability on the pore surface of H-Y is greater for 2-propanol compared to that for cyclohexane or mesitylene. Therefore, it is considered that the 2-propanol molecules find it easier to undergo adsorption onto the pore surfaces of H-Y compared to mesitylene and cyclohexane due to their stronger adsorption affinity.

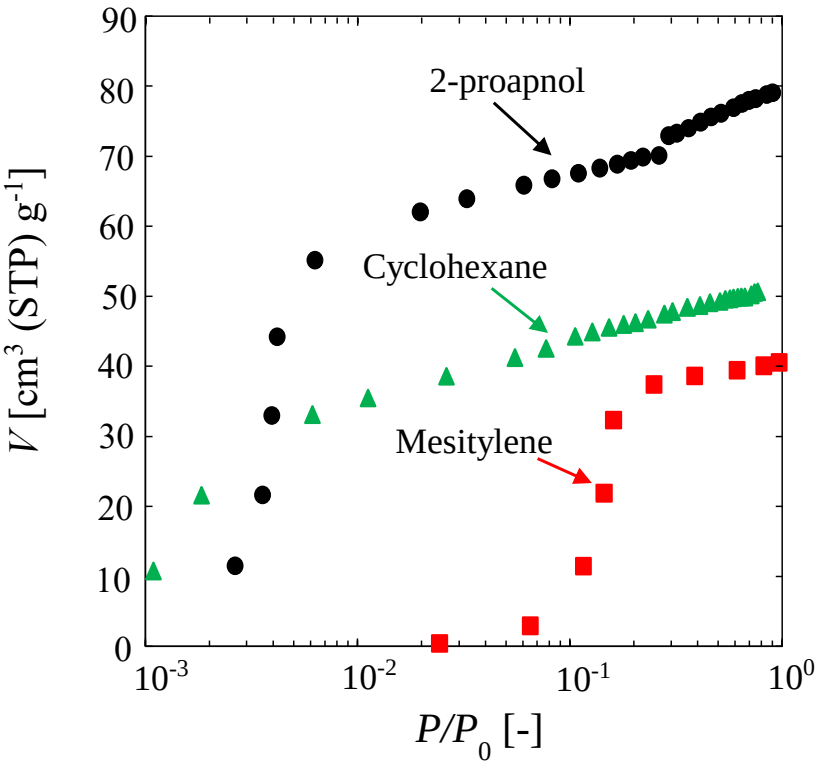

Fig. 3.4 Vaper adsorption isotherm of mesitylene (P_0 = 0.41), cyclohexane (P_0 = 10.77) and 2-propanol (P_0 = 11.55) on H-Y at 298 K.

3.3.3 Adsorption of phenol and toluene within H-Y

Adsorption isotherms for phenol and toluene within H-Y at 313, 323 and 353 K in mesitylene are presented in Fig.3.5. The adsorption isotherms for phenol and toluene on H-Y exhibit a Henry-type equation with a linear correlation:

$$Q=KC_e \quad (3\text{-}4)$$

where Q is amount of adsorbed diffusion substance, K is the equilibrium constant.

The adsorption enthalpies for phenol and toluene on H-Y from the following Van't Hoff equation:

$$K=\exp(-\Delta H/RT) \quad (3\text{-}5)$$

Where ΔH is adsorption enthalpy, R is the universal gas constant (8.314 $JK^{-1}mol^{-1}$), T is the absolute temperature (kelvin)

Phenol exhibits stronger adsorption within H-Y compared to toluene at each temperature. The adsorption enthalpies (ΔH) for phenol and toluene in mesitylene solution were calculated from the respective equilibrium constants. During the adsorption of phenol or toluene, replacement of mesitylene, which was adsorbed on the micropore surface of Y-type zeolite, with a molecule of phenol or toluene (via diffusion) occurred. The phenol molecules have a stronger interaction with the Brønsted acid sites on the H-Y pore surfaces by hydrogen bonding compared to the interactions between the aromatic rings and the acid sites [19, 33, 37]. Thus, the replacement of mesitylene with phenol more readily occurred relative to that for toluene.

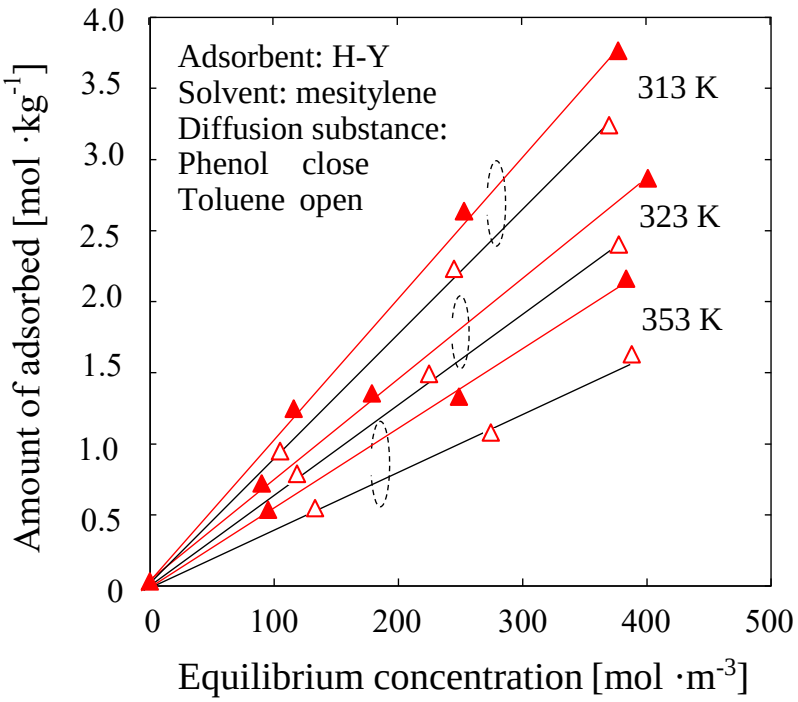

Fig.3.5 Adsorption isotherms for phenol and toluene on H-Y.

To investigate the effect of solvent type on the adsorption and diffusivity of phenol, 2-propanol, cyclohexane and mesitylene were used as solvents. The adsorption isotherms for phenol on H-Y in these solvents are presented in Fig.3.6. The adsorption isotherms for phenol on H-Y at specific temperatures in mesitylene, cyclohexane and 2-propanol can also be expressed by Eq. (3-4) for the concentration range examined.

The amount of adsorbed phenol within H-Y was the smallest in 2-propanol. As shown in Fig.3.4, the amount of 2-propanol adsorbed on H-Y in the gas phase was higher than that for cyclohexane or mesitylene, indicating that 2-propanol was strongly adsorbed on the pore surface of H-Y. Thus, it is considered that the affinity between the solvent and zeolite pore surface would affect the amount of phenol being adsorbed. The adsorption enthalpies (ΔH) for phenol in the three solvents were calculated from the equilibrium constants. The adsorption enthalpies for phenol in 2-propanol, cyclohexane and mesitylene were -33.1, -21.7 and -20.7 kJ/mol, respectively. Clearly, ΔH for phenol in 2-propanol is much larger than that for cyclohexane and mesitylene due to a stronger adsorption on the Brønsted acid sites of H-Y, which make it difficult for phenol to undergo adsorption.

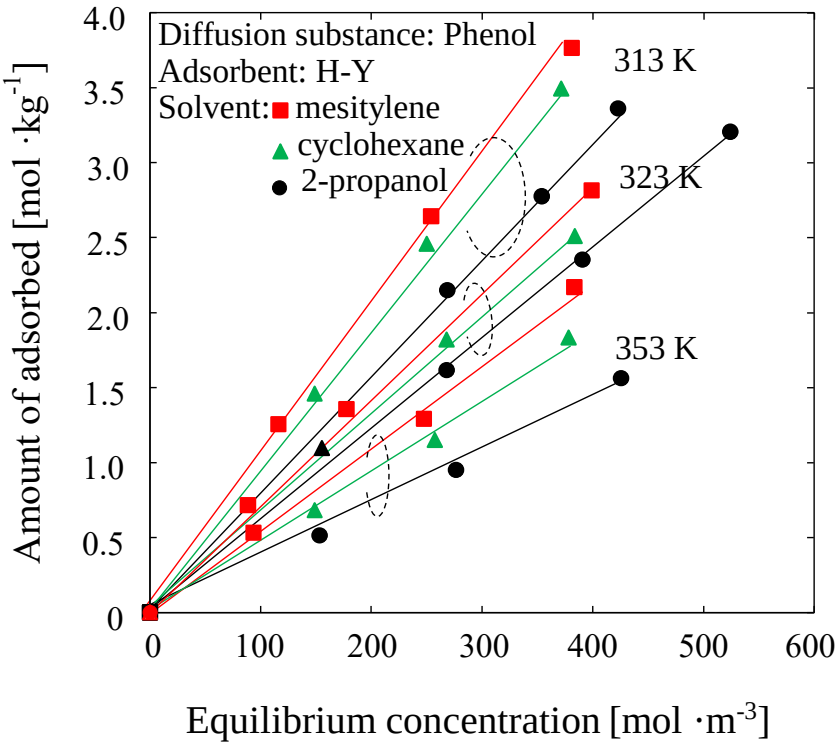

Fig.3.6 Adsorption isotherms for phenol on H-Y in mesitylene, cyclohexane and 2-popanol solutions.

3.3.4 Adsorption of phenol within deAl-Y

In order to prove the hydroxy group in phenol was adsorbed strongly on the Brønsted acid sites of H-Y, we investigated the adsorption of phenol within H-Y and deAl-Y in 2-propanl and mesitylene solution. The adsorption isotherms of phenol within H-Y and deAl-Y in the 2-propanol or mesitylene solution at 313 and 353 K are shown in Fig.3.7. The deAl-Y exhibits lower phenol adsorption ability compared with H-Y in 2-propanol or mesitylene. The result indicated that hydrogen bonding between the OH group in phenol and the Brønsted acid sites within H-Y is considered to enhance the adsorption of phenol.

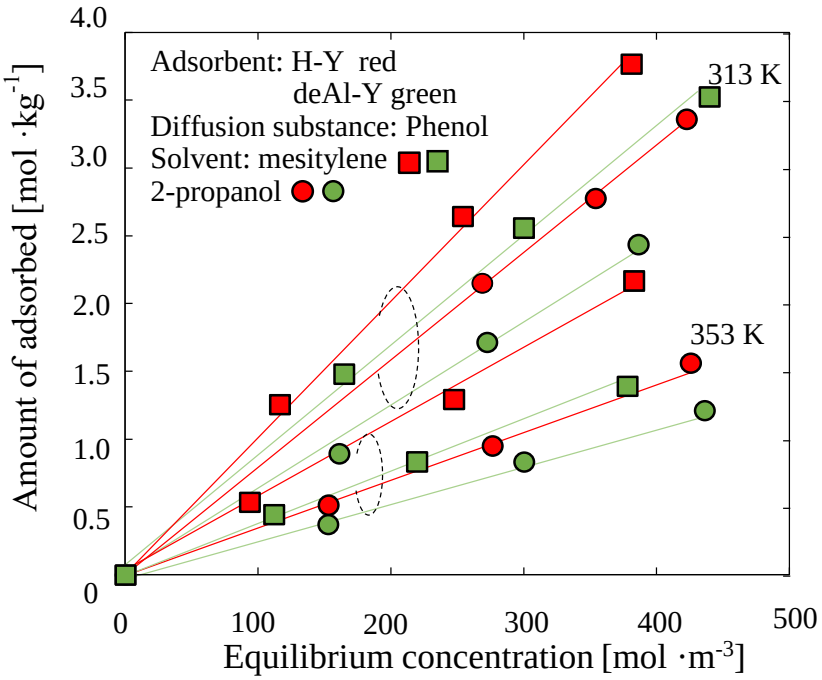

Fig.3.7 Adsorption isotherms for phenol on H-Y and deAl-Y in mesitylene or 2-propanol.

3.3.5 Intracrystalline diffusivities of phenol and toluene within Y-type zeolite in mesitylene, cyclohexane and 2-propanol.

The effects of temperature on the intracrystalline diffusivities of phenol and toluene within H-Y in mesitylene solution are illustrated in Fig.3.8. The activation energy for the intracrystalline diffusivity of toluene within H-Y in mesitylene was 17.2

kJ/mol, and this value is larger than the reported value (8.1 kJ/mol) for the gas phase [36]. When a molecule diffuses within a zeolite pore, the molecule undergoes repeated adsorption and desorption processes within the pore structure. There are geometrical limitations to this process as determined by the relationship between the pore structure and the geometry of diffusion molecules; moreover, the acid sites of the zeolite affect the diffusivity of the diffusion molecule [13]. H-Y has a super-cage-like structure, whose size is much larger than the diameter of the aromatic ring. In the gas phase, diffusion molecules undergo repeated adsorption and desorption processes inside the super-cage and the molecules adsorbed near the pore mouth of the super-cage further diffuse inside the zeolite crystal. This lower activation energy is a reflection of the relatively small geometrical limitations. In contrast, in the liquid phase, both the diffusion molecules and solvent exist inside the pores of H-Y. In this study, at first, solvent was introduced to the zeolite pores, and then the target molecule (toluene) would diffuse into the zeolite pore. Thus, the toluene molecules underwent diffusion and adsorption on the acid sites inside the pores by replacing the mesitylene molecules that were adsorbed on the acid sites. In addition, it is considered that the diffusion molecules and the solvent molecules adsorbed on the surface of the pores (channel and the super-cage) inhibited the diffusion of toluene. Therefore, the activation energy for the diffusion of toluene in the liquid phase was different from that in the gas phase.

The intracrystalline diffusivity of toluene within H-Y in mesitylene solution exhibited a higher value compared with that for phenol. In addition, the activation energy for the intracrystalline diffusivity of phenol (27.9 kJ/mol) within H-Y was much higher than that for toluene (17.2 kJ/mol). It has been reported that the adsorption of diffusion molecules on the acid sites reduces the diffusivity of the molecules because the residence time on the acid sites becomes extended. As shown above, phenol has higher affinity for acid sites compared to toluene due to hydrogen bonding, which makes the residence time for phenol on the acid sites of H-Y longer than toluene.

The dependence of the intracrystalline diffusivity of phenol on temperature within H-Y for mesitylene, cyclohexane and 2-propanol are shown in Fig.3.8. The intracrystalline diffusivities of phenol within H-Y for the three solvents occur in the following order: 2-propanol > cyclohexane > mesitylene, and the corresponding activation energies for phenol in 2-propanol, cyclohexane and mesitylene are 10.8, 26.9 and 27.9 kJ/mol, respectively. These data indicate that the solvent coexisting within the H-Y pores affects the diffusivity of phenol. As mentioned above, the amount of phenol adsorbed depends on the solvent, and the amount of phenol adsorbed on H-Y in 2-propanol was the lowest among the solvents investigated in this study. Given that

2-propanol has a higher affinity for the acid sites than phenol, the extent of adsorption of phenol on the acid sites decreased. In contrast, phenol has a higher affinity for the acid sites than cyclohexane and mesitylene, and hence the amount of phenol adsorption on the acid sites became relatively high (Fig.3.6). It is considered that the residence time of phenol on the acid sites in cyclohexane (as well as mesitylene) is longer than that in 2-propanol. As a consequence, the diffusivity of phenol within H-Y in cyclohexane and mesitylene was lower than that in 2-propanol. In addition, because the kinetic diameter of 2-propanol is smaller than that of cyclohexane and mesitylene, it is considered that the effective pore space for diffusion of 2-propanol that is unoccupied by adsorbed molecules becomes large. Therefore, the effect of adsorbed 2-propanol on phenol diffusion (adsorption inhibited) is small compared with cyclohexane and mesitylene; these conditions thus lead to a high intracrystalline diffusivity for phenol and a low activation energy.

The effective diffusivity of molecules, which does not have a physical meaning, may be used to assess the overall reaction rate in reaction kinetics via the Thiele modulus and the effectiveness factor. Arrhenius plots of the effective diffusivity values for phenol and toluene within H-Y for the three solvents are presented in Fig.3.8. For phenol diffusion within H-Y, 2-propanol displayed the highest effective diffusivity than that in mesitylene and cyclohexane.

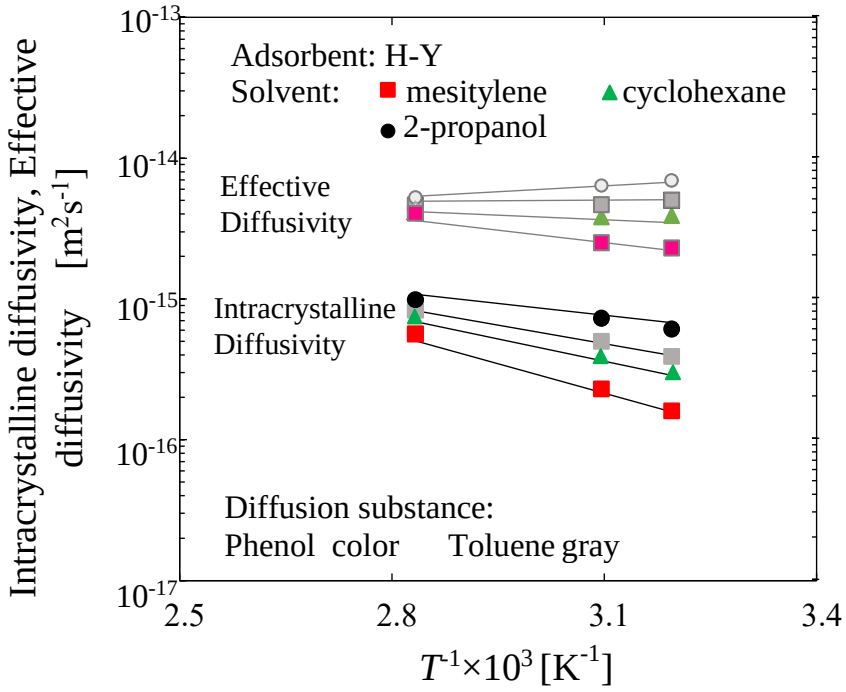

Fig.3.8 Arrhenius plots of the intracrystallinediffusivity and effective diffusivity of phenol and toluene within H-Y in mesitylene, cyclohexane and 2-propanol.

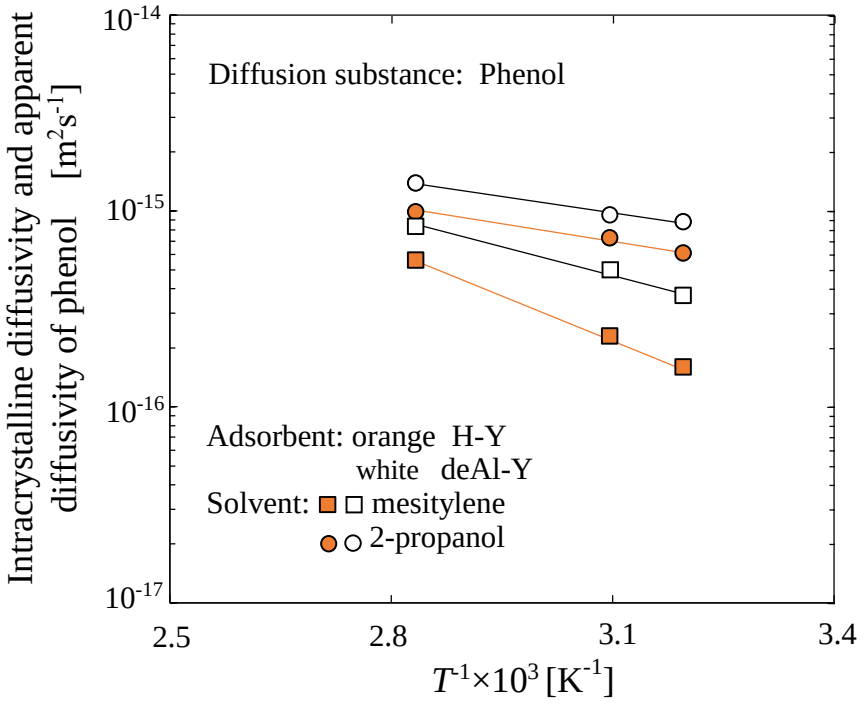

Fig.3.9 Temperature dependency of the intracrystalline diffusivity of phenol within H-Y and the apparent diffusivity within deAl-Y in mesitylene and 2-propanol.

Apparent diffusion resistance can be expressed as follow:

$$L^2/D=L_m^2/D_m+L_z^2/D_z \quad (3\text{-}6)$$

Here, D, D_m and D_z indicate the apparent intracrystalline diffusivity (m^2s^{-1}), diffusivity in the mesopore (m^2s^{-1}) and diffusivity inside zeolite pore (m^2s^{-1}), respectively. L, L_m and L_z indicate the diffusion length of zeolite of H-Y, diffusion length of mesopore and diffusion length of zeolite in deAl-Y, respectively.

From the nitrogen adsorption data (Table 3.1), ratio of external surface area to specific surface area of deAl-Y is 6 %. Indicating that large part of deAl-Y has Y-type zeolite structure and L_m is much smaller than L_z, which considered that diffusion and adsorption in the remaining zeolite structure is dominant. However, because it is very difficult to decide actual diffusion length of remaining zeolite structure, diffusivity of phenols within deAl-Y was evaluated using diffusion length of H-Y (before dealumination) as tentative value. Thus, the diffusivity of phenols within deAl-Y in the

previous manuscript is the apparent intracrystalline diffusivity.

The dependence of the intracrystalline diffusivity of phenol on temperature within H-Y and the dependence of the apparent diffusivity of phenol on temperature within deAl-Y in the 2-propanol and mesitylene solution are shown in Fig.3.9. The activation energy of phenol within H-Y and deAl-Y in 2-propanol are approximately same (10.8 kJ/mol). This indicate that effect of acid site on diffusion mechanism of phenol within Y-type zeolite in 2-propanol is small. Because 2-propanol are preferentially adsorbed on the acid site of zeolite pore surface, it can be assumed that frequency of phenol adsorption is decreased and interaction between phenol and 2-propanol is dominant resistance for diffusion. In addition, the activation energy of phenol within H-Y (27.9 kJ/mol) in mesitylene is higher than that within deAl-Y (17.7 kJ/mol). Indicating that the presence of Brønsted acid sites affect the diffusion of phenol in the H-Y pores in mesitylene solutions. The results suggest that the hydroxy group in phenol was adsorbed strongly on the Brønsted acid sites of H-Y in mesitylene.

Based on above results, the assumed diffusion mechanisms for phenol within H-Y in the liquid phase are summarized in Fig.3.10. In the gas phase, the pore size of the H-Y is large enough to neglect the mass transfer resistance at the pore mouth, and the molecules can diffuse within the pores with minimal geometrical limitations (as previously mentioned) [13]. In contrast, in the liquid phase, because the diffusion molecules and the solvent coexist within the pores of H-Y, the molecules adsorbed on the acid sites of the pore surface affect the diffusivity. The ease of adsorption of the diffusion molecules and the solvent molecules coexisting inside the pores on the acid sites of H-Y as well as the kinetic diameter of the solvent molecules adsorbed on the acidic sites affect the diffusivity of the molecules and their activation energy. Therefore, toluene can readily undergo diffusion and be adsorbed on the acid sites within H-Y, because there is no solvent effect. However, in the liquid phase, the target molecules and the solvent molecules both co-exist within the pores of H-Y.

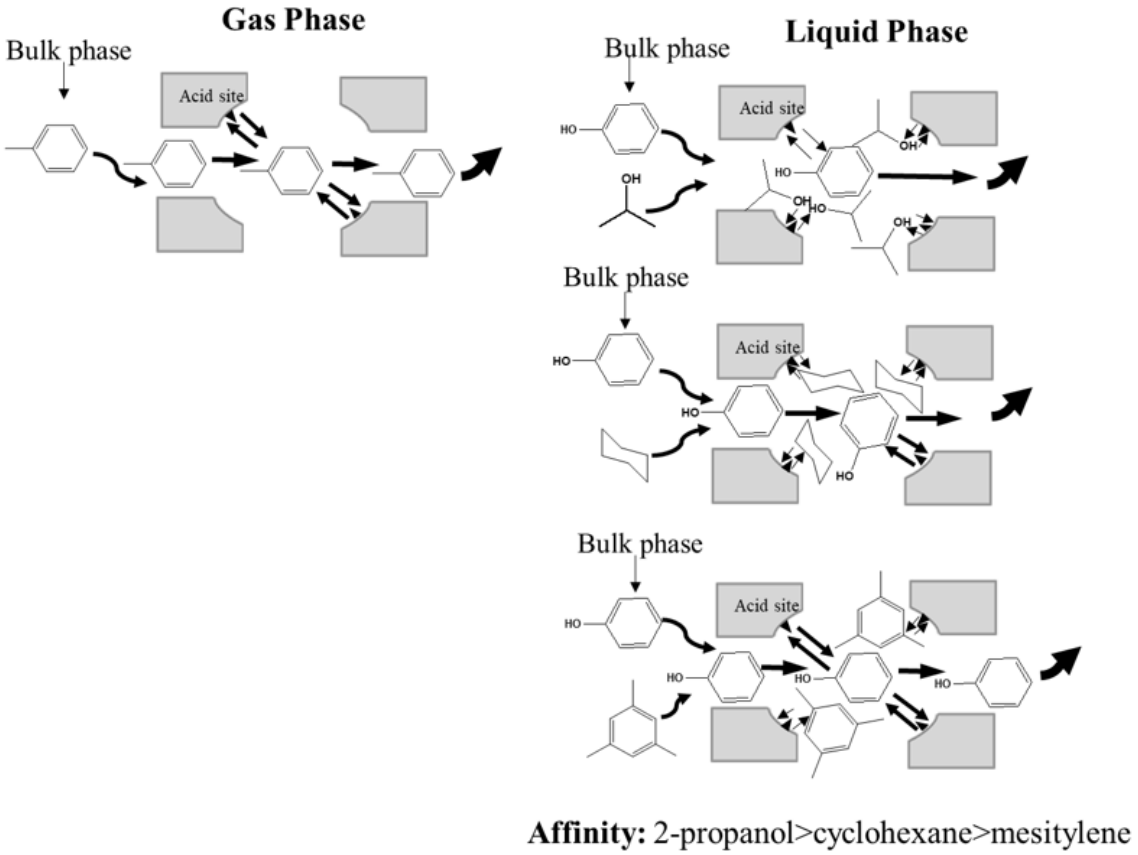

Fig.3.10 Possible diffusion mechanisms for phenol within H-Y in mesitylene, cyclohexane and 2-propanol solutions

3.4. Conclusions

The intracrystalline diffusivity of phenol and toluene within H-Y zeolites in the liquid phase together with the effect on the diffusivity of phenol and toluene of solvents coexisting in the H-Y zeolite pores were studied. In the gas phase, given that the geometrical limitations are small when toluene diffuses into the zeolite pores, the activation energy for intracrystalline diffusivity was small. In contrast, in the liquid phase, the activation energy for the intracrystalline diffusivity of toluene was larger than that in the gas phase because solvent molecules coexisted inside the pores. To investigate the affinity of the diffusion molecule for the acid sites of H-Y and its effect on the diffusivity, the diffusivities of phenol and toluene were measured in mesitylene solutions. The hydroxy group in phenol was adsorbed strongly on the Brønsted acid

sites of H-Y and this led to a lower intracrystalline diffusivity than that for toluene. Furthermore, the intracrystalline diffusivities of phenol within H-Y for three solvents were measured to investigate the effect of the affinities of the solvents and the acid sites on phenol diffusion and to clarify the order of phenol diffusivity, this being as follows: 2-propanol > cyclohexane > mesitylene. It was clarified that the ease of adsorption of the diffusion molecules and the solvent molecules coexisting within the pores on the acid sites of H-Y as well as the kinetic diameter of the solvent molecules adsorbed on the acid sites affected the diffusivity of the diffusion molecules and their activation energy.

References

[1] K. X. Lee, J.A. Valla, Appl. Catal. B. 201(2017)359-369.
[2] C.Y. Liu, R.P. Wei, G.L. Geng, M.H. Zhou, L.J. Gao, G.M. Xiao, Fuel Process. Technol., 134(2015)168-174.
[3] J. García-Martínez, K. Li, G. Krishnaiah, ChemComm, 48(2012)11841-11843.
[4] A. Westermann, B. Azambre, J. Phys. Chem. C 120(2016)25903-25914.
[5] J. Jiao, B. Qin, Y. Du, J. Ma, W. Li, R. Li, J. Chem. Eng. Data 64(2019)3483-3492.
[6] C. Li. Y. Ren, J. Gou, B. Liu H. Xi, Appl. Surf. Sci. 392 (2017)785-794.
[7] J. Kärger, D. Freude, Chem Eng Technol. 25(2002)769-778.
[8] X. Li, J. Wang, Y. Guo, T. Zhu, W. Xu, Chem. Eng. J. 411 (2021)128558.
[9] S.V. Donk, A.H. Janssen, J.H. Bitter, K.P.D. Jong, Catal Rev, 45(2003)297-319.
[10] J. Pérez-Ramírez, C. H. Christensen, K. Egeblad, C. H. Christensen and J. C. Groen, Chem. Soc. Rev., 37(2008)2530-2542.
[11] P. Losch, A.B. Pinar, M.G. Willinger, K. Soukup, S. Chavan, B. Vincent, B. Louis, J. Catal. 345 (2017) 11-23.
[12] T. Masuda, Chem. Eng. Sci. 56 (2001) 889-896.
[13] T. Masuda, Catal. Surv. from Asia. 7 (2003) 133-144.
[14] T. Masuda, Y. Fujikata, H. Ikeda, K. Hashimoto, Microporous Mesoporous Mater. 38 (2000) 323-332.
[15] T. Masuda, Y. Fujikata, T. Nishida, K. Hashimoto, Microporous Mesoporous Mater. 23 (1998) 157-167.
[16] Y. Fujikata, T. Masuda, H. Ikeda, K. Hashimoto, Microporous Mesoporous Mater. 21 (1998) 679-686.

[17] T. Masuda, Y. Fujikata, T. Nishida, K. Hashimoto, Microporous Mesoporous Mater. 23 (1998) 157-167.

[18] Y. Nakasaka, T. Tago, K. Odate, T. Masuda, Microporous Mesoporous Mater. 112 (2008) 162-169.

[19] X. Su, Y. Nakasaka, R. Moriwaki, T. Yoshikawa, T. Masuda, Microporous Mesoporous Mater. 319 (2021) 111044.

[20] L. Song, Z. Sun, L. Duan, J. Gui, G. S. McDougall, Microporous Mesoporous Mater. 104 (2007)115-128.

[21] W. Wanmolee, N. Laosiripojana, P. Daorattanachai, L. Moghaddam, J. Rencoret, J.C.D. Rio, W.O.S. Doherty. ACS Sustain. Chem. Eng. 6(2018)3010-3018.

[22] Y. Liu, E. Baráth, H. Shi, J. Hu, D. M. Camaioni, J. A. Lercher, Nat. Catal. 1 (2018)141-147.

[23] M. H. Kamani, I. Eş, J. M. Lorenzo, F. Remize, E. Roselló-Soto, F. J. Barba, J. Clark, A. M. Khaneghah, Green Chem. 21 (2019)3213-3231.

[24] A. Demirbaş, Energy Convers. Manag. 42(2001)1357-1378.

[25] J.C. Serrano-Ruiz, R. Luque, A. Sepúlveda-Escribano. Chem. Soc. Rev. 40.11 (2011): 5266-5281.

[26] S. Wang, Z. Zhang, B. Liu, J. Li, Ind. Eng. Chem. Res. 53(2014)5820-5827.

[27] C.H. Zhou, X. Xia, C.X. Lin. D.S. Tong, J. Beltramini. Chem. Soc. Rev. 40 (2011)5588-5617.

[28] C. Amen-Chen, H. Pakdel, C. Roy. Bioresour. Technol. 79(2001)277-299.

[29] Y. Zhang, H. Lei, Z. Yang, K. Qian, E Villota, ACS Sustain. Chem. Eng. 6(2018)5349-5357.

[30] K. Yang, W. Wu, Q. Jing, L. Zhu, Environ. Sci. Technol. 42(2008)7931-7936.

[31] K.M. Basha, A. Rajendran, V. Thangavelu, Asian J Exp Biol Sci 1(2010)219-234.

[32] W. Zhang, Z. Xu, B. Pan, Q. Zhang, W. Du, Q. Zhang, K. Zheng, Q. Zhang, J. Chen, Chemosphere.66(2007)2044-2049.

[33] I. Khalil, H. Jabraoui, S. Lebegue, W.J. Kim, L-J. Aguilera, K. Thomas, F. Mauge, M. Badawi, Chem. Eng. J. 402 (2020): 126264.

[34] D.Verboekend, Y. Liao, W. Schutysera, B. F. Sels, Green Chem.18(2016)297-306.

[35] N. P. Rhodes, R. Rudham. J. Chem. Soc., Faraday trans. 89 (1993) 2551-2557, https://doi.org/10.1039/FT9938902551

[36] T. Masuda, K. Fukada, Y. Fujikata, H. Ikeda, K. Hashimoto, Chem. Eng. Sci. 51 (1996) 1879-1888, https://doi.org/10.1016/0009-2509(96)00045-0.

[37] S. Javadian and F. Ektefa, RSC Adv. 122 (2015)100799-100808, https://doi.org/10.1039/C5RA20657J.

Chapter 4
Measurement of diffusivity of toluene and 1-methylnaphathlene within silicalite-1 and Si-beta in the sub- and super-critical fluids

4.1. Introduction

Zeolite has various functions such as strong acid, shape selectivity and ion exchange ability, which an important porous material as catalyst and adsorbent in industrial process [1-2]. It is known that the pore size of zeolite is close to the molecular size of some hydrocarbons. Most of the acid sites of the zeolite are located on the surface of the pore, and the reaction proceeds to the first reaction by diffusing the inside of the zeolite pore from the bulk fluid and adsorbing it to the active sites [3]. The apparent reaction rate of the catalytic reaction with zeolite is evaluated by the reaction of the zeolite particle and the molar flux of the product [4]. The observed maximum reaction rate is the diffusion rate in zeolite crystals. Therefore, the reaction of zeolite catalysts is influenced by the diffusion, and the information about the diffusion rate of molecules in the zeolite crystal is indispensable for the reaction engineering analysis and the catalyst design using the zeolite catalyst.

For the gas phase, various methods for measuring the diffusion coefficient of molecules within zeolite crystals, such as microscopic methods using NMR [5-7] and macroscopic methods using the constant volume method, and discussions on the diffusion mechanism have been conducted. We also reported that diffusivity within zeolite by constant volume method [8-14].

On the other hand, there are some reports on the low-temperature liquid phase including our laboratory [15-17]. Furthermore, there are few research reports on the diffusion mechanism in zeolite crystals in high-temperature liquid phases, subcritical and supercritical fluids. Liu et al. studied HZSM-5@Al-MCM-41 exhibits the excellent catalytic performance with the highest catalytic activities to enhanced diffusivity and the lowest deactivation rate for the improved performances of catalytic cracking of supercritical n-dodecane (773 K, 4 MPa) [18]. We found that the concentration of diffusing substances in the high-temperature liquid phase, subcritical and supercritical fluids can be measured by using a Raman spectrophotometer, and there has been no

report so far by applying this concentration measurement method for measurement of diffusion coefficient of aromatic compounds within zeolite crystals in subcritical and supercritical fluids.

The main objectives of this study were to develop a method for the direct and continuous measurement of intracrystalline diffusivity of 1-methylnaphathlene and toluene within Si-beta, silicalite-1 and K-ZSM-5 using a Raman spectrometer in the sub- and super-critical fluids has been investigated. Moreover, the intracrystalline diffusivity of toluene within Silicalite-1 in the sub- and super-critical fluids was compared with that in the gas phase.

4.2. Experimental

4.2.1. Preparation of silicalite-1, Si-beta and K-ZSM-5

Si-beta zeolite was supplied from Kubota, Japan. The silicalite-1 were prepared by traditional hydrothermal method. The silicalte-1 and ZSM-5 (pore size: 0.53×0.56nm) were prepared by traditional hydrothermal method. The Na_2SiO_3, $Al_2(SO_4)_3$ (only for ZSM-5), and tetra-n-propylammoniumbromide (TPABr) were dissolved in deionized water. An aqueous solution was stirred for 24 h when a gel was formed. Then transfer into a Teflon-lined steel autoclave, and heated to 423 K for 72 h. After the hydrothermal crystallization, the obtained zeolites suspensions were washed with deionized water by centrifugation and then dried in the air atmosphere. The resulting powders was calcined at 823K. All the samples were essential to ion-exchange to H-type with NH_4NO_3 aqueous solution at 348 K for 3 h. The H-type samples were washed with deionized water by centrifugation and dried overnight at 383 K. The ZSM-5 with Si/Al ratio of 110 was obtained. K-type samples (K-ZSM-5) were prepared by impregnating K-type samples with a KNO_3 aqueous solution of appropriate concentration at 348 K for 2 h. Finally, the targeted K-type zeolites were washed with deionized water, calcined at 823 K for 12 h.

4.2.2. Characterization of silicalite-1, Si-beta and K-ZSM-5

Morphology (crystal sizes) and crystallinity of the zeolites were analyzed by field emission scanning electron microscopy (FE-SEM; JSM-6500F, JEOL) and X-ray diffraction (XRD; Ultima IV, Rigaku Co. Ltd.), respectively. The pore volumes and the external and specific surface areas of the zeolites at 77 K were calculated using the BET- and the t-methods based on N_2 adsorption isotherms (Microtrac BEL Corp., Belsorp-mini.).

4.2.3. Measurement of intracrystalline diffusivity in the sub- and super-critical fluids

The intracrystalline diffusivity of 1-methylnaphthalene and toluene within Si-beta and silicalite-1 in the sub- and super-critical fluids by a constant volumetric method using Raman spectroscopy, respectively. Cyclohexane and cyclopentane served as the respective solvents. The transient change process can be described the following theoretical equations for the zeolites with a spherical shape (Si-beta) and a hexagonal slab shape (silicalite-1 and K-ZSM-5).

Fig.4.1 show the change in the toluene concentration with time, where silicalite-1 was used as the catalyst. The benzene concentrations in cyclohexane solution at initial time (C_0) were 203 mol/m^3. The symbols and the curve represent the experimental results and the numerical result calculated using Eq. (1). Toluene concentrations decreased with time in silicalite-1 due to toluene molecules diffuse into the pores of the catalyst and are adsorbed on the pore surface.

.

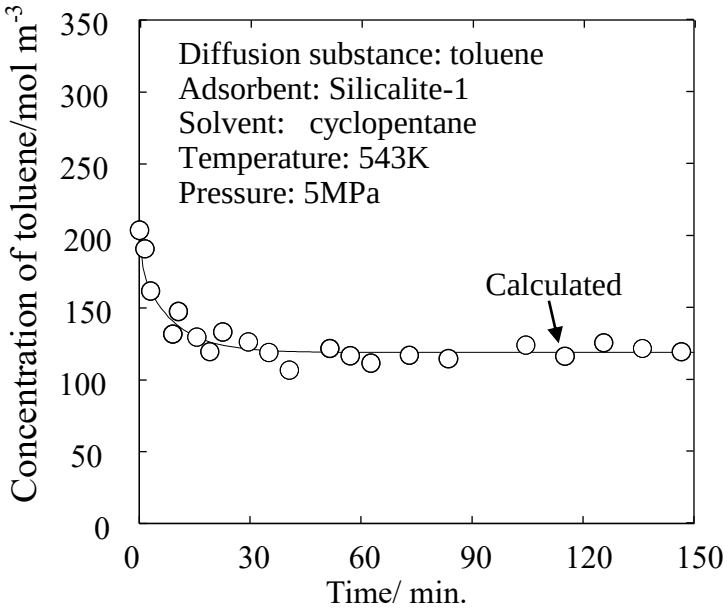

Fig. 4.1. Change in the toluene concentrations with time.

Hexagonal slab shape

$$\frac{M_t}{M_e} = \frac{C_0 - C_t}{C_0 - C_e} = 1 - \sum_{n=1}^{\infty} \frac{2\alpha(1+\alpha)}{1+\alpha+\alpha^2 q_n^2} \exp\left(-\frac{D q_n^2 t}{L^2}\right) \quad (4\text{-}1)$$

$\alpha = V/(a_m WHL)$ and q_n are the non-zero positive root of $\tan q_n = -\alpha q_n$

Spherical shape

$$\frac{M_t}{M_e} = \frac{C_0 - C_t}{C_0 - C_e} = 1 - \sum_{n=1}^{\infty} \frac{6\alpha(1+\alpha)}{9+9\alpha+\alpha^2 q_n^2} \exp\left(-\frac{D q_n^2 t}{R^2}\right) \quad (4\text{-}2)$$

$\alpha = V/(a_m WHR)$ and q_n are the non-zero positive root of $\tan q_n = -\alpha(3q_n/3+\alpha q_n^2)$

where, M_t is the amount of aromatic hydrocarbon adsorbed at time t; M_e is the M_t value at equilibrium; C_t is the aromatic hydrocarbon in cyclopentane at time t; C_0 and C_e are the initial and equilibrium C_t values, respectively; D is the intracrystalline diffusivity of the aromatic hydrocarbon; R and L are the radius and half-thickness of the spherically

shape zeolites and the hexagonal slab-shaped zeolite crystals, respectively; a_m is the outer surface area of the zeolite crystal, *V* is the volume of the sub- and super-critical fluids; *W* is the weight of the zeolites; and *H* is the partition factor.

The intracrystalline diffusivity was calculated in the sub- and super-critical fluids using the experimental apparatus shown in Fig.4.2. Cyclohexane and cyclopentane were used as the solvents, which can fill with the pores of Si-beta or silicalite-1 or K-ZSM-5. Si-beta or silicalite-1 or K-ZSM-5 zeolites were put in a Pt basket and immersed in the cyclohexane or cyclopentane solution and placed into the vacuum drier for 3 h. Thereafter, the Pt basket was fixed into a stainless-steel autoclave with one of the solutions (critical point of cyclohexane and cyclopentane are 553 K, 4.1 MPa and 511 K, 4.5 MPa, respectively), and then reached the target pressure of 5 Mpa using the pump. The autoclave was heated to the experimental temperature (373-573 K), and the solution was magnetically stirred. After reached the desired temperature and pressure, 1-methylnaphthalene or toluene was injected by syringe into the autoclave and pump. Hence, *in situ* measurement of 1-methylnaphthalene or toluene concentration changes in respective solution with time was conducted to calculate the intracrystalline diffusivity in the sub- and super-critical fluids.

Through the Raman spectrum of the mixed solution of diffusion substance and solvent, it can be seen that the concentration of diffusion substance in the solvent is different at different temperatures. This may be due to the density of diffusion substance varies at different temperatures and pressures. According to this situation, under the condition of constant pressure, we made calibration curves at different temperatures.

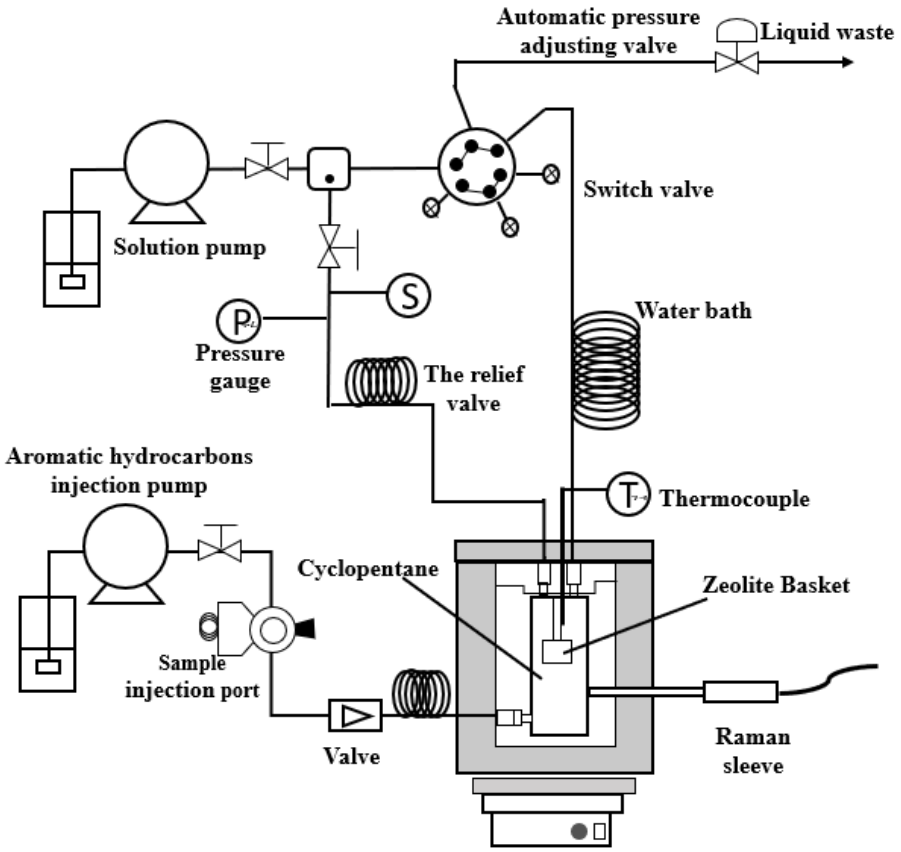

Fig.4.2 Experimental apparatus for measuring the intracrystalline diffusivity of 1-methylnaphthalene and toluene in the sub- and super-critical fluids of cyclohexane and cyclopentane, respectively.

4.3. Result and discussion

4.3.1. Characterization of the silicalite-1，Si-beta and K-ZSM-5

The powder XRD patterns of the silicalite-1 and K-ZSM-5 are presented in Fig.4.3. All of the diffraction peaks in the patterns of the silicalite-1 and K-ZSM-5 correspond to typical characteristic diffraction peaks of MFI-type zeolites. SEM image of the silicalite-1, Si-beta and K-ZSM-5 zeolites are showed in Fig. 4.4. The image reveal that H-silicalte-1 and K-ZSM-5 particles have hexagonal slab shape with a mean crystal size (thickness) of 1.8 and 2.9 μm, respectively; Si-beta particles have spherical

shape. The N_2 adsorption-desorption isotherms of silicalite-1, Si-beta and K-ZSM-5 exhibited type I behavior (not shown here), which is consistent with the presence of micropores. N_2 adsorption isotherms of silicalite-1, Si-beta and K-ZSM-5 were recorded at 77K, and the BET specific surface area (S_{BET}), external surface area (S_{EXT}), and the micropore volume (V_m) of the silicalite-1, Si-beta and K-ZSM-5 were estimated (Table 1). The NH_3-TPD profiles of K-ZSM-5 is shown in Fig. 5. In the profile of K-ZSM-5, one NH_3 desorption peaks are observed at approximately 483 K. A total acid site amount of 0.073 mol/kg (Table 4.1). The Si/Al ratio (100) of K-ZSM-5 obtained by XRF analyze is also shown in Table 4.1.

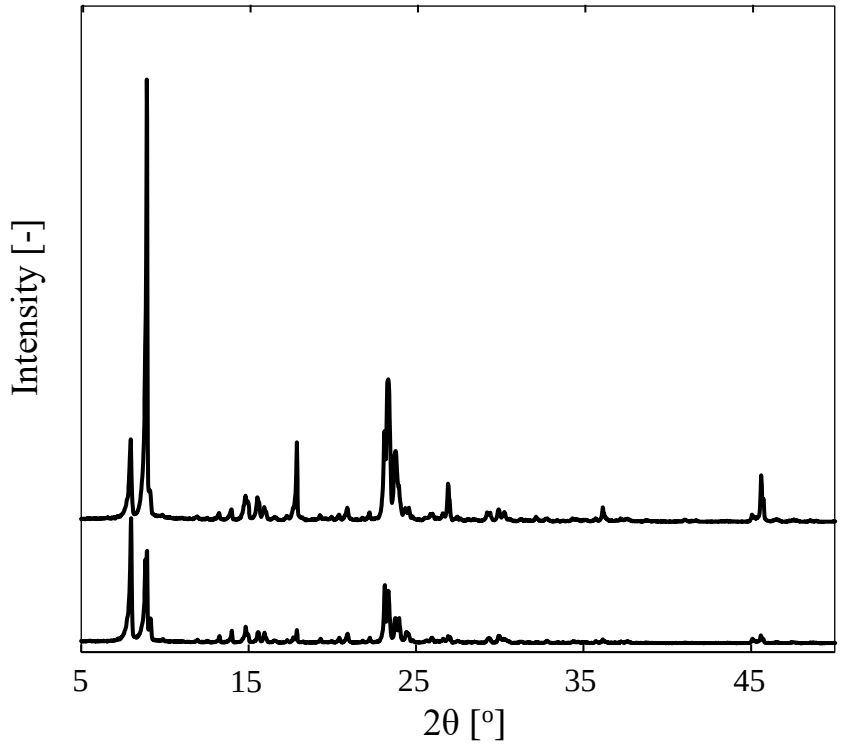

Fig.4.3 XRD patterns of silicalite-1 and K-ZSM-5.

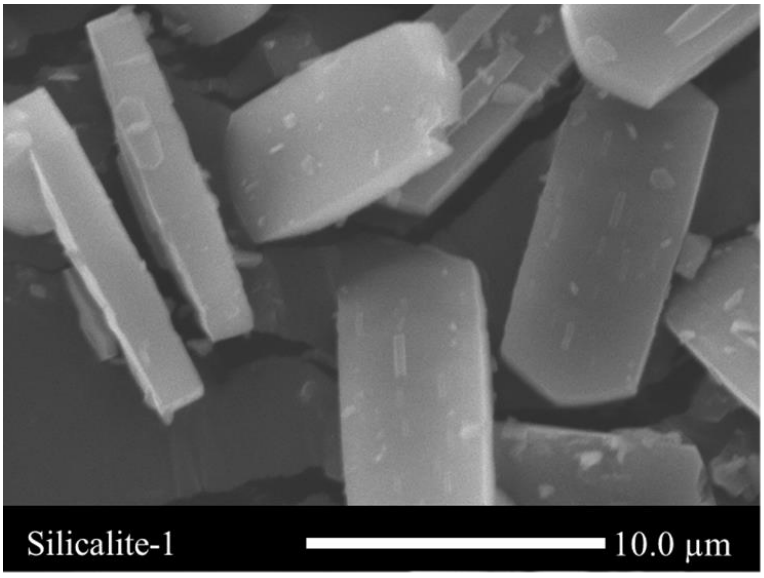
Silicalite-1
10.0 μm

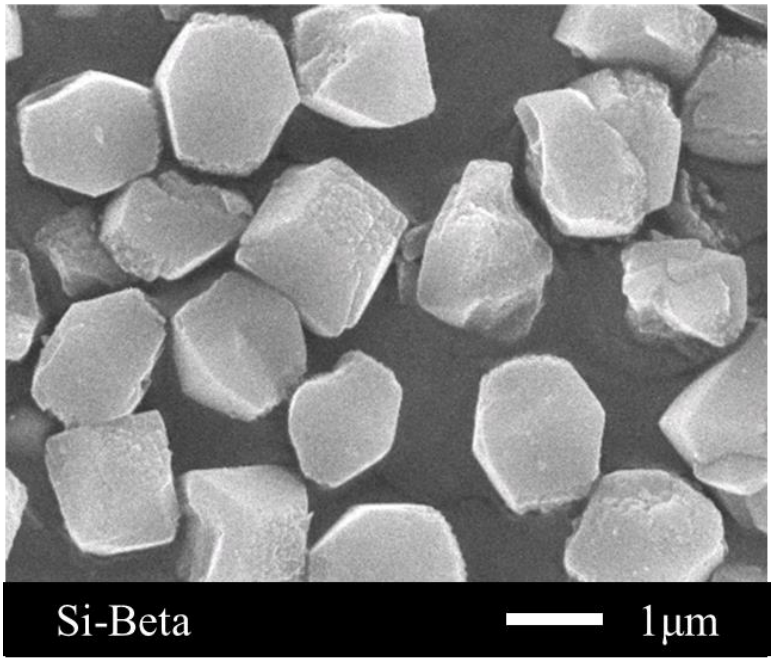
Si-Beta
1μm

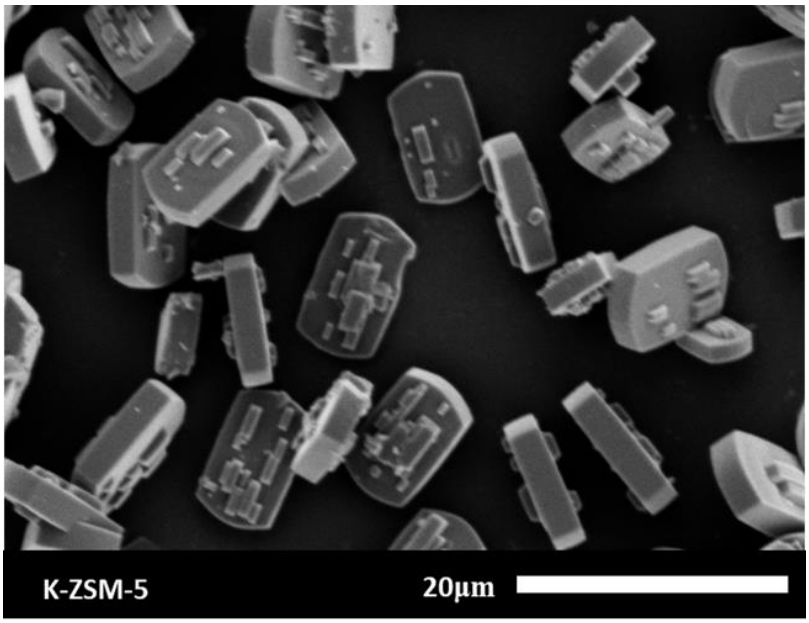

Fig.4.4 SEM image of silicalite-1, Si-beta and K-ZSM-5

Table 4.1 Properties of H-silicalite-1, Si-beta and K-ZSM-5 zeolites

Zeolites	S_{BET} [$m^2\ g^{-1}$]	S_{EXT} [$m^2\ g^{-1}$]	V_m* [$cm^3\ g^{-1}$]	Number of acid sites [$mol\ kg^{-1}$]	Si/Al ratio* [-]
Silicalite-1	401	0.27	0.17	—	—
Si-beta	533	20.6	0.20	—	—
K-ZSM-5	387	15.2	0.17	0.26	110

* Pore volume (V_m) was calculated by the BJH method and the Si/Al ratio obtained by XRF analyze.

4.3.2. Diffusivity of 1-Methylnaphthalene or toluene within Si-beta or H-silicalite-1 in the respective solvents

The typical temperature dependency of diffusivities of 1-Methylnaphthalene (within Si-beta in cyclohexane), and toluene (within H-silicalite-1 in cyclopentane) were shown in Fig 4.5. The diffusivity of toluene within H-silicalite-1 in the gas phase [11] is much higher than that in the liquid phase, sub- and super-critical of cyclopentane. In the gas phase, diffusion molecules go through repeated adsorption and desorption processes inside the zeolite. In contrast, both the diffusion molecules and

solvent exist inside the pores of H-silicalite-1 in the liquid phase, sub- and super-critical fluids. In this study, at first, solvent was introduced to the zeolite pores, and then the toluene would diffuse into the zeolite pore. Thus, the toluene molecules went through diffusion inside the pores by replacing the cyclopentane molecules. It is considered that the diffusing molecules and the solvent molecules adsorbed on the surface of the pores inhibited the diffusion of toluene. Therefore, the intracrystalline diffusivities of toluene in the liquid phase, sub- and super-critical fluid were different from that in the gas phase.

Logarithm of diffusivities of toluene within H-silicalite-1 measured under 5 MPa and liquid phase were correlated with a single line against inverse number of temperatures indicating that the diffusivity only depends on temperature. In contrast, above 473 K, the diffusivity of toluene within silicalite-1 was decreased and the almost minimum value at critical temperature (513 K) was obtained in the supercritical fluids. In addition, the diffusivities of 1-Methylnaphthalene within Si-beta in the sub-critical fluids under 5 MPa and in liquid phase were increased with increasing the temperature while the diffusivity of 1-Methylnaphthalene within Si-beta was decreased and also took almost minimum value at critical temperature (553 K).

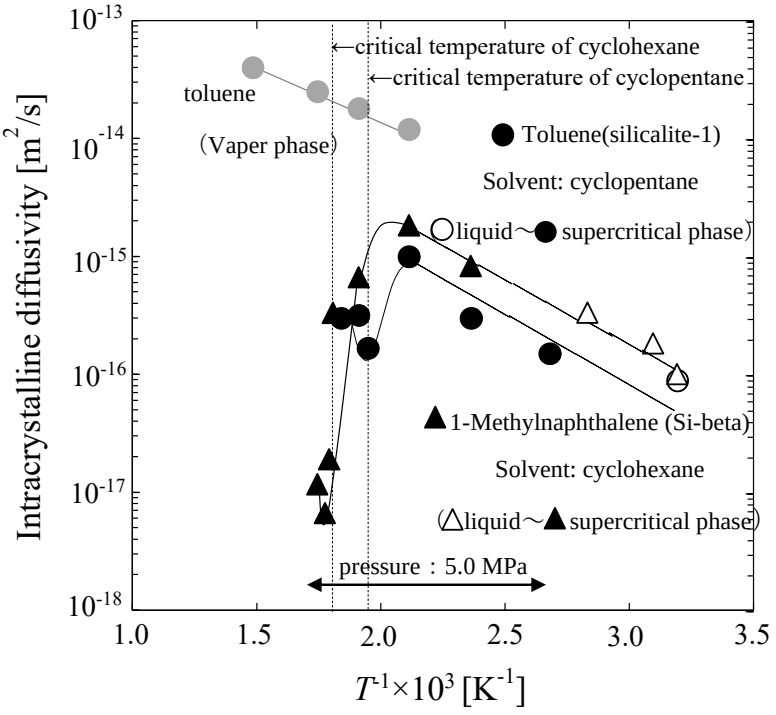

Fig.4.5 Diffusivities of toluene in gas, liquld phase and sub-, super-critical fluids(solvent:cyclopentane, adsorbent: silicalite-1);1-methylnaphthalene(solvent:cyclohexane, adsorbent: Si-beta).

It has been reported that dynamic structure of a cluster formed around a solute in the supercritical fluids was observed. This phenomenon suggestion that cluster of solvent would be formed easily in the supercritical fluids [19]. With the assumption described above, formation of clusters between diffusion substance and solvent molecules near the critical point of solvent was considered, which lead to increased mass transfer resistance at pore mouth near the outer surface of the silicalite-1or Si-beta.

4.3.3. Analysis of mixed solution by using Raman spectrometer

To demonstrate the formation of clusters between diffusion substance and solvent, the Raman study of mixed solution of toluene and cyclopentane (mole ratio is 0.1or 0.3) at 5 MPa in the temperature range from 313 to 573 K were investigated. The experimental results of Raman shift of cyclopentane and toluene in toluene/cyclopentane mixture under 5 MPa at different temperature were shown in Fig. 4.6. CH_2 contrastively symmetric stretching vibration of cyclopentane (Fig.6a) and coupled vibration of toluene ring and substituent-ring stretching of toluene (Fig.6b) were observed. Zerda et al. studied Raman Shifts to a higher frequency is attributed to increased repulsive interaction in the intermolecular; Raman Shifts to a lower frequency is attributed to increased attractive forces in the intermolecular [20]. The peak of cyclopentane was shifted to the lower frequency with decreasing concentration of cyclopentane, and took the almost minimum value around the critical temperature, which suggestion that attractive interactions in the intermolecular of cyclopentane molecules became stronger and vibration of cyclopentane was suppressed (Fig.4.6 a). The peak of toluene was shifted to the higher frequency with increasing the concentration of toluene, which suggestion that increased repulsive interaction in the intermolecular of toluene molecules (Fig.4.6 b). The results indicated that cluster of solvent would be formed easily around the critical temperature. Moreover, we also used 1-Methylnaphthalene /cyclohexane mixture solution (mole ratio is 0.1) did the same experiment and the peak of cyclohexane was also shifted to the lower frequency around the critical temperature. It is considered that formation of clusters between diffusion substance and solvent molecules near the critical point of solvent, which lead to increased mass transfer resistance at pore mouth near the outer surface of the zeolite.

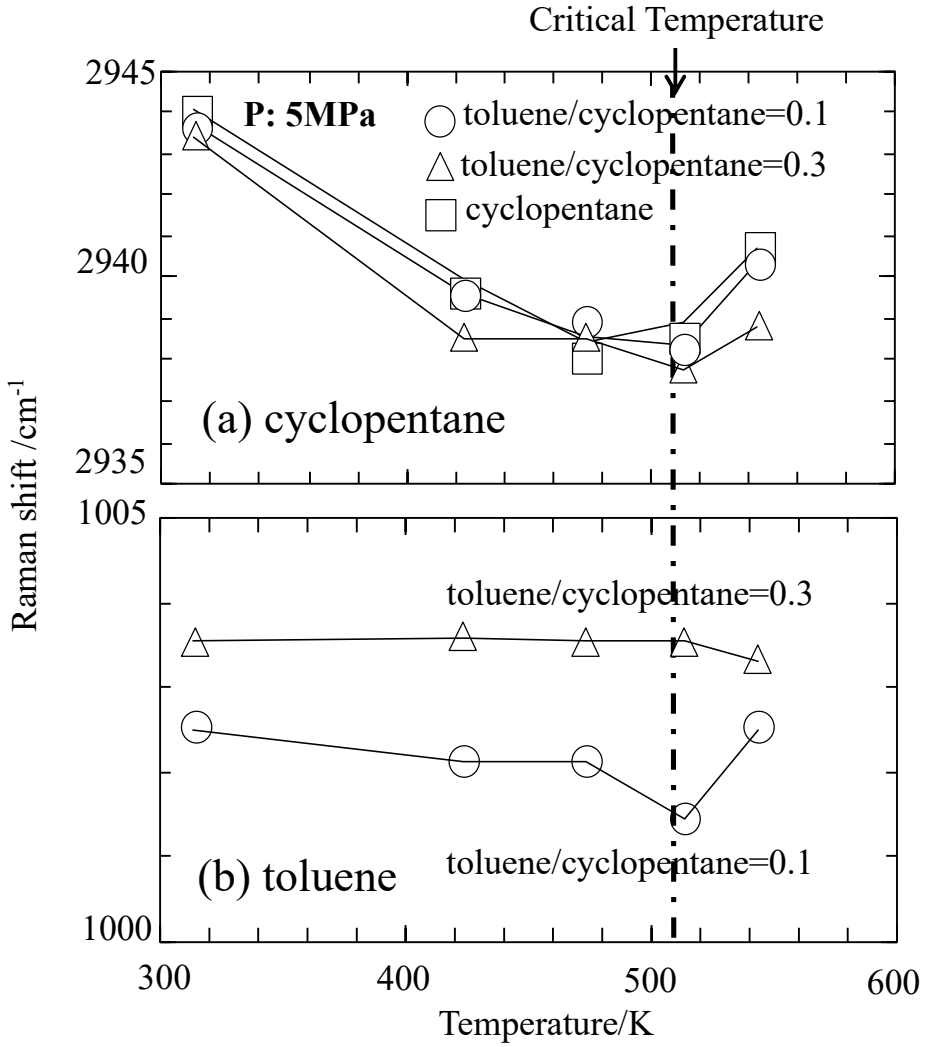

Fig.4.6 Raman shift of cyclopentane and toluene in toluene/cyclopentane mixture under 5 MPa at different temperature. [molar ratio of toluene to cyclopentane:0.1 (circle), 0.3 (triangle), cyclopentane without toluene (square)]

4.3.4 Effects of the crystal size of Silicalite-1 on the intracrystalline diffusivity

The pore surfaces of silicalite-1 and Si-beta have no acid sites. Therefore, diffusion molecules in zeolite pore diffusion process, the pore mouth of zeolite diffusion

and the internal pore wall of zeolite - intermolecular physical diffusion are resistant. The overall resistance to mass transfer for the diffusion can be expressed by

$$\frac{L^2}{D} = \frac{\Delta L^2}{D_m} + \frac{L^2}{D_p} \tag{4-3}$$

where D is apparent diffusivity within pore; D_m is intracrystalline diffusivity at pore mouth; D_p is intracrystalline diffusivity in the gas phase. and ΔL is a hypothetical diffusion distance at the pore mouth where the molecules diffuse at the rate of $D_m / \Delta L$ [12].

Hypothetical that formation of clusters between diffusion substance molecules and solvent molecules near the critical temperature, resulting in a low diffusivity. Thus, diffusion resistance will form at the pore mouth of zeolite. The equation (4-3) can transform into equation (4-4)

$$\left(\frac{1}{D} - \frac{1}{D_p}\right) = \frac{\Delta L^2}{D_m} \cdot \frac{1}{L^2} \tag{4-4}$$

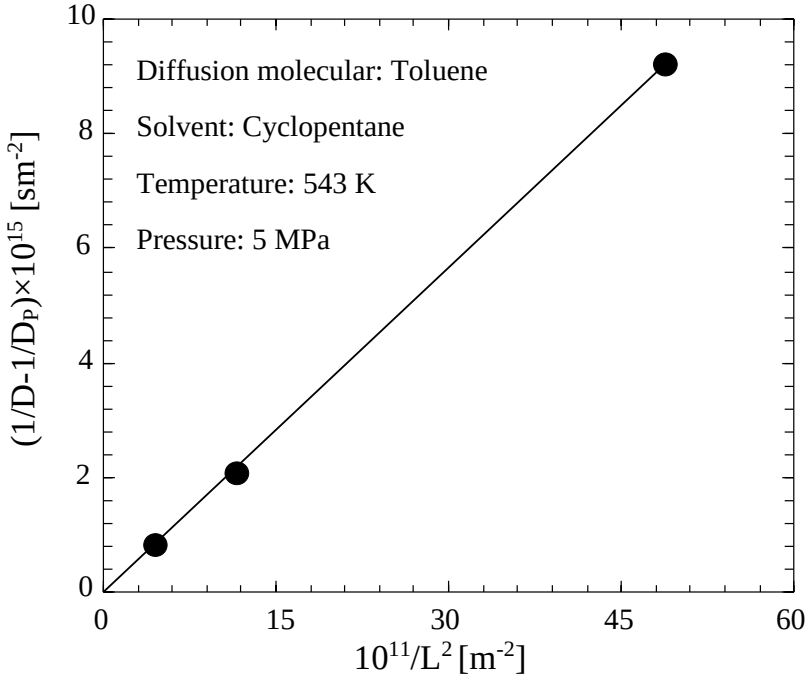

Fig.4.7 Relationship between $1/D-1/D_P$ value and $1/L^2$ value.

Accordingly, the intracrystalline diffusivity of toluene within silicalite-1 at 543 K and 5 MPa in the cyclopentane solution with different crystal sizes of silicalite-1 were measured. Relationship between $1/D-1/D_p$ value and $1/L^2$ value was shown in Fig.4.7. Here, D_p is intracrystalline diffusivity of silicalite1 in the gas phase. Relationship between $1/D-1/D_p$ value and $1/L^2$ value were found to lie on a single line through the origin. Indicating that the mass transfer resistance across pore mouth near the outer surface of the silicalite-1 was existence around critical points of cyclopentane. This was further demonstrated that formation of clusters between diffusion substance and solvent molecules near the critical point of solvent at pore mouth of zeolite (without acid sites).

4.3.5 Intracrystalline diffusivity of toluene within K-ZSM-5 in sub- and supercritical fluids

In addition, the intracrystalline diffusivity of toluene within K-ZSM-5 in supercritical fluid of cyclopentane was also measured. The typical temperature dependency of intracrystalline diffusivity of toluene within K-ZSM-5 in the sub- and super-critical of cyclopentane was shown in Fig.4.8. The intracrystalline diffusivity showed much higher value than that within silicalite-1. Because of toluene concentration at outer surface of the K-ZSM-5 was increased, formation of the cluster may be suppressed and decreased diffusion resistance at pore mouth, which leading to increase the diffusivity. It has been reported that the adsorption of diffusion molecules on the acid sites reduces the diffusivity of the molecules in the gas and liquid phase, which indicated that the diffusivity of diffusion molecules within silicalite-1 (without acid sites) is much higher than that within ZSM-5 (with acid sites). In contrast, we got the opposite results in the supercritical fluids, which may ascribe to the formation of clusters between diffusion substance and solvent molecules near the critical point of solvent at pore mouth of siliclite-1. In order to demonstrate this point, we also did the further investigate.

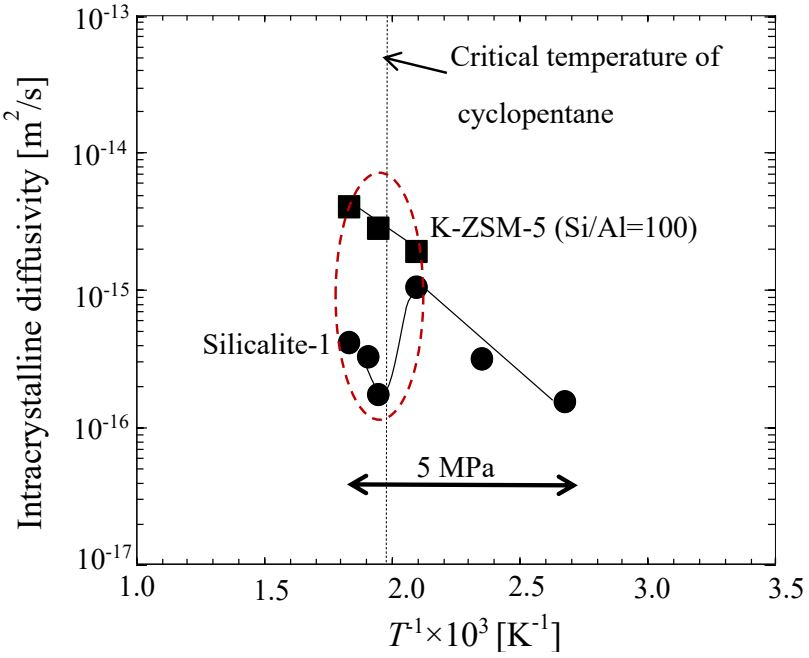

Fig.4.8 The typical temperature dependency of intracrystalline diffusivity of toluene within K-ZSM-5 in the sub- and super-critical of cyclopentane.

4.3.6 Intracrystalline diffusivity of toluene within K-ZSM-5 with different Si/Al ratio in supercritical fluids

The effect of Al content in K-ZSM-5 on intracrystalline diffusivity of toluene within K-ZSM-5 under 5 MPa at 543 K was shown in Fig.4.9. The diffusivity of toluene was reduced with decreasing Al content in K-ZSM-5, which was further confirmed diffusion resistance at the pore mouth was increased with decreasing the acid site leading to increase the diffusivity within K-ZSM-5 due to toluene molecular adsorbed on the acid sites of pore mouth of K-ZSM-5 to make the toluene concentration at outer surface of the K-ZSM-5 was increased. And formation of the cluster may be suppressed and decreased diffusion resistance at pore mouth, which leading to enhance the diffusivity with increasing the Al content.

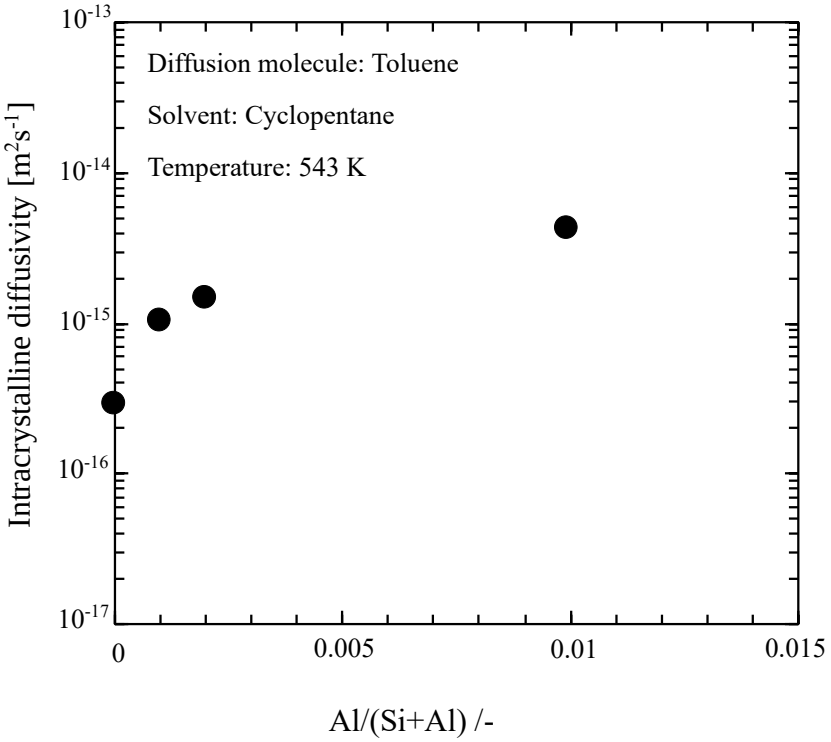

Fig.4.9 Effect of Al content in K-ZSM-5 on intracrystalline diffusivity of toluene within K-ZSM-5 under 5 MPa at 543 K.

4.4. Conclusions

The intracrystalline diffusivity of 1-Methylnaphthalene or toluene within Si-beta or silicalite-1 and K-ZSM-5 in the sub- and super-critical fluids. In the gas phase, the geometrical limitations are small when toluene diffuses into the zeolite pores, the activation energy for intracrystalline diffusivity was small. Moreover, in the sub- and super-critical fluids, the intracrystalline diffusivity of 1-Methylnaphthalene or toluene was much larger than that in the gas phase because solvent molecules coexisted inside the pores. The intracrystalline diffusivity of 1-Methylnaphthalene or toluene in the cyclohexane or cyclopentane solvent was also investigated. During 313 ~ 473 K, the intracrystalline diffusivity increased with increasing the temperature. Above 473 K, the intracrystalline diffusivity of 1-Methylnaphthalene or toluene within Si-beta or

silicalite-1 was decreased and the almost minimum value at critical temperature was obtained in the supercritical fluids. This may be because solvent molecules gather around diffusion molecules near the critical point to forming clusters. For this point, the resistance at the pore mouth of the Si-beta or silicalite-1 increases and the intracrystalline diffusivity decreases. In contrast, intracrystalline diffusivity of toluene within K-ZSM-5 in the sub- and super-critical of cyclopentane showed much higher value than that within silicalite-1 as well as the diffusivity of toluene was reduced with decreasing Al content in K-ZSM-5. Because of toluene concentration at outer surface of the K-ZSM-5 was increased, formation of the cluster may be suppressed and decreased diffusion resistance at pore mouth, which leading to increase the diffusivity.

Referrence

[1] M. E. Davis, Nature, 417 (2002) 813-821.
[2] S. Mintova, M. Jaber, V. Valtchev, Chem. Soc. Rev., 44 (2015)7207-7233.
[3] M. Gao, H. Li, M. Yang, J. Zhou, X. Yuan, P. Tian, M. Ye, Z. Gao, Chem. Eng. J., 377(2019)119668.
[4] J. Kärger, S. Vasenkov, S.M. Auerbach. CRC Press, (2003)458-560.
[5] R. Q. Snurr, J. Kärger, J. Phys. Chem. B, 101(1997)6469-6473.
[6] P. Kortunov, S. Vasenkov, J. Kärger, R. Valiullin, P. Gottschalk, M. Fé Elía, M. Perez, M. Stöcker, B. Drescher, G. McElhiney, C. Berger, R. Gläser, and J. Weitkamp, J. Am. Chem. Soc., 127(2005)13055-13059.
[7] Mehlhorn D, Valiullin R, Kärger J, et al. Microporous Mesoporous Mater., 164(2012)273-279.
[8] T. Masuda, Chem. Eng. Sci. 56 (2001) 889-896.
[9] T. Masuda, Catal. Surv. from Asia. 7 (2003) 133-144.
[10] T. Masuda, Y. Fujikata, H. Ikeda, K. Hashimoto, Microporous Mesoporous Mater. 38 (2000) 323-332.
[11] T. Masuda, Y. Fujikata, T. Nishida, K. Hashimoto, Microporous Mesoporous Mater. 23 (1998) 157-167.
[12] Y. Fujikata, T. Masuda, H. Ikeda, K. Hashimoto, Microporous Mesoporous Mater. 21 (1998) 679-686.
[13] T. Masuda, Y. Fujikata, T. Nishida, K. Hashimoto, Microporous Mesoporous Mater. 23 (1998) 157-167.

[14] T. Masuda, K. Fukada, Y. Fujikata, H. Ikeda, K. Hashimoto, Chem. Eng. Sci. 51 (1996) 1879-1888.

[15] Y. Nakasaka, T. Tago, K. Odate, T. Masuda, Microporous Mesoporous Mater. 112 (2008) 162-169.

[16] X. Su, Y. Nakasaka, R. Moriwaki, T. Yoshikawa, T. Masuda, Microporous Mesoporous Mater. 319 (2021) 111044.

[17] L. Song, Z. Sun, L. Duan, J. Gui, G. S. McDougall, Microporous Mesoporous Mater. 104 (2007)115-128.

[18] Z. Diao, L. Wang, X. Zhang, G. Liu, Chem. Eng. Sci., 135(2015)452-460.

[19] C. C. Liew, H. Inomata, S. Saito, Fluid Phase Equilibria, 104 (1995) 317-329.

[20] T. W. Zerda, X. Song, J. Jonas, Appl. Spectrosc., 40 (1986) 1194.

Chapter 5
The diffusion mechanism of aromatic hydrocarbons within silicalite-1, K-ZSM-5, and K-Y in the sub- and super-critical fluids

5.1. Introduction

The ordered crystalline porous materials such as zeolite catalysts are crystalline alumino-silicate with ultra-fine nano-pores, the diameters of which are almost the same as those of minimum molecular diameters of lighter hydrocarbons [1-6]. Therefore, the zeolite exhibits unique catalysis caused by molecular sieving effect and shape selective catalysis, which are exploited as adsorbents, catalysis, and separation membrane in the variety of application fields of petroleum, fine chemical, and chemical biomass conversion [7-11]. The pore size and structure sometimes strengthen limitations to the mass transport processes that contact activity and selectivity of the reaction because surface active sites in zeolite crystals are not fully utilized. Generally, apparent reaction rates of zeolites-catalyzed reactions can be controlled by diffusion resistance of reactants and products inside the zeolite [12]. Because the diffusion coefficient of the hydrocarbon substrate depends on its size relative to the size of catalyst pores and the physicochemical features of the fluid where the catalysts and the substrate exist. In addition, investigating the intrinsic kinetics of heterogeneous reactions as well as designing reactors hinge on their diffusivity. Therefore, understanding diffusion mechanisms of molecules in the porous catalysts under different conditions are very critical for designing the catalysis and supply more useful information on reaction processes using those catalysts, since the degree of the diffusion limitations are observed differently by depending on molecular size and circumstance around the catalysts, such as gas, liquid, sub-critical and supercritical fluids.

Several research works have been reported to measure the diffusivity of hydrocarbon within porous materials in the gas and have been few reported in the liquid phase [13-21]. Nevertheless, the desulfurization and denitrogenation of hydrocarbons in the process of oil refinery, and the production of useful aromatic chemicals from carbohydrate [22], and low molecular lignin in the biomass [23] need to be carried out at high temperature and high pressure. Among the different high temperature and high pressure systems, the supercritical fluids have gained growing attention in a variety processes, which attributed to its physicochemical properties of solubility, high

diffusivity, lower viscosity and liquid-like density that can enhance the mass transfer of substrates to the active sites of catalysts [24-29]. These properties make it as green solvent for various applications because of supercritical fluids are environmentally friendly, sustainable and low chemical toxicity [30]. Many studies have displayed that gasification, liquefaction, carbonization, and upgrading of biomass, petroleum oil, microalgae and waste sources by using supercritical water [31-38]. Peng et al. studied esterification of acids into ester with HZSM-5 catalyzed in supercritical ethanol, which effectively cracked and hydrogenated compounds in bio-oil [39]. Moreover, supercritical fluids are effective way to suppresses the formation of coke on the outer surface of zeolites during reaction [40], and some literatures from our previously work [41-42]. However, diffusivity of aromatic hydrocarbons within porous materials in the sub and super-critical fluid have not been proposed.

Our group demonstrated a method for measurement of intracrystalline diffusivity of hydrocarbon within porous materials in sub- and super-critical fluids by a constant volumetric method using Raman spectroscopy, which can directly and continuously measure the change in the diffusion substance concentration with time and explore the diffusion mechanism in the sub- and super-critical fluids. This study aimed to measuring the intracrystalline diffusivities of aromatic hydrocarbons within silicalite-1, K-ZSM-5 and K-Y in the in sub- and super-critical fluids. Moreover, the mechanism of aromatic hydrocarbons diffusion within silicalite-1, K-ZSM-5 and K-Y in super-critical fluids were investigated.

5.2. Experimental

5.2.1. Preparation of K-ZSM-5 and K-Y

The ZSM-5 (pore size: 0.53×0.56nm) were prepared by traditional hydrothermal method. The Na_2SiO_3, $Al_2(SO_4)_3$, and tetra-n-propylammoniumbromide (TPABr) were dissolved in deionized water. An aqueous solution was stirred for 24 h when a gel was formed. Then transfer into a Teflon-lined steel autoclave, and heated to 423 K for 72 h. After the hydrothermal crystallization, the obtained zeolites suspensions were washed with deionized water by centrifugation and then dried in the air atmosphere. The resulting powders was calcined at 823 K. Y-type zeolite (pore size: 0.74×0.74nm) with SiO_2/Al_2O_3 ratio of 5.5 was purchased by Wako Chemical Ltd., Japan. All the samples were essential to ion-exchange to H-type with NH_4NO_3 aqueous solution at 348 K for 3 h. The H-type samples were washed with deionized water by

centrifugation and dried overnight at 383 K. K-type samples (K-ZSM-5 and K-Y) were prepared by impregnating K-type samples with a KNO_3 aqueous solution of appropriate concentration at 348 K for 3 h. Finally, the targeted K-type zeolites were washed with deionized water, calcined at 823 K for 12 h. The samples were labeled K-ZSM-5 and K-Y, respectively.

5.2.2. Characterization of silicalite-1, K-ZSM-5 and K-Y zeolites

Morphology (crystal sizes) and crystallinity of the zeolites were analyzed by field emission scanning electron microscopy (FE-SEM; JSM-6500F, JEOL) and X-ray diffraction (XRD; Ultima IV, Rigaku Co. Ltd.), respectively. The Si/Al ratios of the samples were determined by X-ray fluorescence measurements (XRF; Shimadzu, EDX-700HS). Acidity of the zeolites were evaluated by NH_3-temperature programmed desorption (NH_3-TPD; BEL CAT Ⅱ (MicrotracBEL Corp.) with a Q-mass spectrometer (Bel-mass, MicrotracBEL Corp.)). The pore volumes and the external and specific surface areas of the zeolites at 77K were calculated using the BET- and the t-methods based on N_2 adsorption isotherms (Microtrac BEL Corp., Belsorp-mini.).

5.2.2. Measurement of intracrystalline diffusivity in the sub- and super-critical fluids

The intracrystalline diffusivity of aromatic hydrocarbons within silicalite-1, K-ZSM-5 and K-Y in the sub- and super-critical fluids (cyclopentane as a solvent) by a constant volumetric method using Raman spectroscopy. The transient change process can be described the following theoretical equations for the porous materials with a hexagonal slab shape (silicalite-1and K-ZSM-5) and a spherical shape (K-Y).

Hexagonal slab shape

$$\frac{M_t}{M_e} = \frac{C_0 - C_t}{C_0 - C_e} = 1 - \sum_{n=1}^{\infty} \frac{2\alpha(1+\alpha)}{1+\alpha+\alpha^2 q_n^2} \exp\left(-\frac{D q_n^2 t}{L^2}\right) \quad (5\text{-}1)$$

$\alpha = V/(a_m WHL)$ and q_n are the non-zero positive root of $\tan q_n = -\alpha q_n$

Spherical shape

$$\frac{M_t}{M_e} = \frac{C_0 - C_t}{C_0 - C_e} = 1 - \sum_{n=1}^{\infty} \frac{6\alpha(1+\alpha)}{9 + 9\alpha + \alpha^2 q_n^2} \exp\left(-\frac{D q_n^2 t}{R^2}\right) \quad (5\text{-}2)$$

$\alpha = V/(a_m WHR)$ and q_n are the non-zero positive root of $\tan q_n = -\alpha(3q_n/3 + \alpha q_n^2)$

where, M_t is the amount of aromatic hydrocarbon adsorbed at time t; M_e is the M_t value at equilibrium pressure; C_t is the aromatic hydrocarbon in cyclopentane at time t; C_0 and C_e are the initial and equilibrium C_t values, respectively; D is the intracrystalline diffusivity of the aromatic hydrocarbon; R and L are the radius and the half-thickness of the spherically shape zeolites and the hexagonal slab-shaped zeolite crystals, respectively; a_m is the outer surface area of the zeolite crystal, V is the volume of the sub- and super-critical fluids; W is the weight of the zeolites; and H is the partition factor.

The intracrystalline diffusivity was calculated in the sub- and super-critical fluids using the experimental apparatus shown in Fig.1, which includes a pump and a stainless-steel autoclave with a Raman spectrophotometer. Cyclopentane was used as a solvent, which can enter the pores of silicalite-1, K-ZSM-5 and K-Y. The weight of the zeolite sample, which was put in a Pt basket and was immersed in the volume of the cyclopentane solution, which placed them into the vacuum drier for 3 h. Thereafter, the Pt basket with zeolite was fixed into a stainless-steel autoclave with cyclopentane solution (critical point of cyclopentane is 511 K, 4.5 MPa), and then filled 5 MPa pressure by using the pump. The autoclave was reached to the experimental temperature (473 K-543 K) and cyclopentane solution with magnetically stirred. After reached the desired temperature, aromatic hydrocarbons (toluene, xylene isomers, *p*-propylphenol, propylbenzene and *p*-cresol) was injected by syringe into the autoclave and pump. Hence, in situ measurement of aromatic hydrocarbon concentration changes in cyclopentane solution with time was conducted to calculate the intracrystalline diffusivity in the sub- and super-critical fluids.

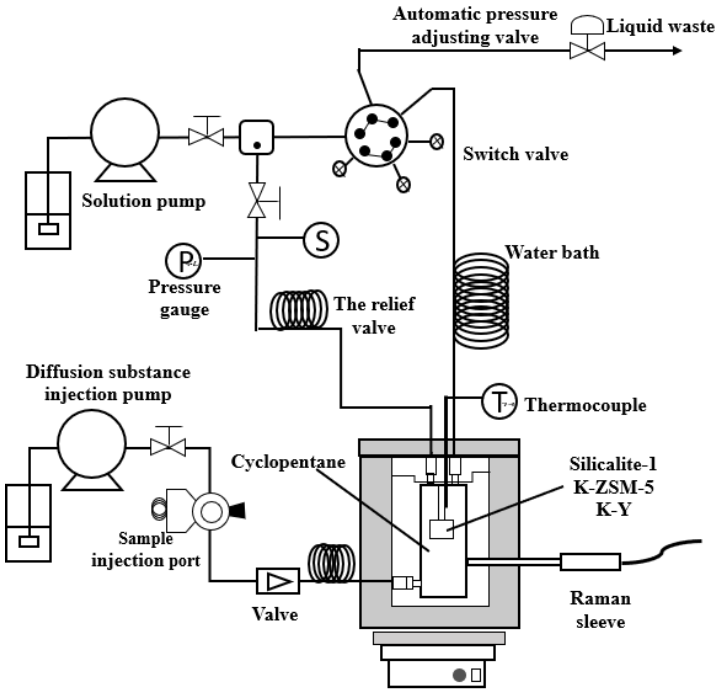

Fig.5.1 Experimental apparatus for measuring the intracrystalline diffusivity in the sub- and super-critical fluids

5.3. Results and discussion

5.3.1. Characterization of the silicalite-1, K-ZSM-5 and K-Y

The XRD patterns were conducted for all the samples and the results are shown in Fig.5.2. Prominently, all diffraction peaks of samples a and b showed a broad diffraction peak in the 2θ range of 7–9.5° and 22−25°, confirming that the acquired samples are crystallized in the MFI structure. The sample c showed diffraction peaks over the angular range of 5°-50°and all diffraction peaks were corresponding to the Y zeolites. The morphologies of all samples were investigate using FE-SEM. Fig.5.3 shows SEM images recorded for silicalite-1, K-ZSM-5 and K-Y. The surface morphology of silicalite-1 and K-ZSM-5 are hexagonal platelet-shape, whereas the SEM image of K-Y has a spherical structured. The crystal size of silicalite-1, K-ZSM-5 and K-Y is approximately 1.8 μm, 2.46 μm and 3.88 μm, respectively.

N_2 adsorption isotherms profile of silicalite-1, K-ZSM-5 and K-Y are depicted in Fig.5.4. All the samples exhibit a type I isotherm and a strong uptake at low

p/p_0, confirming the existence of micropores. Table 1 listed specific properties in surface area, external surface area and the micropore volume of silicalite-1, K-ZSM-5 and K-Y based on N_2 adsorption/desorption isotherms.

Fig.5.5 shows the NH_3-TPD profiles of K-ZSM-5 and K-Y. With the addition of K^+, both K-ZSM-5 and K-Y exhibited one NH_3 desorption peaks at about 473 K, which can be correspond to the desorption of the weak acid sites. The total acid site (Table 1) of K-ZSM-5 and K-Y was 0.26 and 3.29 mol/kg, respectively.

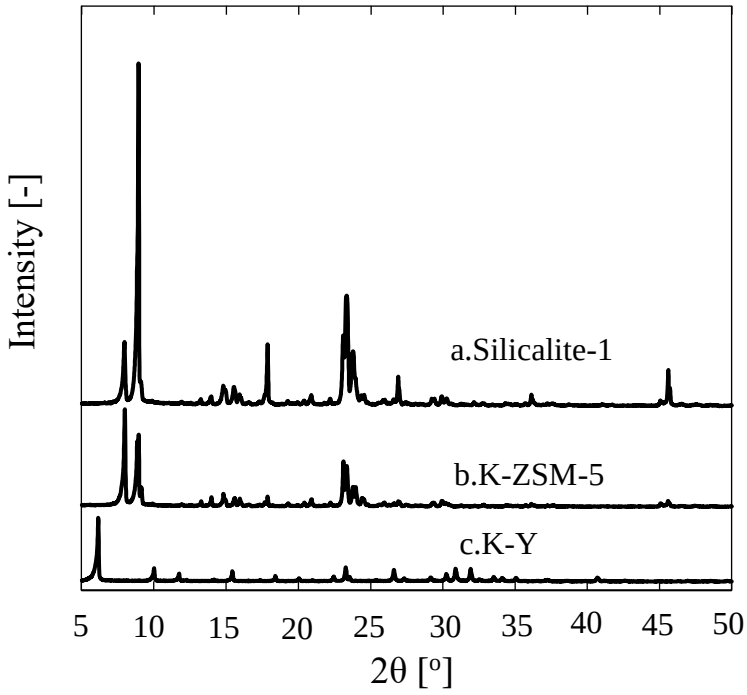

Fig.5.2 XRD patterns of silicalite-1, K-ZSM-5 and K-Y.

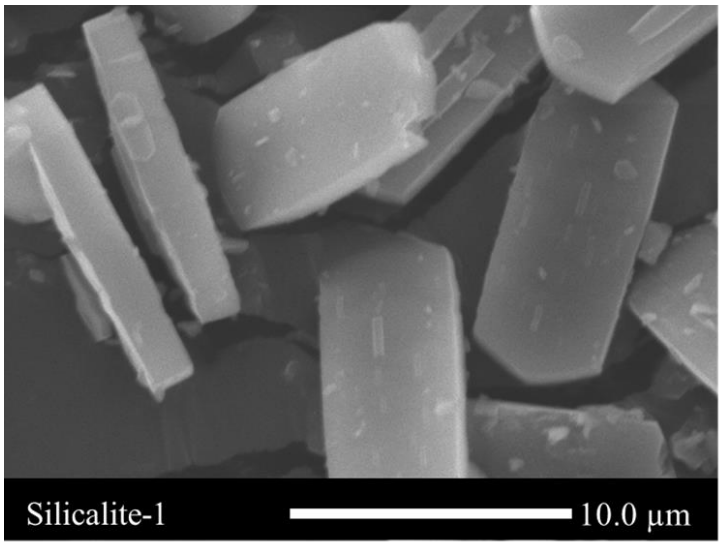

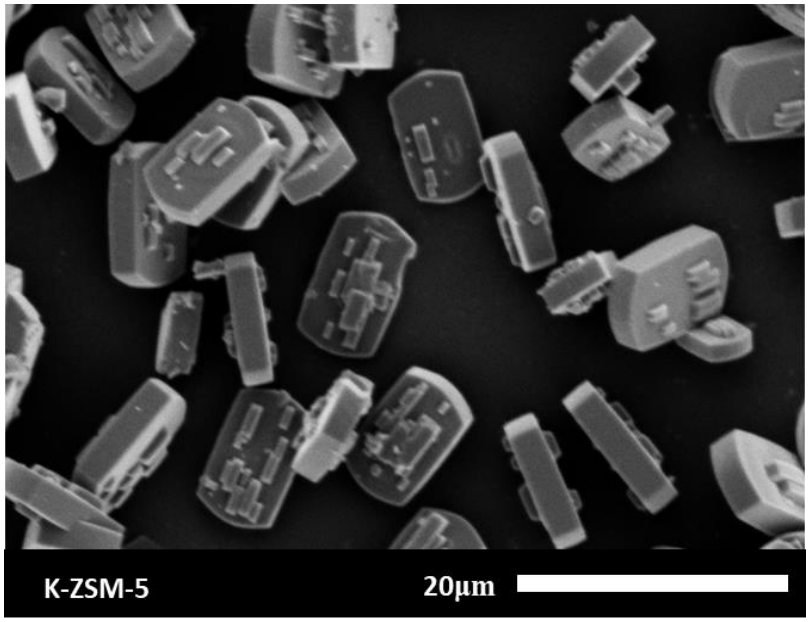

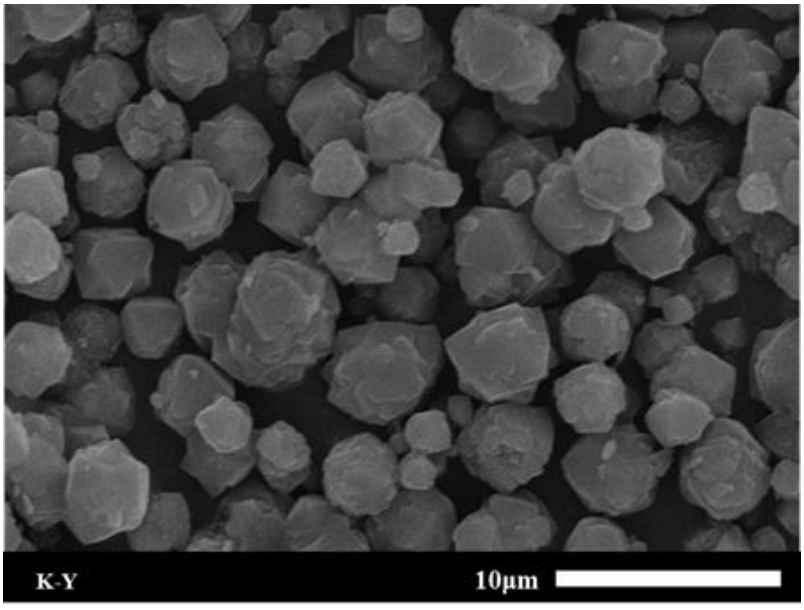

Fig.5.4 SEM image of silicalite-1, K-ZSM-5 and K-Y.

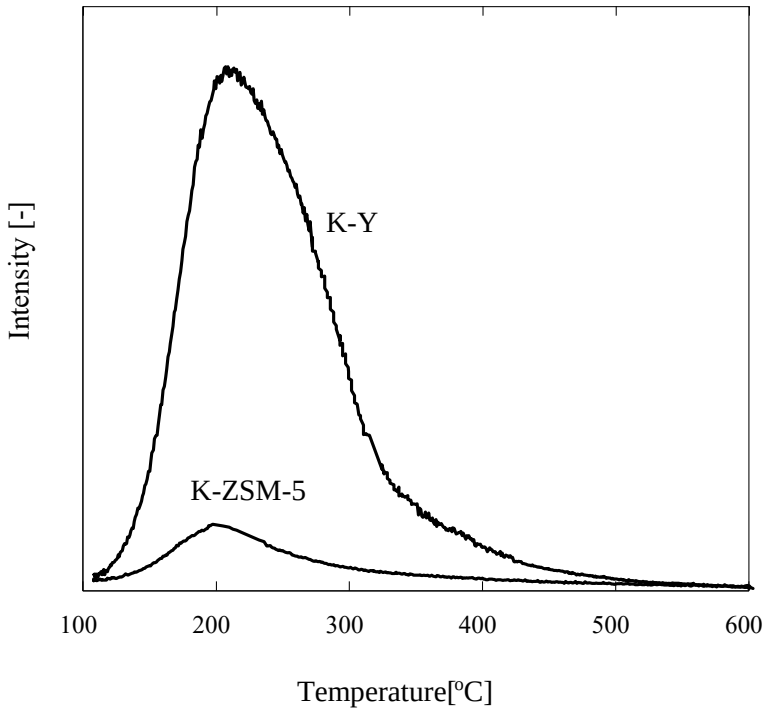

Fig.5.5 NH_3-TPD profile of K-ZSM-5 and K-Y.

Table 1 Properties of Silicalite-1, K-ZSM-5 and K-Y

Zeolites	S_{BET} [$m^2\ g^{-1}$]	S_{EXT} [$m^2\ g^{-1}$]	V_m* [$cm^3\ g^{-1}$]	Number of acid sites [mol kg^{-1}]	Si/Al ratio* [-]
Silicalite-1	401	0.27	0.17	—	—
K-ZSM-5	387	15.2	0.17	0.26	110
K-Y	622	15.7	0.24	3.29	3.2

* Pore volume (V_m) was calculated by the BJH method and the Si/Al ratio obtained by XRF analyze

5.3.2. Diffusivities of aromatic hydrocarbons within Silicalite-1 in the sub- and super-critical fluids of cyclopentane

The Temperature dependency of *p*-xylene, *p*-cresol, *p*-propylphenol and toluene intracrystalline diffusivities of within silicalite-1 in the sub- and super-critical fluids are presented in Fig.6. The diffusivity of toluene within silicalite-1 in sub- and super-critical fluids of cyclopentane was much lower than that in the gas phase, which indicated that the solvent coexisting within the silicalite-1 pores affected the diffusion of toluene. The diffusivities of p-xylene, p-cresol, p-propylphenol and toluene within silicalite-1 in the sub-critical fluids under 5 MPa were correlated with a single line, indicating that the diffusivity only depends on temperature (313K-473K). On the contrary, the almost minimum value at critical temperature of cyclopentane (513 K) was obtained in the supercritical fluids. Liew et al. reported that dynamic structure of a cluster formed around a solute in the supercritical fluids was observed. This phenomenon suggestion that cluster of solvent would be formed easily in the supercritical fluids [43]. With the assumption described above, formation of clusters between diffusion substance and solvent molecules near the critical point of solvent was considered, which lead to increased mass transfer resistance at pore mouth near the outer surface of the silicalite-1. The diffusivities of *p*-xylene, *p*-cresol, *and* *p*-propylphenol within silicalite-1 are approximately the same as that of toluene in the sub-critical and super-critical fluid irrespective of the para-position functional groups on the benzene ring. Moreover, the diffusivities for *p*-xylene, *m*-xylene and *o*-xylene at 473 K, 513 K and 543 K are list in Table 5.2. From the table, it can be seen that the diffusivities for three xylene isomers within silicalite-1 in sub-critical and super-critical fluids are in the following order: *p*-xylene > *m*-xylene > *o*-xylene, which shows the values as expected according to their molecular kinetic diameter.

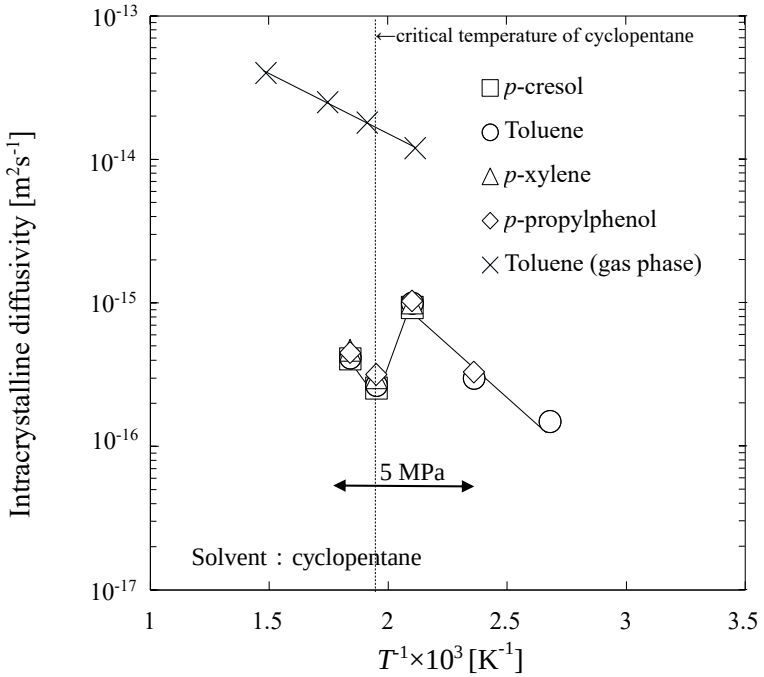

Fig.5.6 Temperature dependency of the diffusivity of aromatic hydrocarbons within silicalite-1 in gas, sub- and super-critical fluids (solvent: cyclopentane).

Table 5.2 The intracrystalline diffusivity of three xylene isomers within silicalite-1, K-ZSM-5 and K-Y

Zeolite	Diffusivity of Sorbate	T（K）		
		473	513	543
Silicalite-1	*p*-xylene	1.0×10^{-15}	3.0×10^{-16}	4.6×10^{-16}
	m-xylene	6.3×10^{-16}	2.3×10^{-16}	3.7×10^{-16}
	o-xylene	4.2×10^{-16}	2.0×10^{-16}	3.1×10^{-16}
K-ZSM-5	*p*-xylene	1.8×10^{-15}	2.4×10^{-15}	3.7×10^{-15}
	m-xylene	1.0×10^{-15}	1.8×10^{-15}	2.4×10^{-15}
	o-xylene	6.0×10^{-16}	8.8×10^{-16}	1.5×10^{-15}
K-Y	*p*-xylene	1.5×10^{-15}	1.4×10^{-15}	2.0×10^{-15}
	m-xylene	7.3×10^{-16}	1.2×10^{-15}	1.5×10^{-15}
	o-xylene	5.6×10^{-16}	9.2×10^{-16}	1.1×10^{-15}

5.3.3. Intracrystalline diffusivities of aromatic hydrocarbons within K-ZSM-5 in the sub- and super-critical fluids of cyclopentane

The typical temperature dependency of intracrystalline diffusivities of toluene, *p*-xylene, *p*-cresol, and propylbenzene within K-ZSM-5 in the sub- and super-critical fluids are shown in Fig.5.7. The intracrystalline diffusivities of toluene, p-xylene, p-cresol, and propylbenzene in the supercritical fluids were correlated with a single line and shows much higher value than that within silicalite-1. It is considered that aromatic hydrocarbons adsorb on the outer surface of K^+ of the K-ZSM-5 to make aromatic hydrocarbons concentrations were increased, formation of the cluster may be suppressed and decreased diffusion resistance at pore mouth, which leading to increase the diffusivity. The intracrystalline diffusivities of toluene, p-xylene and propylbenzene are approximately the same without affected by functional groups on the benzene ring, whereas *p*-cresol shows low value within K-ZSM-5 compared to toluene. The results reflecting the enhanced molecular transport resistance of *p*-cresol in K-ZSM-5. Moreover, the relation of corresponding activation energy values calculated according to the relationship between the temperature and intracrystalline diffusivity, *p*-cresol within K-ZSM-5 is 29 kJ/mol, which is greater than that of toluene, p-xylene and propylbenzene (21 kJ/mol). It is attributed that the formation of hydrogen bonding between *p*-cresol and K-ZSM-5, and *p*-cresol molecules are strongly adsorbed on K^+ of K-ZSM-5 to the residence time of p-cresol on the K^+ becomes extended in the framework, which lead to the intracrystalline diffusivity decreased within K-ZSM-5. The intracrystalline diffusivity for three xylene isomers followed the order of o-xylene < m-xylene < p-xylene at the same temperature range (Table 5.2), which is attributed to the smaller molecular kinetic diameter and weaker interaction between p-xylene and K-ZSM-5 compared with m-xylene and o-xylene. In addition, activation energies for p-xylene, m-xylene and o-xylene, which exhibited the opposite trend with intracrystalline diffusivities. (23.3 kJ/mol for p-xylene, 27.7 kJ/mol for m-xylene and 28.8 kJ/mol for o-xylene, respectively)

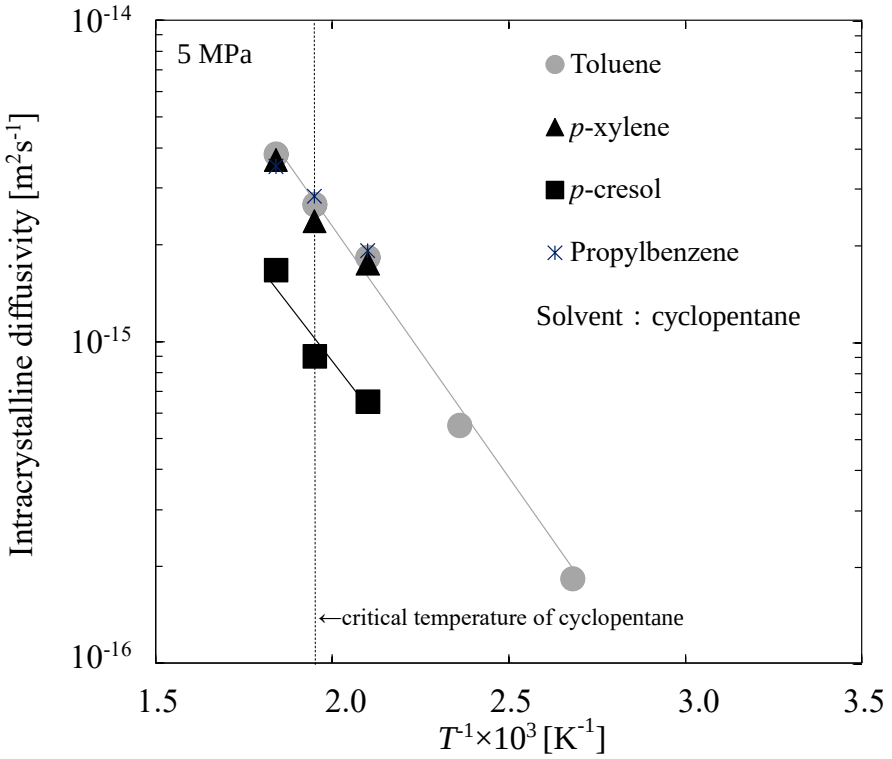

Fig.5.7 Temperature dependency of the intracrystalline diffusivity of aromatic hydrocarbons within K-ZSM-5 in sub- and super-critical of cyclopentane.

5.3.4. Intracrystalline diffusivities of aromatic hydrocarbons within K-Y in the sub- and super-critical fluids of cyclopentane

The temperature dependency on K-Y for toluene, *p*-cresol, *p*-xylene and propylbenzene intracrystalline diffusivities in the sub- and super-critical fluids are investigated in Fig. 5.8. For toluene and propylbenzene, the intracrystalline diffusivities also shows almost the same values. Moreover, intracrystalline diffusivity of *p*-cresol exhibits lower within K-Y than that of toluene. In addition, calculate activation energies for toluene and *p*-cresol within K-Y were 16.0 and 22.1 kJ/mol, respectively. It indicated that *p*-cresol diffused through the K-Y zeolite forming hydrogen bonding interacts with oxygen atoms of the framework of K-Y and adsorbed on K^+ of K-Y for decreased the diffusivity. Furthermore, intracrystalline diffusivity of *p*-xylene within K-Y is lower than that of *p*-cresol while intracrystalline diffusivity of *p*-xylene and *p*-cresol within

K-ZSM-5 got the opposite results. It is considered that the *p*-xylene may undergo repeated adsorption and desorption processes inside the super-cage of the K-Y, which make the low diffusivity while *p*-creasol can adsorbed on the K+ near the pore mouth of the super-cage further diffuse inside the zeolite crystal. The Y-type zeolite depend on its porous structure and surface property (acid sites), which lead to complex process in diffusion of hydrocarbon within Y zeolite.

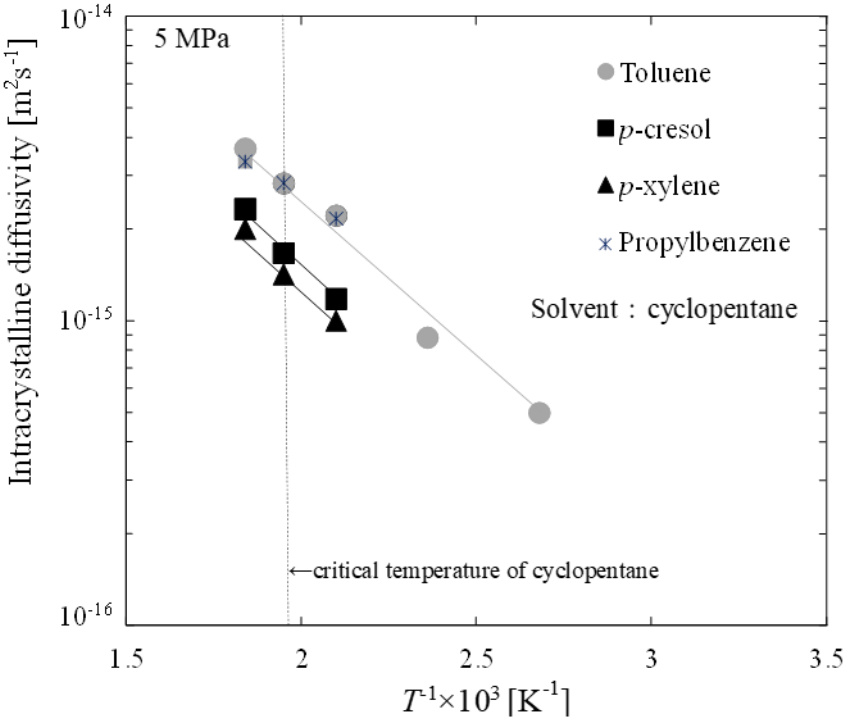

Fig.5.8 Temperature dependency of the intracrystalline diffusivity of aromatic hydrocarbons within K-Y in sub- and super-critical of cyclopentane

From the Table 5.2, it was also observed that the diffusivities of xylene isomers within K-Y exhibited the same trend as the silicalite-1 and K-ZSM-5 (*p*-xylene > *m*-xylene > *o*-xylene) in sub- and super-critical fluids, while their activation energies values displayed the opposite phenomenon (22.6 kJ/mol for *p*-xylene, 23.2 kJ/mol for *m*-xylene and 23.7 kJ/mol for *o*-xylene, respectively). In addition, a significant downward tendency can be seen for all diffusion substances within K-Y compared to that within K-ZSM-5, which reveals that the activation energy involved in diffusion within zeolite with large pore size (K-Y) would be relatively lower than that within

zeolite with small pore size (K-ZSM-5).

5.3.5. Possible diffusion mechanism within silicalite-1 and K-ZSM-5 in gas, sub- and super-critical fluids

On the basis of the experimental results, possible diffusion mechanism within silicalite-1 and K-ZSM-5 (K-Y) in the gas, sub- and super-critical fluids can be described, as shown in Fig.5.9. In the gas phase, the toluene can easily adsorb and diffusion within silicalite-1, because there is no solvent effect. However, in the sub- and super-critical fluids, the diffusion molecule and solvent can exist inside the pore of silicalite-1 and K-ZSM-5. For the silicalite-1, Formation of clusters between solvent molecules and diffusion substance near the critical point of solvent was considered to lead to the increase of diffusion resistance at pore mouth of silicalite-1, intracrystalline diffusivity was decreased. For the K-ZSM-5, diffusion substance adsorbed on the acid site at outer surface of the zeolite was considered to lead to increase diffusion substance concentration near critical point of solvent. And then, formation of the cluster of solvent solution may be suppressed for decreasing diffusion resistance at pore mouth, which intracrystalline diffusivity increased with increasing the acid site at pore mouth, compared to diffusivity within silicalite-1. For the K-Y, the diffusion mechanism of some diffusion substances worked the same way as within K-ZSM-5. However, K-Y has the super-cage size, which make some diffusion substances such as *p*-xylene may undergo repeated adsorption and desorption processes inside the super-cage of the K-Y, which make the low diffusivity while *p*-cresol can adsorbed on the acid site near the pore mouth of the super-cage further diffuse inside the zeolite crystal, which make the high diffusivity. The Y-type zeolite depend on its porous structure and surface property (acid sites), which lead to complex process in diffusion of hydrocarbon within Y zeolite.

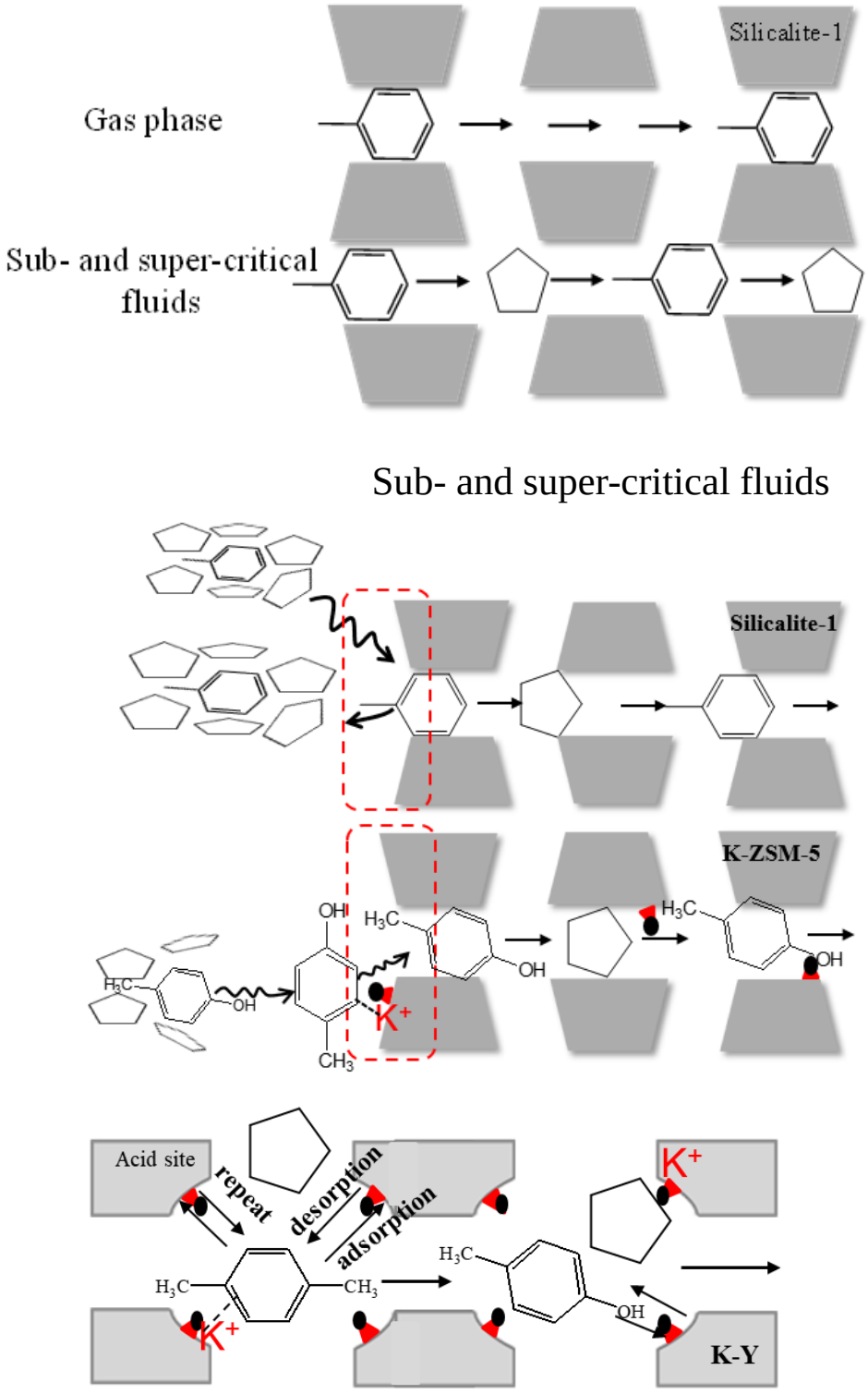

Fig.5.9 Possible diffusion mechanisms for toluene within H-silicalite-1, K-ZSM-5 and p-cresol and p-xylene within K-Y in the gas phase, the sub- and super-critical of cyclopentane.

5.4. Conclusions

The intracrystalline diffusivities of toluene, xylene isomers, *p*-propylphenol, propylbenzene, and *p*-cresol within silicalite-1, K-ZSM-5, and K-Y in sub-, and super-critical fluid of cyclopentane (473-543 K, 5 MPa) and the diffusion mechanism of aromatic hydrocarbons within silicalite-1, K-ZSM-5, and K-Y zeolite pores has been investigated. The intracrystalline diffusivity of *p*-xylene, *p*-cresol and *p*-propylphenol within silicalite-1 under sub-, and super-critical fluid shows approximately same irrespective of the para-position functional groups on the benzene ring and made the almost minimum value at critical temperature (513 K). This result suggested that formation of cluster between solvent and diffusion substance near the critical point of solvent. Moreover, the intracrystalline diffusivities of toluene and propylbenzene within K-ZSM-5, and K-Y showed almost the same value, and *p*-cresol exhibited lower intracrystalline diffusivity. It is attributed that the hydroxy group in p-cresol was adsorbed strongly on K^+ of K-ZSM-5 (or K-Y) and this led to a lower intracrystalline diffusivity. However, the diffusion mechanism of *p*-xylene within K-ZSM-5 and K-Y are different may be due to the different pore structure between K-ZSM-5 and K-Y. The intracrystalline diffusivity for three xylene isomers within silicalite-1, K-ZSM-5 and K-Y in sub-critical and super-critical fluids follow the order of *o*-xylene < *m*-xylene < *p*-xylene, which shows the values as expected according to their molecular kinetic diameter.

Reference

[1] T. F. Willems, C. H. Rycroft, M. Kazi, J. C. Meza, M. Haranczyk, Microporous Mesoporous Mater., 149 (2012) 134-14.
[2] J. Liang, Z. Liang, R. Zou, Y. Zhao, Adv. Mater., 29 (2017) 1701139.
[3] M. Choi, H. S. Cho, R. Srivastava, C. Venkatesan, D. Choi and R. Ryoo, Nature mater., 5 (2006) 718-723.
[4] C. H. Christensen, K. Johannsen, I. Schmidt and C. H. Christensen, J. Am. Chem. Soc., 15 (2003) 13370-13371.
[5] L. Huang, Z. Wang, J. Sun, L. Miao, Q. Li, Y. Yan and D. Zhao, J. Am. Chem. Soc., 122 (2000) 3530-3531.
[6] A. Corma, Chem. Rev., 97 (1997) 2373-2420.
[7] M. E. Davis, Nature, 417 (2002) 813-821.

[8] M. O. Daramola, E. F. Aransiola and T. V. Ojumu, Materials, 5 (2012) 2101-2136.
[9] C. S. Cundy and P. A. Cox, Chem. Rev., 103 (2003) 663-702.
[10] S. Mitchell, A. B. Pinar, J. Kenvin, P. Crivelli, J. Kärger and J. Pérez-Ramírez, Nat. Commun., 6 (2015) 1-14.
[11] T. Ennaert, J. V. Aelst, J. Dijkmans, R. D. Clercq, W. Schutyser, M. Dusselier, D. Verboekend and B. F. Sels, Chem Soc Rev., 45 (2016) 584-611.
[12] R. Li, J. A. Fowler and B. A. Todd, Phys. Rev. Lett., 113 (2014) 028303.
[13] T. Masuda, Chem. Eng. Sci. 56 (2001) 889-896.
[14] T. Masuda, Catal. Surv. from Asia. 7 (2003) 133-144.
[15] T. Masuda, Y. Fujikata, H. Ikeda, K. Hashimoto, Microporous Mesoporous Mater. 38 (2000) 323-332.
[16] T. Masuda, Y. Fujikata, T. Nishida, K. Hashimoto, Microporous Mesoporous Mater. 23 (1998) 157-167.
[17] Y. Fujikata, T. Masuda, H. Ikeda, K. Hashimoto, Microporous Mesoporous Mater. 21 (1998) 679-686.
[18] T. Masuda, Y. Fujikata, T. Nishida, K. Hashimoto, Microporous Mesoporous Mater. 23 (1998) 157-167.
[19] Y. Nakasaka, T. Tago, K. Odate, T. Masuda, Microporous Mesoporous Mater. 112 (2008) 162-169.
[20] X. Su, Y. Nakasaka, R. Moriwaki, T. Yoshikawa, T. Masuda, Microporous Mesoporous Mater. 319 (2021) 111044.
[21] L. Song, Z. Sun, L. Duan, J. Gui, G. S. McDougall, Microporous Mesoporous Mater. 104 (2007)115-128.
[22] S. Yang, J. Zhang, Q. Yang and Y. Qian, Energy Fuels, 28 (2014) 5557-5564.
[23] S. Kang, X. Li, J. Fan, J. Chang, Renew. Sust. Energ. Rev., 27 (2013) 546-558.
[24] A. M. Vorobei, O. I. Pokrovskiy, K. B. Ustinovich, O. O. Parenago, V. V. Lunin, J. Mol. Liq., 280 (2019) 212-217.
[25] S-M. Kang, M-W. Cho, K-M. Kim, D-Y. Kang, W-M. Koo, K-H. Kim, J-Y. Park, S-S. Lee, Wood Sci. Technol., 46 (2012) 643-656.
[26] J. Zhang, Z. Luo, Q. Dang, J. Wang and W. Chen, Energy & Fuels., 26 (2012) 2990-2995.
[27] S. Oh, H. Hwang, H. S. Choi, J. W. Choi, Chemosphere., 117 (2014) 806-814.
[28] H-J. Huang, X-Z. Yuan, G-M. Zeng, Y. Liu, H. Li, J. Yin, X-L. Wang, J ANAL APPL PYROL., 102 (2013) 60-67.
[29] W. Li, C. Pan, Q. Zhang, Z. Liu, J. Peng, P. Chen, H. Lou, X. Zheng, Bioresour.

technol., 102 (2011) 4884-4889.
[30] Ž. Knez, M. Pantić, D. Cör, Z. Novak, M. K. Hrnčič, Chem Eng Technol.,141 (2019) 107532.
[31] M. T. Timko, A. F. Ghoniem, W. H. Green, J Supercrit Fluids., 96 (2015) 114-123.
[32] D. C. Elliott, T. R. Hart, A. J. Schmidt, G. G. Neuenschwander, L. J. Rotness, M. V. Olarte, A. H. Zacher, K. O. Albrecht, R. T. Hallen, J. E. Holladay, Algal Res., 2 (2013) 445-454.
[33] D. R. Vardon, B. K. Sharma, J. Scott, G. Yu, Z. Wang, L. Schideman, Y. Zhang, T. J.Strathmanna, Bioresource Technol., 102 (2011) 8295-8303.
[34] G. Yu, Y. Zhang, L. Schideman, T. Funk and Z. Wang, Energy Environ. Sci., 4 (2011) 4587-4595.
[35] A. A. Peterson, F. Vogel, R. P. Lachance, M. Fröling, M. J. Antal, Jr. and J. W. Tester, Energy Environ. Sci., 1 (2008) 32-65.
[36] M. Mosteiro-Romero, F. Vogel, A. Wokaun, Energy Environ. Sci., 109 (2014) 111-122.
[37] I. Okajima, T. Sako, J. Biosci. Bioeng., 117 (2014) 1-9.
[38] I. Pavlovič, Ž. Knez, and M. Škerget, J. Agr. Food Chem., 61 (2013) 8003-8025.
[39] J. Peng, P. Chen, H. Lou, X. Zheng, Bioresour. technol., 100 (2009) 3415-3418.
[40] X. Zhang, Q. Zhang, T. Wang, B. Li, Y. Xu, L. Ma, Fuel, 179 (2016) 312-321.
[41] T. Yoshikawa, T. Umezawa, Y. Nakasaka, T. Masuda, Catal. Today., 347 (2020) 110-114.
[42] G. Watanabe, Y. Nakasaka, T. Taniguchi, T. Yoshikawa, T. Tago, T. Masuda, Chem. Eng. J., 312 (2017) 288-295.
[43] C. C. Liew, H. Inomata, S. Saito, fluid phase equilib., 104 (1995) 317-329.

Summary

The chapter 1 is the introduction that describes research background including the general characteristics of zeolites, intralystalline diffusion phenomenon within zeolite and the general characteristics of supercritical fluids, and finally introduces the purpose of this study and the structure of this paper.

Chapter 2 This study investigated the intracrystalline diffusivity of phenol, p-propylphenol, m-cresol, and toluene within silicalite-1 and H-MFI in the liquid phase. The amounts of phenol, p-propylphenol and toluene adsorbed within silicalite-1 are approximately the same, whereas the amounts of adsorbed m-cresol is small, which is attributed to the larger kinetic diameter of m-cresol. In addition, compared with toluene, phenol exhibits a greater adsorption amount in H-MFI, because of strong interaction between hydrogen bonds in phenol molecules and Brønsted acid sites within H-MFI. The investigation of the intracrystalline diffusivity of phenol, p-propylphenol, and toluene within silicalite-1 indicates that they exhibit approximately the same diffusivity, which is ascribed to geometrical limitations alone determining the intracrystalline diffusivity. However, the m-cresol exhibited a lower intracrystalline diffusivity and effective diffusivity, and a higher activation energy (21.8 kJ/mol) than the other phenolic compounds (~17 kJ/mol). This result is attributed to the larger molecular size of m-cresol strongly limiting its diffusion inside the micropores of silicalite-1. In H-MFI zeolite, the acid sites affect phenol diffusion, leading to a low intracrystalline diffusivity and a high activation energy compared with silicalite-1, indicating a difference in the hydrogen bonding interaction between phenol and H-MFI than between toluene and H-MFI, it is considered that the residence time of phenol on the acid sites was longer than that of toluene, which led to the difference in intracrystalline diffusivity within H-MFI.

Chapter 3 The intracrystalline diffusivity of phenol and toluene within H-Y zeolites in the liquid phase together with the effect on the diffusivity of phenol and toluene of solvents coexisting in the H-Y zeolite pores were studied. In the gas phase, given that the geometrical limitations are small when toluene diffuses into the zeolite pores, the activation energy for intracrystalline diffusivity was small. In contrast, in the liquid phase, the activation energy for the intracrystalline diffusivity of toluene was larger than that in the gas phase because solvent molecules coexisted inside the pores.

To investigate the affinity of the diffusion molecule for the acid sites of H-Y and its effect on the diffusivity, the diffusivities of phenol and toluene were measured in mesitylene solutions. The hydroxy group in phenol was adsorbed strongly on the Brønsted acid sites of H-Y and this led to a lower intracrystalline diffusivity than that for toluene. Furthermore, the intracrystalline diffusivities of phenol within H-Y for three solvents were measured to investigate the effect of the affinities of the solvents and the acid sites on phenol diffusion and to clarify the order of phenol diffusivity, this being as follows: 2-propanol > cyclohexane > mesitylene. It was clarified that the ease of adsorption of the diffusion molecules and the solvent molecules coexisting within the pores on the acid sites of H-Y as well as the kinetic diameter of the solvent molecules adsorbed on the acid sites affected the diffusivity of the diffusion molecules and their activation energy.

Chapter 4 The intracrystalline diffusivity of 1-Methylnaphthalene or toluene within Si-beta or silicalite-1 and K-ZSM-5 in the sub- and super-critical fluids. In the gas phase, the geometrical limitations are small when toluene diffuses into the zeolite pores, the activation energy for intracrystalline diffusivity was small. In contrast, in the sub- and super-critical fluids, the intracrystalline diffusivity of 1-Methylnaphthalene or toluene was much larger than that in the gas phase because solvent molecules coexisted inside the pores. The intracrystalline diffusivity of 1-Methylnaphthalene or toluene in the cyclohexane or cyclopentane solvent was also investigated. During 313 ~ 473 K, the intracrystalline diffusivity increased with increasing the temperature. Above 473 K, the intracrystalline diffusivity of 1-Methylnaphthalene or toluene within Si-beta or silicalite-1 was decreased and the almost minimum value at critical temperature was obtained in the supercritical fluids. This may be because solvent molecules gather around diffusion molecules near the critical point to forming clusters. For this point, the resistance at the pore mouth of the Si-beta or silicalite-1 increases and the intracrystalline diffusivity decreases. In contrast, intracrystalline diffusivity of toluene within K-ZSM-5 in the sub- and super-critical of cyclopentane showed much higher value than that within silicalite-1 as well as the diffusivity of toluene was reduced with decreasing Al content in K-ZSM-5. Because of toluene concentration at outer surface of the K-ZSM-5 was increased, formation of the cluster may be suppressed and decreased diffusion resistance at pore mouth, which leading to increase the diffusivity.

Chapter 5 The intracrystalline diffusivities of toluene, xylene isomers, p-propylphenol, propylbenzene, and p-cresol within silicalite-1, K-ZSM-5, and K-Y in sub-, and super-critical fluid of cyclopentane (473-543 K, 5 MPa) were investigated. The Arrhenius plots of the intracrystalline diffusivity of p-xylene, p-cresol and

p-propylphenol within silicalite-1 under 5 MPa shows similar values and made the almost minimum value at critical temperature (513 K). This result suggested that formation of cluster between solvent and diffusion substance near the critical point of solvent. In addition, the intracrystalline diffusivities of toluene and propylbenzene within K-ZSM-5, and K-Y showed almost the same value, and p-cresol exhibited lower intracrystalline diffusivity. It is attributed that the hydroxy group in p-cresol was adsorbed strongly on K^+ of K-ZSM-5 (or K-Y) and this led to a lower intracrystalline diffusivity. The diffusion mechanism of p-xylene within K-ZSM-5 and K-Y are different may be due to the different pore structure of K-ZSM-5 and K-Y. The intracrystalline diffusivity for three xylene isomers within silicalite-1, K-ZSM-5 and K-Y in sub-critical and super-critical fluids follow the order of o-xylene < m-xylene < p-xylene, which shows the values as expected according to their molecular kinetic diameter.

Outlook

supercritical carbon dioxide (SCO_2) as solvent

With the continuous growth of the world's population and economy, the global demand for energy has increased dramatically. To meet this demand, the global community relies heavily on the burning of fossil fuels (coal, petroleum, and crude oil). The massive use of fossil fuels has led to serious environmental problems such as Nitrogen dioxide pollution from vehicle exhaust Global warming caused by the emitted CO_2. As awareness of these problems and effective alternatives has increased, considerable efforts have been put into achieving substantial reductions in CO2 emissions. Therefore, the utilization and conversion of CO_2 as renewable resources have been important issues and paid much attention in the field of green and sustainable chemistry. The conversion of CO_2 to chemicals and fuels has attracted much interest as CO_2 is a nontoxic, non-flammable, and cheap carbon–oxygen source.

Moreover, most of the chemical reactions that can take place depend on solvents, but most solvents also cause environmental pollution of varying degrees. Therefore, the use of supercritical carbon dioxide (SCO_2) as a fluid has been identified as a promising energy technology for reduced environmental impact and high conversion efficiency.

In the supercritical state, CO_2 as a fluid in an energy conversion system presents interesting properties. When the temperature is higher than the critical temperature (31^oC) and the pressure is higher than the critical pressure (7.4 MPa), ATM, the properties of carbon dioxide will change. Its density is close to that of liquid, its viscosity is close to that of gas, and its diffusion coefficient is 100 times that of liquid, so it has amazing solubility. It can be used to dissolve a variety of substances, and then extract the active components, which has a wide application prospect. Therefore, in recent decades, many researchers have used SCO_2 as a solvent to convert chemicals and fuels, such as supercritical carbon dioxide extraction technology, oxidizing reaction and catalytic hydrogenation.

Theses chemical reactions need to be carried out using SCO_2, which attributed to its physicochemical properties of solubility, high diffusivity, lower viscosity and liquid-like density that can enhance the mass transfer of substrates to the active sites of

catalysts. However, diffusivity of reactant within zeolites in the super-critical fluid have not been proposed. Therefore, understanding diffusion mechanisms of molecules in the porous catalysts under different conditions are very critical for designing the catalysis and supply more useful information on reaction processes using zeolites. Moreover, since the degree of the diffusion limitations are observed differently by depending on molecular size and circumstance around the catalysts, such as gas, liquid, sub-critical and supercritical fluids. SCO_2 will be used as the most suitable solvent to explore the diffusion mechanism of aromatic compounds within zeolites in supercritical fluids.

Acknowledgements

During the preparation of the PhD dissertation, I have received a lot of valuable help from many people. Their advice and comments contribute to the accomplishment of the dissertation.

Firstly, I profound gratitude my supervisor Professor Takao Masuda and Associate Professor Yuta Nakasaka for providing me with the opportunity to following PhD studies. They have given me great instructions and deeply throughout the process of selecting research direction and writing the dissertation and publications, which provide me many enlightening ideas. I also thankful to Professor Shin Mukai, Professor Atsushi Fukuoka, Professor Toshifumi Satoh and Associate Professor Isao Ogino. Their insightful comments for my research process and writing the dissertation. I also wish to thank Associate Professor Takuya Yoshikawa for his comments, criticism and advice to research work.

Secondly, special thanks go to Ms. Miki Oda and Ms. Hiromi Aoki and Ms. Sayaka Fukasawa for their assistance in both study and daily life in Japan. I also grateful to all the members in Chemical System Engineering Laboratory that helped and encouraged me in the entire process of finishing this dissertation, such as Dr. Yuki Kawamata, Mr. Hiroya Ishimaru, Mr. Takumi Kanda, Mr. Haruki Iwauchi, Mr. Naoki Kumagai, Mr. Yuta Ishizu, Mr. Ren Moriwaki, Ms. Mai Hasegawa, Mr. Hernandez Jose, and other colleagues and friends for their kind assistant and friendships.

Finally, I would like to express my sincere thanks to my family in China thanks to Professor Masahiko Arai in Japan and thanks to friends who unconditionally supported my studies and gave me spiritual encouragement to finish my study in Japan. Thank you very much for my greatest parents, Mr. Fubin Su and Ms. Ying Xin.

Xinluona Su

Jan.2022

Study Achievements

Scientific publications

(1) **Xinluona Su**, Yuta Nakasaka, Ren Moriwaki, Takuya Yoshikawa, Takao Masuda. Diffusion of phenolic compounds within high-silica MFI-type zeolite in the mesitylene solution, Microprus and Mesoporous Materials, 2021, 319, 111044.5.
(2) **Xinluona Su**, Yuta Nakasaka, Ren Moriwaki, Takuya Yoshikawa, Takao Masuda. Effect of solvents coexistence on the intracrystalline diffusivity of toluene and phenol within Y-type zeolite in the liquid phase. (in press)

Oral or Poster Presentations

Academic activity:
International Conference
(3) **Xinluona Su**, Yuta Nakasaka, Ryo Nakano, Yoshihiro Kubota, Satoshi Inagaki, Takao Masuda, "Measurement of Intracrystalline Diffusivity of Toluene within Silicalite-1 and K-ZSM-5 in Sub- and Super-critical Fluids" APCChE 2019, 23rd-27th/09/2019, Sapporo, Japan. (oral presenter)
(4) **Xinluona Su**, Yuta Nakasaka, Ryo Nakano, Yoshihiro Kubota, Satoshi Inagaki, Takao Masuda, "Diffusion of Toluene within Silicalite-1 and K-ZSM-5 in Sub- and Super-critical Fluids of cyclopentane" International symposium on porous materials, 17th-19th/11/2019, Tokyo, Japan. (poster presenter)
(5) **Xinluona Su**, Yuta Nakasaka, Ryo Nakano, Yoshihiro Kubota, Satoshi Inagaki, Takao Masuda, "Measurement of toluene diffusivity within MFI-type zeolites in sub- and super-critical fluids of cyclopentane" Winter Research Presentation, 28th-29th/01/2020, Sapporo, Japan. (oral presenter)
(6) 森脇蓮, **Xinluona Su**, 中坂佑太, 吉川琢也, 増田隆夫, Silicalite-1, ZSM-5 結晶内におけるフェノール類の液相拡散係数測定" 第 124 回触媒討論会, 2019 年 9 月, 長崎
(7) 森脇 蓮, 中坂 佑太, **Xinluona Su**, 吉川 琢也, 増田 隆夫, "液相におけるフェノール類の MFI 型ゼオライト細孔内拡散機構の解明"第 30 回化学工学・粉体工学研究発表会、オンライン、 2021 年